JOINT DETECTION AND CLASSIFICATION OF THE OFDM-BASED MOBILE WIMAX AND LTE SIGNALS FOR COGNITIVE RADIO

ALA'A AL-HABASHNA

JOINT DETECTION AND CLASSIFICATION OF THE OFDM-BASED MOBILE WIMAX AND LTE SIGNALS FOR COGNITIVE RADIO

by

© Ala'a Al-Habashna

A Thesis submitted to the School of Graduate Studies
in partial fulfillment of the requirements for the degree of
Master of Engineering

Faculty of Engineering and Applied Science
Memorial University of Newfoundland

August 2010

St. John's Newfoundland

Abstract

Spectrum awareness is one of the most challenging requirements in cognitive radio (CR). To adequately adapt to the changing radio environment, it is necessary for the CR to be able to perform joint detection and classification of low signal-to-noise ratio (SNR) signals. The wireless industry has recently shown great interest in orthogonal frequency division multiplexing (OFDM) technology, due to advantages, such as efficient use of the spectrum, resistance to frequency selective fading, and elimination of intersymbol interference. As such, joint detection and classification of OFDM signals has been intensively researched recently.

The existing techniques for joint detection and classification of OFDM signals either involve complex feature recognition procedures or introduce new overheads by creating features in the signals for detection and classification purposes. As such, the OFDM standard signals should be investigated and existing features should be exploited for their joint detection and classification. The cyclostationarity of OFDM signals in two of the most popular wireless communications standards, namely, mobile Worldwide Interoperability for Microwave Access (WiMAX) and third Generation Partnership Project Long Term Evolution (3GPP LTE), is studied here for the purpose of their joint detection and classification.

In this thesis, the second-order cyclostationarity of the OFDM-based mobile WiMAX and LTE signals is studied, and closed-from expressions for the cyclic autocorrelation function (CAF) and cyclic frequencies (CFs) of both signals are derived. Furthermore,

two cyclostationarity-based algorithms for joint detection and classification of these signals are developed, and the joint detection and classification performance, as well as the complexity of the proposed algorithms are investigated. Simulation results show the efficiency of the proposed algorithms under low SNRs, short sensing times, and diverse channel conditions.

Acknowledgements

I would like to thank my supervisors, Dr. Octavia Dobre and Dr. Ramachandran Venkatesan, from Memorial University of Newfoundland for their suggestions, encouragements, and technical guidance and support which helped me a lot throughout my master's program.

I would also like to thank the students in the Computer Engineering Research Laboratory (CERL) at Memorial University of Newfoundland, for the pleasant working environment.

I would like to express gratitude to my brother and sisters for their encouragement and love over the years.

Finally, and most importantly, I am grateful to my parents. They borne, raised, and supported me. Their endless love and belief in me have been a constant source of inspiration, and this thesis is dedicated to them.

Table of Contents

List of Tables

List of Figures

List of Abbreviations

AWGN	Additive white Gaussian noise
CAF	Cyclic autocorrelation function
CF	Cyclic frequency
CP	Cyclic prefix
CR	Cognitive radio
DL	Downlink
DSA	Dynamic spectrum access
FCC	Federal communication commission
FDD	Frequency division duplexing
FFT	Fast Fourier transform
IDFT	Inverse discrete Fourier transform
i.i.d.	Independent and identically distributed
LTE	Long term evolution
MBSFN	Multicast broadcast single frequency network
OFDM	Orthogonal frequency division multiplexing
PSK	Phase shift keying
QAM	Quadrature amplitude modulation
RS	Reference signal
RTG	Receive/transmit transition gap
SNR	Signal-to-noise ratio
TDD	Time division duplexing
TTG	Transmit/receive transition gap
UL	Uplink
WiMAX	Worldwide interoperability for microwave access
WRAN	Wireless regional area network
3GPP	Third generation partnership project

List of Symbols

$r(t)$	Continuous-time received signal
$r(n)$	Discrete-time received signal
f_s	Sampling rate
$r_{\mathrm{P}}(n)$	Discrete-time received mobile WiMAX signal component corresponding to the preamble
$r_{\mathrm{DL}}(n)$	Discrete-time received mobile WiMAX signal component corresponding to the DL
$r_{\mathrm{UL}}(n)$	Discrete-time received mobile WiMAX signal component corresponding to the UL
$w(n)$	Discrete-time additive zero-mean Gaussian noise
K_{P}	The number of used subcarriers in the preamble symbol
K_{DL}	The number of used subcarriers in the DL symbols
K_{UL}	The number of used subcarriers in the UL symbols
a_{P}	Amplitude factor equals to $1/\sqrt{K_{\mathrm{P}}}$
a_{DL}	Amplitude factor equals to $1/\sqrt{K_{\mathrm{DL}}}$
a_{UL}	Amplitude factor equals to $1/\sqrt{K_{\mathrm{UL}}}$
u_q	The qth preamble data symbol
Δf	The subcarriers frequency separation
$g(n)$	The impulse response of the transmit and the receive filters in cascade
N_{F}	The number of OFDM symbols in the mobile WiMAX frame
N_{DL}	The number of OFDM symbols in the mobile WiMAX DL subframe (excluding the preamble)
N_{UL}	The number of OFDM symbols in the mobile WiMAX UL subframe
T_{u}	The useful OFDM symbol time duration
T_{cp}	The CP time duration
T	The OFDM symbol time duration
T_{TG}	The TTG time duration
T_{RG}	The RTG time duration
D_{u}	The useful OFDM symbol duration (in number of samples)
D_{cp}	The CP duration (in number of samples)
D	The OFDM symbol duration (in number of samples)
D_{TG}	The TTG duration (in number of samples)

D_{RG}	The RTG duration (in number of samples)
D_{G}	Total duration of the transition gaps within each mobile WiMAX frame (in number of samples)
$K_{\mathrm{DL},\lambda,d}$	The number of data subcarriers in the λth DL OFDM symbol in the frame
$K_{\mathrm{DL},\lambda,p}$	The number of pilot subcarriers in the λth DL OFDM symbol in the frame
$\sigma^2_{\mathrm{DL},\lambda,d}$	The variance of the data symbol transmitted on the λth DL OFDM symbol in the frame
$\sigma^2_{\mathrm{DL},\lambda,p}$	The variance of the pilot symbol transmitted on the λth DL OFDM symbol in the frame
$K_{\mathrm{UL},\lambda,d}$	The number of data subcarriers in the λth UL OFDM symbol in the frame
$K_{\mathrm{UL},\lambda,p}$	The number of pilot subcarriers in the λth UL OFDM symbol in the frame
$\sigma^2_{\mathrm{UL},\lambda,d}$	The variance of the data symbol transmitted on the UL OFDM symbol in the frame
$\sigma^2_{\mathrm{UL},\lambda,p}$	The variance of the pilot symbol transmitted on the UL OFDM symbol in the frame
$K_{\mathrm{P},d}$	The number of subcarriers in the preamble used to transmit preamble date
$K_{\mathrm{DL},p}$	The number of pilot subcarriers in a DL OFDM symbol
$s_{\mathrm{P}}(n)$	A preamble symbol
$s_{\mathrm{DL}}(n)$	A DL OFDM symbol
$R_r(n,\tau)$	The autocorrelation function of $r(n)$ at time n and delay τ
$R_r(\alpha,\tau)$	The CAF of $r(n)$ at CF α and delay τ
$\lvert R_r(n,\tau)\rvert$	The magnitude of the $R_r(n,\tau)$
$\lvert R_r(\alpha,\tau)\rvert$	The magnitude of the $R_r(\alpha,\tau)$
$\hat{R}_r(n,\tau)$	The estimation of $R_r(n,\tau)$
$\hat{R}_r(\alpha,\tau)$	The estimation of $R_r(\alpha,\tau)$
$\lvert\hat{R}_r(n,\tau)\rvert$	The magnitude of $\hat{R}_r(n,\tau)$
$\lvert\hat{R}_r(\alpha,\tau)\rvert$	The magnitude of $\hat{R}_r(\alpha,\tau)$
$R_{s_{\mathrm{P}}}(n,\tau_i)$	The autocorrelation function of $s_{\mathrm{P}}(n)$ at time n and delay τ_i
$R_{s^{(2)}_{\mathrm{DL}}}(n,\tau_i)$	The autocorrelation function of $s^{(2)}_{\mathrm{DL}}(n)$ at time n and delay τ_i
$\mathcal{K}$	The set of CFs
K	Total number of subcarriers in LTE OFDM symbol
a	Amplitude factor equal to $1/\sqrt{K}$
$N^{\mathrm{DL}}_{\mathrm{RB}}$	The number of resource blocks in an OFDM symbol

N_{sc}^{RB}	The number of subcarriers in a resource block
N_{symb}^{DL}	The number of OFDM symbols in an LTE slot
N_z	The repetition period for the RS distribution (in number of OFDM symbols)
$\mathcal{Z}_1$	A set of the OFDM symbols in which the RS is transmitted
$\mathcal{Z}_2$	A set of the OFDM symbols in which the RS is transmitted
D_1	The duration of the first OFDM in the slot of the LTE signal with short CP
D_z	The repetition period for the RS distribution (in number of samples)
K_d	The number of data subcarriers in an LTE OFDM symbol
K_r	The number of RS subcarriers in an LTE OFDM symbol
A_1	the set of subcarriers on which the RS is transmitted in the OFDM symbols belonging to $\mathcal{Z}_1$
A_2	the set of subcarriers on which the RS is transmitted in the OFDM symbols belonging to $\mathcal{Z}_2$
K_1	The number of subcarriers in A_1
K_2	The number of subcarriers in A_2
$\Im\{.\}$	Fourier transform
H_0	The hypothesis used in the cyclostationarity test under which, the tested frequency is not a CF
H_1	The hypothesis used in the cyclostationarity test under which, the tested frequency is a CF
L	Number of samples available at the receive-side
$\hat{\Sigma}$	Covariance matrix used in the cyclostationarity test
Q_0	Components of the covariance matrix used in the cyclostationarity test
Q_1	Components of the covariance matrix used in the cyclostationarity test
$\hat{Q}_0$	Estimation of Q_0
$\hat{Q}_1$	Estimation of Q_1
$f(i;\tau)$	lag product in the cyclostationarity test
Ψ_r^{α}	The test statistic used in the cyclostationarity test for a CF α
$W^{(L_{sw})}$	Spectral window
L_{sw}	Length of the spectral window
Ψ_r	The test statistic used in the cyclostationarity test for multiple CFs
N_α	The set of tested frequencies
Γ	Threshold value used in the cyclostationarity test
$P_{dc}(i \mid i)$	Probability of correct joint detection and classification
$E(.)$	The expectation operator

cum(.)	The cumulant operator
Re{.}	The real part
Im{.}	The imaginary part
$\otimes$	Convolution operator
$\lceil . \rceil$	The ceiling function
$\lfloor . \rfloor$	The floor function

Chapter 1

Introduction

1.1. Cognitive Radio

The radio spectrum is a valuable and scarce resource, and the need for spectrum access for mobile services is steadily increasing [1]. Fixed spectrum assignment policies are usually used for regulating the spectrum, which means that users are granted licenses by governmental agencies to operate in certain spectrum bands and geographical areas. As more and more networks need to access the limited spectrum, the available spectrum becomes insufficient for the increasing number of users and services. On the other hand, the spectrum usage measurements obtained by the Federal Communication Commission (FCC) spectrum policy task force indicate that although the radio spectrum is highly utilized in some areas, most of the licensed spectrum lies idle. According to the FCC, the utilization of the spectrum ranges from 15% to 85% [1]. The above facts make it necessary to start looking for new approaches for spectrum management, outside of the fixed spectrum assignment policies.

There are many open research areas on the dynamic spectrum access (DSA) to increase the spectrum utilization. Cognitive radio (CR) represents one of the promising solutions for the spectrum scarcity problem. There are many potential and military applications for

CR. Using CR, the spectrum utilization will be significantly improved by opening the licensed bands to be used by other users, without interfering with the licensed users. One of the potential applications of CRs is in military radio environment, where military radios can operate in different bands. The CR technology opens the licensed spectrum to be used by unlicensed (secondary or cognitive) users by giving these users the ability to determine which bands of the spectrum are not currently used by the primary users (spectrum holes), and the opportunity to exploit these bands on the fly.

Fig. 1.1 shows a typical architecture for a CR network. As one can easily notice, there are two types of networks, the primary network and the secondary network. The primary networks are infrastructured and have the license to operate in some spectrum bands. An example of the primary network is the conventional cellular network, where the users have the right to use the spectrum at any time and their access is controlled by primary base-stations that are components of the infrastructured network. The secondary or cognitive networks, which can be either infrastructured or infrastructureless, are unlicensed networks. Hence, their access to the spectrum is performed opportunistically, which means that they can employ the spectrum when this is not used by the primary networks. It is very important that the operation of the primary users should not be affected by that of the secondary users. As such, the secondary users should access the spectrum opportunistically and be able to detect the spectrum holes and perform their transmission adaptively, according to the available frequency bands. Regulations require that secondary users must constantly monitor the spectrum to see if the primary users resumed access, and if so, withdraw themselves within a short period of time.

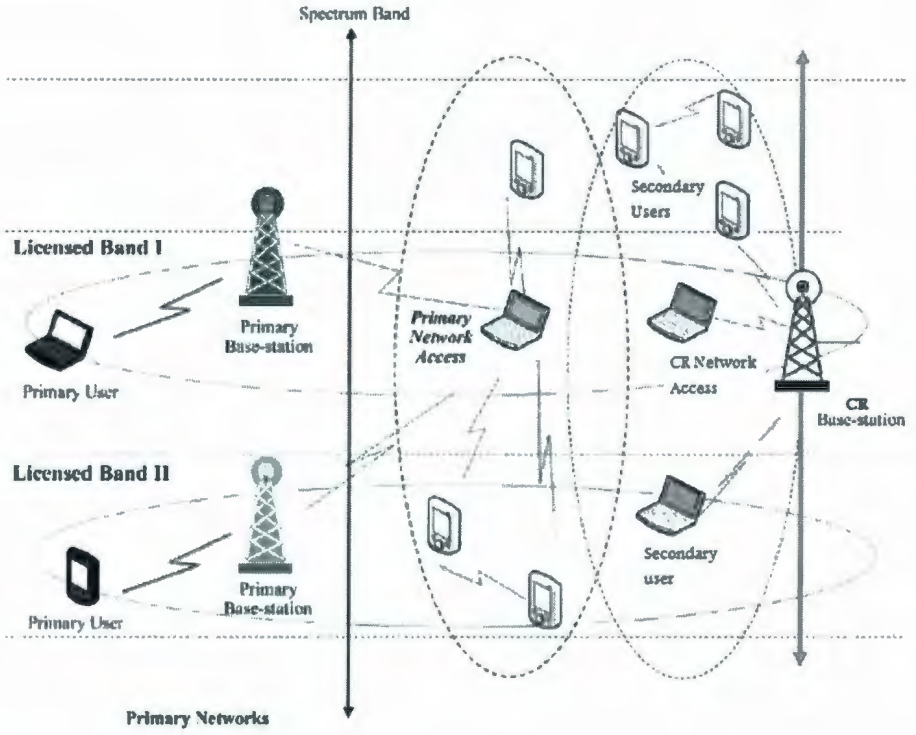

Fig. 1.1. A sample CR network (taken from [2]).

For the start, TV bands have been considered by the FCC for CR usage. The IEEE established the IEEE 802.22 Wireless Regional Area Networks (WRAN) international standard for utilizing the idle bands in TV frequency spectrum [2]. With the 802.22, restrictions are imposed on the 80.22 users to avoid interference with the licensed users. This involves the transmission power of these users. Therefore, effective power control mechanisms are employed in WRAN networks. Frequency agility is another important requirement for the coexistence mechanisms of the 802.22. The 802.22 users should be able to adjust their frequency of operation within short periods of time and as often as necessary.

There are two main approaches for implementing DSA in CR networks, the overlay and underlay approaches. In the overlay approach, secondary users access the spectrum when

this is not used by the primary users [1]-[3]. These have to reliably detect the presence of primary users in the channel at low SNRs. In the underlay approach [4]-[5], the secondary users are allowed to transmit at the same time and spectrum bands with the primary users. A restriction is imposed on the transmission power of the secondary users, such that this will not raise the noise floor for the primary users beyond a specific value. In this work, we focus on the overlay approach, where secondary users access the spectrum when this is not used by the primary users. As such, the most efficient way to detect spectrum holes is to detect the primary users' signals by sensing the channel.

There are three major digital signal processing approaches for the detection of the primary users, i.e., the energy detector, the matched filter detector, and the cyclostationary feature detector [1]-[3]. The energy detector is the simplest approach for detecting signals which are in the air. The advantage is that this is simple to implement and requires minimum information (carrier frequency and signal bandwidth) about the received signals to be detected. The energy of the received signal is measured and compared against a threshold to detect the existence of primary users' signals. The disadvantage of the energy detector is that the threshold value depends on the noise level. Therefore, performance of this detector will degrade under noise uncertainty, and detection of weak signals will not be reliably performed. The matched filter detector is the best detection approach when the properties of the primary user's signal, such as the modulation type or pulse shaping, are known to the secondary users. As coherent detection is used in this approach, it performs much better than the energy detector in low SNR regimes and requires less observation time. However, this approach requires information about the primary users' signal at the secondary users. Most man-made signals exhibit cyclostationarity, i.e., their time-varying

statistics are periodic functions of time. Modulated signals are cyclostationary, with a periodicity related to the symbol period, carrier frequency, or chip rate [1]-[3]. On the other hand, the additive Gaussian noise does not exhibit cyclostationarity. This can be employed as a distinctive characteristic to detect the presence of the modulated signals in noise. The cyclostationarity-based methods have the advantage over the matched filter approach of not relying on prior information on the received signal, and has the advantage over the energy detector of being less sensitive to noise uncertainty. In this work, we focus on the cyclostationarity-based approach for signal detection and classification.

1.2. OFDM Signal Classification

Orthogonal frequency division multiplexing (OFDM) represents one of the main candidates for high data rate transmission for current and next generation wireless applications, being adopted by several wireless standards. Recently, OFDM signal detection and classification has been intensively researched in the context of CR [5]-[15]. Most of the proposed methods for detection and classification of OFDM signals are cyclostationarity-based [6]-[15], with some of them employing the detection of the cyclic prefix (CP)-induced peaks in the cyclic autocorrelation function (CAF) [6]-[11]. In [6]-[7], many cyclostationarity-based algorithms are proposed for the classification of OFDM signals versus single carrier signals utilizing the CP-induced cyclostationarity. In these methods, the CAF of the received signal is estimated over a wide range of delays. Then, the CAF is searched over this delay range to find the CP-induced peaks and exploit these peaks for signal detection and classification. In [8]-[9], the CP-induced cyclostationarity is

also exploited for detection and classification of different OFDM signals. The CAF of the received signal is estimated for zero cyclic frequency, and searched over the delay for symmetric peaks that are due to the CP. The location of these peaks can be used for the classification of different OFDM signals with different transmission parameters. The drawback of these algorithms is that they require searching the CAF over a large delay range to find the peaks which introduces a high computational complexity. The CP-induced cyclostationarity in the CAF is used in [10]-[11] for OFDM signal detection and classification. These methods assume that the locations of the peaks in the CAF are known *a priori* which eliminates the need for searching the CAF over some delays. However, the location of the peaks in the CAF could be different for the same signal, as different transmission parameters could be used with different transmission modes and different transmission rates.

Some of the existing methods involve the detection of cyclostationary signatures that are artificially created and intentionally embedded in the OFDM signals [12]-[13] for detection and classification purposes. In these methods, message symbols are redundantly transmitted on more than one subcarrier such that a correlation pattern is created and a cyclostationary feature is embedded in the signal. Subcarrier set mapping permits cyclostationary signatures to be embedded in data-carrying waveforms without adding significant complexity to existing transmitter designs. Using this approach, signals may be uniquely classified by the cyclic frequency of the signature embedded. The problem in this case is that the embedding of these signatures comes at the price of additional overhead and reduction in the data rate. The reduction of the data rate is caused by wasting some

subcarriers for signature embedding while these can otherwise be used for data transmission.

Other methods rely on the existence of pilot symbols for channel estimation or synchronization [14]. It is assumed that these symbols are replicated according to a predefined time/frequency distribution, which induces a non-zero correlation. However, in many cases of practical interest, such as the mobile Worldwide Interoperability for Microwave Access (WiMAX), the pilot symbols are randomly generated, which yields zero correlation [16]-[19].

1.3. Thesis Objective

The drawbacks of the previous methods (that are discussed in Section 1.2) make it necessary to further study the cyclostationarity-based features of the existing OFDM standard signals and exploit the existing cyclostationarity of these signals for the purpose of their joint detection and classification. In this thesis, the mobile WiMAX and third Generation Partnership Project Long Term Evolution (3GPP LTE) are considered, as these are two popular wireless communication standards that employ the OFDM in their transmission. The objective of this work is to develop cyclostationarity-based algorithms for the joint detection and classification of the OFDM-based mobile WiMAX and LTE signals. The mobile WiMAX employs the OFDM in both its uplink (UL) and downlink (DL) transmission and all the current mobility certification profiles of the mobile WiMAX adopt the time division duplexing (TDD) in their transmission. Henceforth, we focus on the mobile WiMAX signals with the TDD transmission and we refer to them as the mobile

WiMAX OFDM-based signals. The LTE employs the OFDM in its DL transmission. Henceforth, we focus on the LTE signals with the frequency division duplexing (FDD) DL transmission and we refer to them as the OFDM-based LTE signals. The algorithms to be developed should not reduce the transmission rate (by exploiting the existing features instead of introducing new overheads) and not be computationally complex (by not requiring complex feature recognition procedures). As such, the second-order cyclostationarity of both signals is studied, and closed-from expressions for the CAF and cyclic frequencies (CFs) of both signals are derived. Furthermore, two cyclostationarity-based algorithms for joint detection and classification of these signals are developed, and the joint detection and classification performance, as well as computational complexity of these algorithms are evaluated.

1.4. Thesis Organization

The rest of the thesis is organized as follows. The mobile WiMAX OFDM-based signals are investigated in Chapter 2 and signal model is provided for these signals. Furthermore, the second-order cyclostationarity of these signals is studied and closed form expressions for the CAF and CFs of these signals are derived. The OFDM-based LTE signals are investigated in Chapter 3 and models for these signals are provided. The second-order cyclostationarity of these signals is studied and closed from expressions for their CAF and CFs are derived. Two feature-based algorithms for joint detection and classification of the OFDM-based mobile WiMAX and LTE signals are proposed in Chapter 4. In Chapter 5, the joint detection and classification performance of the proposed algorithms are evaluated through computer

simulations and their computational complexity is investigated. Conclusions and suggestions for future work are presented in Chapter 6.

1.5. Major Contributions of the Thesis

The new results presented in each chapter are:

- Chapter 2: Signal model for the mobile WiMAX OFDM-based signals and closed-from analytical expressions for their CAF and CFs [A. Al-Habashna et al., *GLOBECOM* 2010].
- Chapter 3: Signal model for the OFDM-based LTE signals and closed-from analytical expressions for their CAF and CFs [A. Al-Habashna et al., *GLOBECOM* 2010].
- Chapter 4: Two proposed algorithms for joint detection and classification of the OFDM-based mobile WiMAX and LTE signals [A. Al-Habashna et al., *ASILOMAR* 2010].
- Chapter 5: Evaluation of the joint detection and classification performance of the proposed algorithms through computer simulations, and study of their computational complexity [A. Al-Habashna et al., *ASILOMAR* 2010].

Here, we present a list of publications out of this work:

- Ala'a Al-Habashna, Octavia A. Dobre, Ramachandran Venkatesan, and Dimitrie C. Popescu "Joint Cyclostationarity-based Detection and Classification of Mobile WiMAX and LTE OFDM Signals," submitted to *IEEE ICC*, 2010.

- Ala'a Al-Habashna, Octavia A. Dobre, Ramachandran Venkatesan, Dimitrie C. Popescu, "WiMAX signal detection algorithm based on preamble-induced second-order cyclostationarity," accepted to *IEEE GLOBECOM*, 2010.
- Ala'a Al-Habashna, Octavia A. Dobre, Ramachandran Venkatesan, Dimitrie C. Popescu, "Cyclostationarity-based detection of LTE OFDM signals for cognitive radio systems," accepted to *IEEE GLOBECOM*, 2010.
- A. Al-Habashna, O. A. Dobre, R. Venkatesan, D. C. Popescu, "Joint signal detection and classification of mobile WiMAX and LTE OFDM signals for cognitive radio," accepted to *IEEE ASILOMAR*, 2010.
- Ala'a S. Al-Habashna, Octavia A. Dobre, Ramachandran Venkatesan, "Cognitive radio: a new paradigm in wireless communications," in *Proc. IEEE NECEC*, 2008.

Chapter 2

Second-Order Cyclostationarity of the Mobile WiMAX OFDM-based Signals

2.1. Introduction

The mobile WiMAX technology, based on the IEEE 802.16e [17]-[18] air Interface Standard, is rapidly proving itself as a technology that will play a major role in broadband wireless metropolitan area networks. Mobile WiMAX employs the scalable OFDM at the physical layer, which allows bandwidth scalability. In this chapter, a description of the structure of the Mobile WiMAX OFDM-based signals is presented. Then, a model is provided for such signals. Furthermore, their second-order cyclostationarity is studied and closed form expressions for the CAF and corresponding set of CFs of these signals are derived. Finally, the CAF results obtained from both analytical findings and computer simulations are presented.

2.2. Mobile WiMAX OFDM-based Signal Model

2.2.1. Signal Description

Fig. 2.1 presents the IEEE 802.16e TDD frame structure, as per the current mobility certification profiles [16]. The standard frame duration can range from 2 ms to 20 ms; however, all WiMAX equipments support only a 5 ms frame [16], [19]. The frame is divided into two subframes, one for the DL and another one for the UL. The DL-to-UL subframe ratio is variable, to support different traffic profiles.

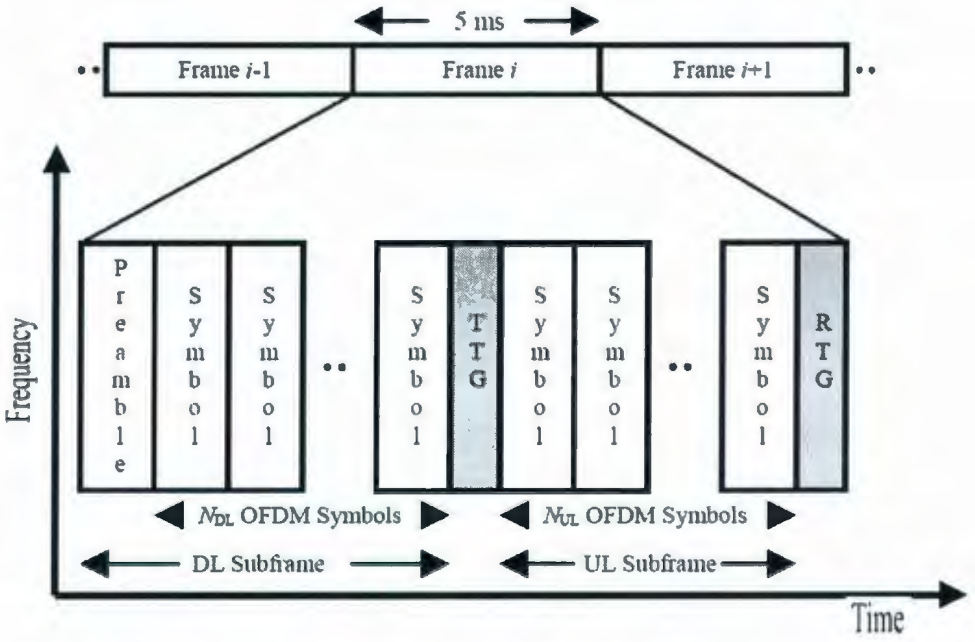

Fig. 2.1. TDD frame structure for mobile WiMAX.

Transition gaps separate the adjacent DL and UL subframes. In Fig. 2.1, TTG represents the DL-UL gap and is referred to as the transmit/receive transition gap, while RTG represents the UL-DL gap and is referred to as the receive/transmit transition gap. Note that the terminology

used here is according to the IEEE 802.16e standard [17]-[18]. The DL subframe starts with a preamble as the first symbol, which is used for time and frequency synchronization and uniquely identifies a serving base-station. Therefore, a cognitive user within the coverage area of a base-station will periodically receive the same preamble.

The OFDM frequency domain description is presented in Fig. 2.2. One can note three types of subcarriers: the data subcarriers to transmit information, the pilot subcarriers for estimation purposes, and the null subcarriers for guard bands and DC subcarrier [18]. The first two types of subcarriers are called the used subcarriers. The pilot symbol on subcarrier k is generated as $8(0.5-w_k)/3$, where w_k is a value taken from a pseudorandom binary sequence that is different for each OFDM symbol. The distribution of the pilot subcarriers might differ from one OFDM symbol to another in the frame, while this repeats every frame, i.e., it is the same for each λth OFDM symbol of the frame. Note that $\lambda = 0$ for the preamble symbol, $1 \le \lambda \le N_{DL}$ for the DL OFDM symbols (excluding the preamble), and $N_{DL}+1 \le \lambda \le N_F - 1$ for the UL OFDM symbols, with N_{DL} and N_F as the number of OFDM symbols in the DL (excluding the preamble) and in the frame, respectively. Note that more than one pilot distribution might be used in the DL or UL subframes; each pilot distribution is used in a certain set of OFDM symbols in the DL or UL subframes. The pilot symbols are usually transmitted with boosted power over that of the data symbols.

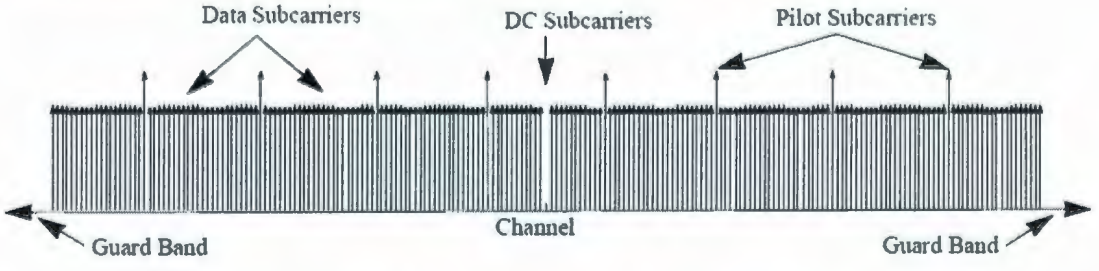

Fig. 2.2. OFDM frequency description (taken from [18]).

The preamble contains only null subcarriers and subcarriers used for transmitting preamble data. According to the standard, the preamble data symbols are transmitted every third subcarrier out of the set of subcarriers, $-K_P/2$, $-K_P/2+1$, ... , $K_P/2$, starting from the subcarrier $-K_P/2 + S_{P,d}$ up to $-K_P/2 + S_{P,d} + 3(K_{P,d} - 1)$, where $S_{P,d}$ = 0, 1, 2 and $K_{P,d}$ is the number of the preamble data symbols. Fig. 2.3 shows the frequency domain description of the preamble when $S_{P,d} = 0$.

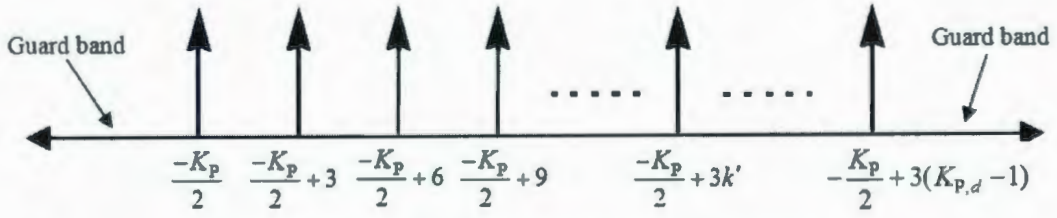

Fig. 2.3. OFDM frequency description of the preamble symbol ($S_{P,d}$=0).

2.2.2. Signal Model

According to the above description, the discrete-time received mobile WiMAX OFDM-based signal can be expressed as

$$r(n) = r_P(n) + r_{DL}(n) + r_{UL}(n) + w(n), \qquad (2.1.a)$$

where $r_P(n)$, $r_{DL}(n)$, and $r_{UL}(n)$ are the signal components corresponding to the preamble, and the DL (excluding the preamble) and UL subframes, respectively, and $w(n)$ is the additive zero-mean Gaussian noise. Furthermore, $r_P(n)$, $r_{DL}(n)$, and $r_{UL}(n)$ are given respectively as,

$$r_{\mathrm{P}}(n)=a_{\mathrm{P}}\sum_{\substack{l=-\infty\\ l \bmod N_{\mathrm{F}}=0}}^{\infty}\sum_{k=-K_{\mathrm{P}}/2}^{K_{\mathrm{P}}/2} b_k g(n-lD-lN_{\mathrm{F}}^{-1}D_{\mathrm{G}})\times e^{j2\pi k(n-lD-lN_{\mathrm{F}}^{-1}D_{\mathrm{G}})/D_{\mathrm{u}}}, \tag{2.1.b}$$

with

$$b_k=\begin{cases} u_q,\ k=3q-\dfrac{K_{\mathrm{P}}}{2}+S_{\mathrm{P},d},\ q=0,\ 1,\ldots,\ K_{\mathrm{P},d}-1,\\ 0,\ \text{otherwise,}\end{cases}$$

which yields

$$r_{\mathrm{P}}(n)=a_{\mathrm{P}}\sum_{\substack{l=-\infty\\ l \bmod N_{\mathrm{F}}=0}}^{\infty}\sum_{k=0}^{K_{\mathrm{P},d}-1} u_k g(n-lD-lN_{\mathrm{F}}^{-1}D_{\mathrm{G}})\times e^{j2\pi(3k-\frac{K_{\mathrm{P}}}{2}+S_{\mathrm{P},d})(n-lD-lN_{\mathrm{F}}^{-1}D_{\mathrm{G}})/D_{\mathrm{u}}}, \tag{2.1.c}$$

$$r_{\mathrm{DL}}(n)=a_{\mathrm{DL}}\sum_{\substack{l=-\infty\\ 1\le l \bmod N_{\mathrm{F}}=\lambda\le N_{\mathrm{DL}}}}^{\infty}\sum_{k=-K_{\mathrm{DL}}/2,k\neq 0}^{K_{\mathrm{DL}}/2} c_{k,l}\, g(n-lD-\left\lfloor lN_{\mathrm{F}}^{-1}\right\rfloor D_{\mathrm{G}})\times e^{j2\pi k(n-lD-\left\lfloor lN_{\mathrm{F}}^{-1}\right\rfloor D_{\mathrm{G}})/D_{\mathrm{u}}}, \tag{2.1.d}$$

and

$$r_{\mathrm{UL}}(n)=a_{\mathrm{UL}}\sum_{\substack{l=-\infty\\ N_{\mathrm{DL}}+1\le l \bmod N_{\mathrm{F}}=\lambda}}^{\infty}\sum_{k=-K_{\mathrm{UL}}/2,k\neq 0}^{K_{\mathrm{UL}}/2} d_{k,l}\, g(n-lD-\left\lfloor lN_{\mathrm{F}}^{-1}\right\rfloor D_{\mathrm{G}}-D_{\mathrm{TG}})$$
$$\times e^{j2\pi k(n-lD-\left\lfloor lN_{\mathrm{F}}^{-1}\right\rfloor D_{\mathrm{G}}-D_{\mathrm{TG}})/D_{\mathrm{u}}}, \tag{2.1.e}$$

where K_{P}, K_{DL}, and K_{UL} are the number of used subcarriers in the preamble, DL, and UL symbols, respectively, a_{P}, a_{DL}, and a_{UL} are the amplitude factors equal to $1/\sqrt{K_{\mathrm{P}}}$, $1/\sqrt{K_{\mathrm{DL}}}$, and $1/\sqrt{K_{\mathrm{UL}}}$, respectively, D is the OFDM symbol period[1] equal to the useful OFDM symbol duration, D_{u}, plus the CP duration, D_{cp}, b_k is the symbol transmitted in the kth subcarrier of the preamble, u_q is the qth preamble data symbol,

[1] Note that all durations are expressed as number of samples. For durations expressed in time periods, we use the symbol T instead of D, e.g., T, T_{u}, and T_{cp}, instead of D, D_{u}, and D_{cp}, respectively.

$q = 0, 1, \ldots, K_{P,d} - 1$, and $-K_P/2 + S_{P,d}$ provides the position of the first subcarrier used to transmit preamble data, with $S_{P,d} = 0, 1, 2,$ $c_{k,l}$ and $d_{k,l}$ are the symbols (data and pilot) transmitted on the kth subcarrier and within the lth[2] OFDM symbol which belongs to the DL and UL subframes, respectively (note that the distribution of pilot subcarriers could be different for different groups of OFDM symbols), N_F is the number of OFDM symbols in the frame, N_{DL} and N_{UL} are the number of OFDM symbols in the DL (excluding the preamble) and UL subframes, respectively, $g(n)$ is the impulse response of the transmit and the receive filters in cascade, $D_G = D_{TG} + D_{RG}$ is the total duration of the transition gaps within each frame, with D_{TG} and D_{RG} as the TTG and RTG transition gaps, respectively, and $\lfloor . \rfloor$ denotes the floor function. Note that the data symbols are taken either from a quadrature amplitude modulation (QAM) or phase shift keying (PSK) signal constellation, and are assumed to be zero-mean independent and identically distributed (i.i.d.) random variables. Note that the subcarrier frequency spacing, Δf, normalized by the sampling rate, f_s, is equal to the reciprocal of the useful OFDM symbol duration, D_u. Also note that the fast Fourier transform (FFT) size for generating OFDM symbols is equal to the total number of subcarriers (used subcarriers and guard band subcarriers), and also equals D_u; since guard bands are used with all OFDM symbols (preamble, DL, and UL OFDM symbols), the FFT size is always greater than the number of used subcarriers.

To ease the understanding of the expressions for the signal model, here we provide an explanation for $r_P(n)$, $r_{DL}(n)$, and $r_{UL}(n)$ given in (2.1.b)-(2.1.e). The inner summation on

---

[2] Note that the OFDM symbol index, l, can be further expressed in terms of the frame index, $\lfloor lN_F^{-1} \rfloor$, and OFDM symbol index within a frame, λ, with $\lambda = l \bmod N_F$. As such, $l = \lfloor lN_F^{-1} \rfloor N_F + \lambda$. Furthermore, $\lambda = 0$ for the preamble symbol, $1 \le \lambda \le N_{DL}$ for the DL OFDM symbols (excluding the preamble), and $N_{DL} + 1 \le \lambda \le N_F - 1$ for the UL OFDM symbols.

the right hand side of these equations is over the number of subcarriers[3], while the outer summation is over the OFDM symbol index. Specific to (2.1.b) is the position of the preamble, which appears at the beginning of each frame. As such, the preamble index, l, is an integer multiple of the number of OFDM symbols in a frame ($\lambda = l \bmod N_F = 0$). Furthermore, for the position of the preamble, we need to take into account the total duration of the transition gaps within all previous frames, which yields the shift of $g(n)$ and $e^{j2\pi k/D_u}$ by $lN_F^{-1}D_G$, with $\lfloor lN_F^{-1} \rfloor = lN_F^{-1}$ providing the frame index (e.g., $\lfloor lN_F^{-1} \rfloor = lN_F^{-1} = 0$ and 1 for the first and second frame, respectively). It is noteworthy that the symbol on each subcarrier, k, is the same for all preambles; as such, b_k does not depend on the preamble index, l. As explained above, the preamble data symbols are transmitted every third subcarrier starting from $-K_P/2+S_{P,d}$. Thus, $r_P(n)$ can be expressed by emphasizing the subcarriers used to transmit preamble data symbols, as in (2.1.c). In (2.1.d) we consider only the OFDM symbols that belong to the DL subframe by having $\lambda = l \bmod N_F$ less than or equal to the number of OFDM symbols in the DL (excluding the preamble), i.e., $1 \le \lambda \le N_{DL}$. Also, the total duration of the transition gaps in previous frames is taken into account by shifting $g(n)$ and $e^{j2\pi k/D_u}$ by $\lfloor lN_F^{-1} \rfloor D_G$, with $\lfloor lN_F^{-1} \rfloor$ accounting for the frame index. For example, for $l = N_F + \lambda$, $\lambda = 1, 2, \ldots, N_{DL}$, we get the λth OFDM symbol (after the preamble) in the second frame ($\lfloor lN_F^{-1} \rfloor = 1$ is the index of the frame; as previously mentioned, the first frame has index zero). Consequently, $g(n)$ and $e^{j2\pi k/D_u}$ will be shifted by D_G, which yields the

[3] Note that the DC subcarrier is not used as shown in Fig. 2.2. As such, we have $c_{k,l}$ and $d_{k,l}$ equal zero at $k = 0$ in (2.1.d) and (2.1.e).

transition gap in the first frame. Another example is $l = 2N_F + \lambda$, which corresponds to the λth OFDM symbol (after the preamble) in the third frame. In this case, $\left\lfloor lN_F^{-1} \right\rfloor = 2$ gives the index of this frame and $g(n)$ and $e^{j2\pi k/D_u}$ are shifted by $2D_G$, which represents the transition gap in the previous two frames. In (2.1.e), only the OFDM symbols in the uplink subframe are considered. The condition that $\lambda = l \bmod N_F$ is greater than N_{DL} (i.e., $N_{DL} + 1 \le \lambda \le N_F - 1$) ensures that. Again, the total duration of the transition gaps is taken into account by shifting $g(n)$ and $e^{j2\pi k/D_u}$ by $\left\lfloor lN_F^{-1} \right\rfloor D_G + D_{TG}$. The shift by $\left\lfloor lN_F^{-1} \right\rfloor D_G$ corresponds to the total duration of transition gaps in the previous frames and can be explained in the same way as for the DL OFDM symbols. On the other hand, the shift by D_{TG} corresponds to the TTG transition gap in the current frame, as the symbols that belong to the UL subframe come after this TTG transition (see Fig. 2.1).

2.3. Second-Order Cyclostationarity of the Mobile WiMAX OFDM-based Signals

2.3.1. Second-Order Signal Cyclostationarity: Definitions

A random process $r(t)$, is said to be second-order cyclostationary if its mean and autocorrelation are almost periodic functions of time [20]. The latter is expressed as a Fourier series as [20]

$$\tilde{R}_r(t, t+\tilde{\tau}) = \sum_{\tilde{\alpha} \in \tilde{\mathcal{K}}} \tilde{R}_r(\tilde{\alpha}, \tilde{\tau}) e^{j2\pi\tilde{\alpha}t}, \tag{2.2}$$

where $\tilde{R}_r(\tilde{\alpha},\tilde{\tau})$ is the CAF at CF $\tilde{\alpha}$ and delay $\tilde{\tau}$, defined as

$$\tilde{R}_r(\tilde{\alpha},\tilde{\tau}) = \lim_{I\to\infty} I^{-1} \int_{-I/2}^{I/2} \tilde{R}_r(t,t+\tilde{\tau}) e^{-j2\pi\tilde{\alpha}t} dt, \tag{2.3}$$

and $\tilde{\mathcal{K}} = \{\tilde{\alpha} : \tilde{R}_r(\tilde{\alpha},\tilde{\tau}) \neq 0\}$ represents the set of CFs.

Furthermore, for the discrete-time signal, $r(n)$, the CAF at CF α and delay τ is given by (under the assumption of no aliasing) [20],

$$R_r(\alpha,\tau) = \tilde{R}_r(\tilde{\alpha},\tilde{\tau}), \tag{2.4}$$

where $\alpha = \tilde{\alpha} f_s^{-1}$ and $\tau = \tilde{\tau} f_s$.

The CAF can be estimated from a finite length sampled signal $\{r(n)\}_{n=0}^{N-1}$, as [20],

$$\hat{R}_r(\alpha,\tau) = \frac{1}{N} \sum_{n=0}^{N-\tau-1} r(n) r^*(n+\tau) e^{j2\pi\alpha n}. \tag{2.5}$$

2.3.2. CAF and CFs of Mobile WiMAX Signals: Analytical Results

Using the signal model in (2.1.c)-(2.1.e), the autocorrelation function of $r(n)$ can be expressed as the sum of autocorrelation functions corresponding to the signal components, signal and noise, and only noise,

$$R_r(n,\tau) = a_{\mathrm{P}}^2 \sum_{\substack{l_1=-\infty \\ l_1 \bmod N_{\mathrm{F}}=0}}^{\infty} \sum_{k_1=0}^{K_{\mathrm{P},d}-1} \sum_{\substack{l_2=-\infty \\ l_2 \bmod N_{\mathrm{F}}=0}}^{\infty} \sum_{k_2=0}^{K_{\mathrm{P},d}-1} E(u_{k_1} u_{k_2}^*)$$

$$\times g(n-l_1 D - l_1 N_{\mathrm{F}}^{-1} D_{\mathrm{G}}) e^{j2\pi(3k_1 - \frac{K_{\mathrm{P}}}{2} + S_{\mathrm{P},d})(n-l_1 D - l_1 N_{\mathrm{F}}^{-1} D_{\mathrm{G}})/D_{\mathrm{u}}}$$

$$\times g^*(n-l_2D-l_2N_F^{-1}D_G+\tau)e^{-j2\pi(3k_2-\frac{K_P}{2}+S_{P,d})(n-l_2D-l_2N_F^{-1}D_G+\tau)/D_u}$$

$$+ \ldots.$$

$$+ \sum_{\substack{l_1=-\infty \\ N_{DL}+1\le l_1 \bmod N_F=\lambda_1}}^{\infty} \sum_{k_1=-K_{UL}/2,k_1\neq 0}^{K_{UL}/2} \sum_{\substack{l_2=-\infty \\ N_{DL}+1\le l_2 \bmod N_F=\lambda_2}}^{\infty} \sum_{k_2=-K_{UL}/2,k_2\neq 0}^{K_{UL}/2} E(d_{k_1,l_1}d^*_{k_2,l_2})$$

$$\times g(n-l_1D-\left\lfloor l_1N_F^{-1}\right\rfloor D_G-D_{TG})\, e^{j2\pi k_1(n-l_1D-\left\lfloor l_1N_F^{-1}\right\rfloor D_G-D_{TG})/D_u}$$

$$\times g^*(n-l_2D-\left\lfloor l_2N_F^{-1}\right\rfloor D_G-D_{TG}+\tau)e^{-j2\pi k_2(n-l_2D-\left\lfloor l_2N_F^{-1}\right\rfloor D_G-D_{TG}+\tau)/D_u}$$

$$+\ldots+E(w(n)w^*(n+\tau)), \qquad (2.6)$$

where $E(.)$ is the expectation operator. To ease the understanding of (2.6), here we provide an explanation. The first term on the right hand side represents the autocorrelation of $r_P(n)$, i.e., the correlation of preamble component with it self. The second shown term represents the autocorrelation of $r_{UL}(n)$, and the last shown term represents the autocorrelation of $w(n)$. the remaining components involve the autocorrelation of $r_{DL}(n)$ and the correlation of components with each others, e.g., correlation of $r_P(n)$ and $r_{DL}(n)$.

We expect that non-zero significant values of $R_r(n,\tau)$ are attained in the following cases:

1) Delays equal to zero (due to the correlation of the signal with itself) and D_u (due to the existence of the CP). This is referred to as Case (1) in the sequel.

2) Delays equal to integer multiples of D_F plus $\lceil iD_u/3\rceil$ and $\lfloor iD_u/3\rfloor$, $i=1, 2$, respectively, with D_F as the frame duration, and $\lceil . \rceil$ denoting the ceiling function (due to the structure of the preamble symbol in the frequency domain, where the preamble data

symbols are transmitted every third subcarrier, along with the time repetition of the preamble every frame). This is referred to as Case (2) in the sequel.

3) Delays equal to $\lceil iD_u / M_{DL} \rceil$ and $\lfloor iD_u / M_{DL} \rfloor$, $i = 1, 2, \ldots, M_{DL}-1$, respectively, and $\lceil iD_u / M_{UL} \rceil$ and $\lfloor iD_u / M_{UL} \rfloor$, $i = 1, 2, \ldots, M_{UL}-1$, respectively, (due to the transmission of boosted pilot symbols every M_{DL}th and M_{UL}th subcarriers in the DL and UL OFDM symbols, respectively). Note that M_{DL} and M_{UL} can take different values for different groups of OFDM symbols in the DL and UL subframes, respectively. This is referred to as Case (3) in the sequel.

4) Delays equal to integer multiples of D_F (due to the time domain repetition of the preamble symbol every frame). This is subsequently referred to as Case (4).

We study $R_r(\alpha,\tau)$ at these delays and its representation as a Fourier series, and determine the expressions for $R_r(\alpha,\tau)$ and set of CFs $\{\alpha\}$.

Case (1): Derivation of the analytical expressions for CAF at delays equal to zero and useful OFDM symbol duration and the corresponding set of CFs

We reiterate that CAF is non-zero at delays equal to zero (due to the correlation of the signal with itself) and D_u (due to the CP). Assuming that the symbols on each subcarrier are i.i.d. and mutually independent for different subcarriers, one can easily see that only $E(u_{k_1}u^*_{k_2})$, $E(c_{k_1,l_1}c^*_{k_2,l_2})$, and $E(d_{k_1,l_1}d^*_{k_2,l_2})$ are non-zero at such delays, and this occurs when $k_1 = k_2 = k$ and $l_1 = l_2 = l$. Based on the above and considering the data and pilot symbols separately in each OFDM symbol in the DL and UL subframes, one can show that

$$R_r(n,\tau)=\Big[a_p^2\sigma_u^2\,K_{P,d}\sum_{\substack{l=-\infty\\ l \bmod N_F=0}}^{\infty}\delta(n-lD-lN_F^{-1}D_G)$$

$$+a_{DL}^2\sum_{\substack{l=-\infty\\ 1\le l \bmod N_F=\lambda\le N_{DL}}}^{\infty}\sigma_{DL,\lambda}^2\delta(n-lD-\lfloor lN_F^{-1}\rfloor D_G)$$

$$+a_{UL}^2\sum_{\substack{l=-\infty\\ N_{DL}+1\le l \bmod N_F=\lambda}}^{\infty}\sigma_{UL,\lambda}^2\delta(n-lD-\lfloor lN_F^{-1}\rfloor D_G-D_{TG})\Big]\otimes g(n)g^*(n+\tau), \qquad (2.7)$$

where $\otimes$ denotes convolution, $\sigma_u^2=E(u_{k_1}u_{k_2}^*)$, $\sigma_{DL,\lambda}^2=(\sigma_{DL,\lambda,d}^2K_{DL,\lambda,d}+\sigma_{DL,\lambda,p}^2K_{DL,\lambda,p})$, $\sigma_{UL,\lambda}^2=(\sigma_{UL,\lambda,d}^2K_{UL,\lambda,d}+\sigma_{UL,\lambda,p}^2K_{UL,\lambda,p})$, with $\lambda=l \bmod N_F$, $1\le\lambda\le N_{DL}$ for the DL OFDM symbols (excluding the preamble), and $N_{DL}+1\le\lambda\le N_F-1$ for the UL OFDM symbols, $K_{DL,\lambda,d}$ and $K_{DL,\lambda,p}$ [4] as the number of data and pilot subcarriers in the λth OFDM symbol in the frame belonging to the DL subframe (excluding the preamble), respectively, $\sigma_{DL,\lambda,d}^2$ and $\sigma_{DL,\lambda,p}^2$ as the variance of the data and pilot symbols in the DL OFDM symbols, respectively, and $K_{UL,\lambda,d}$, $K_{UL,\lambda,p}$, $\sigma_{UL,\lambda,d}^2$, and $\sigma_{UL,\lambda,p}^2$ as their UL counterparts.

By expressing l as $l'+\lambda$, with $l'=\lfloor lN_F^{-1}\rfloor N_F$, (2.7) can be rewritten as,

$$R_r(n,\tau)=\Big[a_p^2\sigma_u^2\,K_{P,d}\sum_{\substack{l'=l=-\infty\\ l' \bmod N_F=0}}^{\infty}\delta(n-l'D-l'N_F^{-1}D_G)$$

[4] Note that the number of pilot subcarriers, the variance of the data symbols, and the variance of the pilot symbols are the same in all the OFDM symbols belonging to the same group. For the simplicity of notations, we consider here a more general case where these parameters are different for each OFDM symbol.

$$+a_{\mathrm{DL}}^2 \sum_{\substack{l'=-\infty \\ l' \bmod N_{\mathrm{F}}=0}}^{\infty} \sum_{\lambda=1}^{N_{\mathrm{DL}}} \sigma_{\mathrm{DL},\lambda}^2 \delta(n-l'D-\lambda D-l'N_{\mathrm{F}}^{-1}D_{\mathrm{G}})$$

$$+a_{\mathrm{UL}}^2 \sum_{\substack{l'=-\infty \\ l' \bmod N_{\mathrm{F}}=0}}^{\infty} \sum_{\lambda=N_{\mathrm{DL}}+1}^{N_{\mathrm{F}}-1} \sigma_{\mathrm{UL},\lambda}^2 \delta(n-l'D-\lambda D-l'N_{\mathrm{F}}^{-1}D_{\mathrm{G}}-D_{\mathrm{TG}})\Big] \otimes g(n)g^*(n+\tau). \quad (2.8)$$

By using that $D_{\mathrm{F}} = N_{\mathrm{F}}D + D_{\mathrm{G}}$, (2.8) can be further expressed as

$$R_r(n,\tau) = \Big[a_{\mathrm{p}}^2\sigma_u^2 K_{\mathrm{P},d} \sum_{\nu=-\infty}^{\infty} \delta(n-\nu D_{\mathrm{F}})$$

$$+a_{\mathrm{DL}}^2 \sum_{\nu=-\infty}^{\infty} \sum_{\lambda=1}^{N_{\mathrm{DL}}} \sigma_{\mathrm{DL},\lambda}^2 \delta(n-\nu D_{\mathrm{F}}-\lambda D)$$

$$+a_{\mathrm{UL}}^2 \sum_{\nu=-\infty}^{\infty} \sum_{\lambda=N_{\mathrm{DL}}+1}^{N_{\mathrm{F}}-1} \sigma_{\mathrm{UL},\lambda}^2 \delta(n-\nu D_{\mathrm{F}}-\lambda D-D_{\mathrm{TG}})\Big] \otimes g(n)g^*(n+\tau). \quad (2.9)$$

Furthermore, by taking the Fourier transform of (2.9), using the convolution theorem and the identity $\Im\{\sum_\nu \delta(n-\nu D_{\mathrm{F}})\} = D_{\mathrm{F}}^{-1}\sum_\nu \delta(\alpha-\nu D_{\mathrm{F}}^{-1})$, one obtains

$$\Im\{R_r(n,\tau)\} = D_{\mathrm{F}}^{-1}\Big[a_{\mathrm{p}}^2\sigma_u^2 K_{\mathrm{P},d} + a_{\mathrm{DL}}^2 \sum_{\lambda=1}^{N_{\mathrm{DL}}} \sigma_{\mathrm{DL},\lambda}^2 e^{-j2\pi\alpha\lambda D} + a_{\mathrm{UL}}^2 e^{-j2\pi\alpha D_{\mathrm{TG}}} \sum_{\lambda=N_{\mathrm{DL}}+1}^{N_{\mathrm{F}}-1} \sigma_{\mathrm{UL},\lambda}^2 e^{-j2\pi\alpha\lambda D}\Big]$$

$$\times \sum_n g(n)g^*(n+\tau)e^{-j2\pi\alpha n} \sum_{\nu=-\infty}^{\infty} \delta(\alpha-\nu D_{\mathrm{F}}^{-1}). \quad (2.10)$$

As one can easily see from (2.10), $\Im\{R_r(n,\tau)\}$ is non zero only for $\alpha = \nu D_{\mathrm{F}}^{-1}$, with ν as an integer. By using the inverse Fourier transform of (2.10), one can further observe that the autocorrelation function has a Fourier series representation. This means that the CF domain is discrete, and the CAF at CF α and delay τ, and the set of CFs are given respectively as

$$R_r(\alpha,\tau) = D_{\mathrm{F}}^{-1}\Big[a_{\mathrm{p}}^2\sigma_u^2 K_{\mathrm{P},d} + a_{\mathrm{DL}}^2 \sum_{\lambda=1}^{N_{\mathrm{DL}}} \sigma_{\mathrm{DL},\lambda}^2 e^{-j2\pi\alpha\lambda D} + a_{\mathrm{UL}}^2 e^{-j2\pi\alpha D_{\mathrm{TG}}} \sum_{\lambda=N_{\mathrm{DL}}+1}^{N_{\mathrm{F}}-1} \sigma_{\mathrm{UL},\lambda}^2 e^{-j2\pi\alpha\lambda D}\Big]$$

$$\times \sum_n g(n)g^*(n+\tau)e^{-j2\pi\alpha n}, \quad (2.11)$$

and

$$\mathcal{K} = \{\alpha : \alpha = \nu D_F^{-1},\ \nu \text{ integer}\}. \tag{2.12}$$

Case (2): Derivation of the analytical expressions for CAF at delays equal to integer multiples of the frame duration, D_F, plus $\lceil D_u/3 \rceil$, $\lceil 2D_u/3 \rceil$, $\lfloor D_u/3 \rfloor$, and $\lfloor 2D_u/3 \rfloor$, respectively, and the corresponding set of CFs

Here we investigate $R_r(n,\tau)$ for delays equal to integer multiples of the frame duration, D_F, plus $\lceil D_u/3 \rceil$, $\lceil 2D_u/3 \rceil$, $\lfloor D_u/3 \rfloor$, and $\lfloor 2D_u/3 \rfloor$, respectively, at which we expect non-zero $R_r(n,\tau)$ based on the structure of the preamble in frequency domain (i.e., the preamble data symbols are transmitted every third subcarrier and all other subcarriers are null), along with its time repetition every frame. We start the analysis by considering a single preamble, then we generalize the results obtained for the autocorrelation function to the case of multiple preambles, which actually corresponds to multiple frames, and finally derive the CAF and CFs analytical expressions.

Without considering its particular position in the frame, a preamble symbol can be expressed in time domain as

$$s_P(n) = a_P \sum_{k=0}^{K_{P,d}-1} u_k e^{j2\pi(3k - \frac{K_P}{2} + S_{P,d})n/D_u} g(n)$$

$$= a_P \sum_{k=0}^{K_{P,d}-1} u_k e^{j2\pi(-\frac{K_P}{2} + S_{P,d})n/D_u} e^{j2\pi(3k)n/D_u} g(n),\ n = 0, 1, \ldots, D_u\text{-}1. \tag{2.13}$$

Note that the window used at the transmit side is usually a raised cosine window with a very low roll-off factor (e.g. 0.025) [21]. Without loss of generality, in the following we consider a rectangular window. Following the procedure in [15], one can define,

$$Z_k = \begin{cases} u_k e^{j2\pi(-\frac{K_P}{2}+S_{P,d})n/D_u} & \text{, if } k = 0, 1, \ldots, K_{P,d}-1 \\ & \text{, } k = 0, 1, \ldots, D_u - 1. \\ 0 & \text{, otherwise.} \end{cases} \quad (2.14)$$

By replacing (2.14) into (2.13), the latter can be re-expressed as

$$s_P(n) = a_P \sum_{k=0}^{D_u-1} Z_k e^{j2\pi(3n)k/D_u}, \; n = 0, 1, \ldots, D_u\text{-}1. \quad (2.15)$$

The right hand side of (2.15) can be seen as $z(3n)$, with $z(n)$ as the inverse discrete Fourier transform (IDFT) of $\{Z_k\}$ [15]. By considering all the subcarriers in the preamble (including the null subcarriers for guard bands), one can easily notice that $K_{P,d} < \lceil D_u/3 \rceil$, and that there is a zero padding in (2.15) with more than $\lceil 2D_u/3 \rceil$ zeros. As n goes from 0 to $D_u - 1$, the argument $3n$ cycles through the range 3 times, and the time domain representation of $r_P(n)$ can be expressed as the concatenation of 3 sequences. Define $z_1(n)$ and $z_2(n)$ as $z(3n+\eta_1)$ and $z(3n+\eta_2)$, respectively, with $\eta_1 = 3 - D_u \bmod 3$ and $\eta_2 = 3 - (2 \times D_u) \bmod 3$; then, one can show that [15],

$$s_P(n) = \begin{cases} z(3n), & n = 0, 1, \ldots, \lceil D_u/3 \rceil - 1 \\ z_1(n - \lceil D_u/3 \rceil) & n = \lceil D_u/3 \rceil, \ldots, \lceil 2D_u/3 \rceil - 1 \\ z_2(n - \lceil 2D_u/3 \rceil) & n = \lceil 2D_u/3 \rceil, \ldots, D_u - 1. \end{cases} \quad (2.16)$$

Note that we use $\lceil . \rceil$ as D_u is not divisible by 3 (D_u is usually a power of 2 as it equals the FFT size used with the OFDM signals). As such, we have $z_1(n - \lceil D_u/3 \rceil)$ and $z_2(n - \lceil 2D_u/3 \rceil)$ when $n = \lceil D_u/3 \rceil, \ldots, \lceil 2D_u/3 \rceil - 1$ and $n = \lceil 2D_u/3 \rceil, \ldots, D_u - 1$, respectively. For example, if $D_u = 512$, $s_P(0) = z(0) = z(512)$, $s_P(171) = z(513) = z(1) = z_1(0)$

for $\eta_1 = 1$ and $n = 171 = \lceil 512/3 \rceil$, and $s_P(342) = z(1026) = z(2) = z_2(0)$ for $\eta_2 = 2$ and $n = 342 = \lceil 2\times 512/3 \rceil$. Furthermore, the 3 sequences become $\{z(3n)\} = \{z(0), z(3), \ldots, z(510)\}$, $\{z(3n+1)\} = \{z(1), z(4), \ldots, z(511)\}$, and $\{z(3n+2)\} = \{z(2), z(5), \ldots, z(509)\}$, respectively. By replacing (2.14) into (2.15), one can easily show that there is a correlation between the sequences $\{z(3n)\}$ and $\{z(3n+1)\}$, $\{z(3n+1)\}$ and $\{z(3n+2)\}$, and $\{z(3n)\}$ and $\{z(3n+2)\}$. Equivalently, there is a correlation between $\{s_P(n), n = 0, \ldots, \lceil D_u/3 \rceil - 1\}$ and $\{s_P(n), n = \lceil D_u/3 \rceil, \ldots, \lceil 2D_u/3 \rceil - 1\}$, $\{s_P(n), n = \lceil D_u/3 \rceil, \ldots, \lceil 2D_u/3 \rceil - 1\}$ and $\{s_P(n), n = \lceil 2D_u/3 \rceil, \ldots, D_u - 1\}$, and $\{s_P(n), n = 0, \ldots, \lceil D_u/3 \rceil - 1\}$ and $\{s_P(n), n = \lceil 2D_u/3 \rceil, \ldots, D_u - 1\}$. One can actually observe that this correlation is practically due to the oversampling by 3 in (2.15). For example, there is a correlation of $s_P(n)$ at delay $n = \lceil D_u/3 \rceil = 171$ which comes from the correlation of the sequences $\{z(3n)\}$ and $\{z(3n+1)\}$, and $\{z(3n+1)\}$ and $\{z(3n+2)\}$, as illustrated in Fig. 2.4, which is given by

$$R_{s_P}(n,171) = a_P^2 e^{j2\pi(-\frac{K_P}{2}+S_{P,d})n/512} e^{-j2\pi(-\frac{K_P}{2}+S_{P,d})(n+171)/512} \sum_{k=0}^{K_{P,d}-1} E(u_k u_k^*) e^{j2\pi k 3n/512} e^{-j2\pi k(3n+1)/512}$$

$$= a_P^2 \sigma_u^2 e^{-j2\pi(-\frac{K_P}{2}+S_{P,d})171/512} \sum_{k=0}^{K_{P,d}-1} e^{-j2\pi k/512}$$

$$= a_P^2 \sigma_u^2 e^{-j2\pi(-\frac{K_P}{2}+S_{P,d})171/512} \frac{1-e^{-j2\pi K_{P,d}/512}}{1-e^{-j2\pi/512}}$$

$$= a_P^2 \sigma_u^2 e^{-j2\pi(-\frac{K_P}{2}+S_{P,d})171/512} e^{-j\pi(K_{P,d}-1)/512} \frac{\sin(\pi K_{P,d}/512)}{\sin(\pi/512)}. \qquad (2.17)$$

This has a reasonably large value. For example, if $K_P = 428$, $\sigma_u^2 = 1$, $S_{P,d} = 0$, $K_{P,d} = 143$, then $|R_{s_P}(n,171)| = 0.2944$. Similar to the analysis in case (1), at delays equal to

$\tau_i = \lceil iD_u/3 \rceil$, $i = 1,\ 2$, one can show that the autocorrelation function of $s_P(n)$ is given by (this is actually a generalization of (2.17))

$$R_{s_P}(n,\tau_i) = a_P^2 \sum_{k=0}^{K_{P,d}-1} E(u_k u_k^*) e^{-j2\pi(-\frac{K_P}{2}+S_{P,d})n/D_u} e^{j2\pi(-\frac{K_P}{2}+S_{P,d})(n+\tau_i)/D_u} e^{j2\pi k 3n/D_u} e^{-j2\pi k(3(n+\tau_i))/D_u}$$

$$= a_P^2 \sigma_u^2 e^{-j2\pi(-\frac{K_P}{2}+S_{P,d})\tau_i/D_u} \sum_{k=0}^{K_{P,d}-1} e^{-j2\pi k 3\tau_i/D_u}$$

$$= a_P^2 \sigma_u^2 e^{-j2\pi(-\frac{K_P}{2}+S_{P,d})\tau_i/D_u} \frac{1-e^{-j2\pi 3\tau_i K_{P,d}/D_u}}{1-e^{-j2\pi 3\tau_i/D_u}}$$

$$= a_P^2 \sigma_u^2 e^{-j2\pi(-\frac{K_P}{2}+S_{P,d})\tau_i/D_u} e^{-j\pi 3\tau_i(K_{P,d}-1)/D_u} \frac{\sin(\pi 3\tau_i K_{P,d}/D_u)}{\sin(\pi 3\tau_i/D_u)}. \qquad (2.18)$$

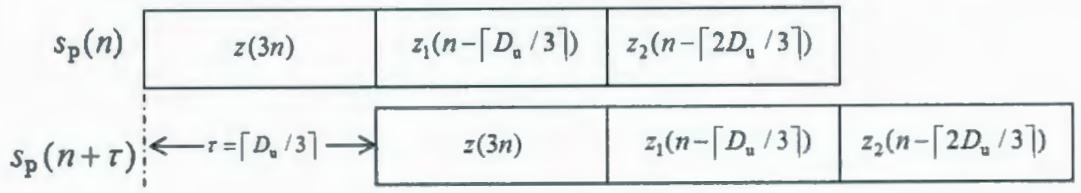

a)

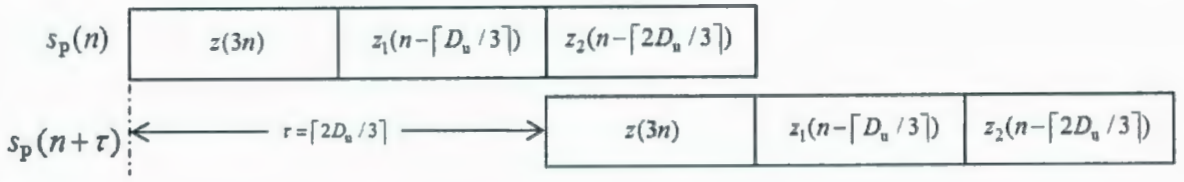

b)

Fig. 2.4. Illustration of the correlation between the components of $s_P(n)$ a) at $\tau = \lceil D_u/3 \rceil$ b) at $\tau = \lceil 2D_u/3 \rceil$.

In addition to delays $\tau_i = \lceil iD_u/3 \rceil$, $i = 1,\ 2$, one can show that the autocorrelation function of $s_P(n)$ is relatively large at delays $\overline{\tau}_i = \lfloor iD_u/3 \rfloor$, $i = 1,\ 2$. As in the previous case, we first look at an example for an easier understanding, and then find the expression for the general case. If

$D_u = 512$, $s_P(0) = z(0) = z(512)$, $s_P(170) = z(510) = z(-2)$, with $n = 170 = \lfloor 512/3 \rfloor$, and $s_P(341) = z(1023) = z(-1)$, with $n = 342 = \lfloor 2\times 512/3 \rfloor$. Furthermore, the 3 sequences become $\{z(3n)\} = \{z(0), z(3), \ldots, z(507)\}$, $\{z(3n-2)\} = \{z(-2), z(1), \ldots, z(508)\}$, and $\{z(3n-1)\} = \{z(-1), z(2), \ldots, z(509)\}$, respectively. As in the previous case, one can easily show that there is a correlation between the sequences $\{z(3n)\}$ and $\{z(3n-2)\}$, $\{z(3n-2)\}$ and $\{z(3n-1)\}$, and $\{z(3n)\}$ and $\{z(3n-1)\}$. Equivalently, there is a correlation between $\{s_P(n), n = 0, \ldots, \lfloor D_u/3 \rfloor - 1\}$ and $\{s_P(n), n = \lfloor D_u/3 \rfloor, \ldots, \lfloor 2D_u/3 \rfloor - 1\}$, $\{s_P(n), n = \lfloor D_u/3 \rfloor, \ldots, \lfloor 2D_u/3 \rfloor - 1\}$ and $\{s_P(n), n = \lfloor 2D_u/3 \rfloor, \ldots, D_u - 1\}$, and $\{s_P(n), n = 0, \ldots, \lfloor D_u/3 \rfloor - 1\}$ and $\{s_P(n), n = \lfloor 2D_u/3 \rfloor, \ldots, D_u - 1\}$. For example, there is a correlation of $s_P(n)$ at delay $n = \lfloor D_u/3 \rfloor = 170$ which comes from the correlation of the sequences $\{z(3n)\}$ and $\{z(3n-2)\}$, and $\{z(3n-2)\}$ and $\{z(3n-1)\}$, which is given by

$$R_{s_P}(n,170) = a_P^2 \sigma_u^2 e^{-j2\pi(-\frac{K_P}{2}+S_{P,d})170/512} e^{j\pi 2(K_{P,d}-1)/D_u} \frac{\sin(\pi 2K_{P,d}/512)}{\sin(\pi 2/512)}. \tag{2.19}$$

By considering the same values used with (2.17), one can find that $\left|R_{s_P}(n,170)\right| = 0.187$. As in the previous case, one can further show that there is a correlation at delays equal to $\overline{\tau}_i = \lfloor iD_u/3 \rfloor$, $i = 1, 2$, with the autocorrelation function of $s_P(n)$ given by (this is actually a generalization of (2.19))

$$R_{s_P}(n,\overline{\tau}_i) = a_P^2 \sigma_u^2 e^{-j2\pi(-\frac{K_P}{2}+S_{P,d})\overline{\tau}_i/D_u} e^{-j\pi 3\overline{\tau}_i(K_{P,d}-1)/D_u} \frac{\sin(\pi 3\overline{\tau}_i K_{P,d}/D_u)}{\sin(\pi 3\overline{\tau}_i/D_u)}. \tag{2.20}$$

Note that the correlation vanishes for other delays, e.g., $\left|R_{s_p}(n,172)\right| = 0.0364$ and $\left|R_{s_p}(n,169)\right| = 0.0337$.

Furthermore, by considering the other components of the mobile WiMAX signal within a single frame, one can show that the only non-zero component of the autocorrelation function at delays equal to $\lceil iD_u/3 \rceil$ and $\lfloor iD_u/3 \rfloor$, $i = 1, 2$, respectively, is due to the preamble. By considering multiple frames ($l = -\infty, \ldots, \infty$) and based on the time domain repetition property of the preamble, one can further show that the values of $R_r(n,\tau)$ for delays equal to $\mu D_F + \lceil iD_u/3 \rceil$ and $\mu D_F + \lfloor iD_u/3 \rfloor$, μ integer and $i = 1, 2$, are equal to those at $\lceil iD_u/3 \rceil$ and $\lfloor iD_u/3 \rfloor$, respectively. By considering $\tau_i = \mu D_F + \lceil iD_u/3 \rceil$, μ integer and $i = 1, 2$, $R_r(n,\tau_i)$ at these delays can be shown to be

$$R_r(n,\tau_i) = a_P^2 \sigma_u^2 e^{-j2\pi(-\frac{K_P}{2}+S_{P,d})(\tau_i \bmod D_F)/D_u} e^{-j\pi 3(\tau_i \bmod D_F)(K_{P,d}-1)/D_u} \frac{\sin(\pi 3(\tau_i \bmod D_F)K_{P,d}/D_u)}{\sin(\pi 3(\tau_i \bmod D_F)/D_u)}$$
$$\times \sum_{\substack{l=-\infty \\ l \bmod N_F = 0}}^{\infty} g(n - lD - lN_F^{-1}D_G) g^*(n - lD - lN_F^{-1}D_G + \tau_i \bmod D_F)$$
$$= a_P^2 \sigma_u^2 e^{-j2\pi(-\frac{K_P}{2}+S_{P,d})(\tau_i \bmod D_F)/D_u} e^{-j\pi 3(\tau_i \bmod D_F)(K_{P,d}-1)/D_u} \frac{\sin(\pi 3(\tau_i \bmod D_F)K_{P,d}/D_u)}{\sin(\pi 3(\tau_i \bmod D_F)/D_u)}$$
$$\times g(n) g^*(n + \tau_i \bmod D_F) \otimes \sum_{\nu=-\infty}^{\infty} \delta(n - \nu D_F), \qquad (2.21)$$

where $\tau_i \bmod D_F$ is used to exclude the dependency on μD_F. By taking the Fourier transform of $R_r(n,\tau_i)$, using the convolution theorem and the identity

$\Im\{\sum_{\nu}\delta(n-\nu D_{\mathrm{F}})\}=D_{\mathrm{F}}^{-1}\sum_{\nu}\delta(\alpha-\nu D_{\mathrm{F}}^{-1})$, the CAF of the mobile WiMAX signal at delays $\tau_i=\mu D_{\mathrm{F}}+\lceil iD_{\mathrm{u}}/3\rceil$, μ integer and $i=1,\ 2,$ can be obtained as

$$R_r(\alpha,\tau_i)=D_{\mathrm{F}}^{-1}a_{\mathrm{P}}^2\sigma_u^2 e^{-j2\pi(-\frac{K_{\mathrm{P}}}{2}+S_{\mathrm{P},d})(\tau_i \bmod D_{\mathrm{F}})/D_{\mathrm{u}}}e^{-j\pi 3(\tau_i \bmod D_{\mathrm{F}})(K_{\mathrm{P},d}-1)/D_{\mathrm{u}}}\frac{\sin(\pi 3(\tau_i \bmod D_{\mathrm{F}})K_{\mathrm{P},d}/D_{\mathrm{u}})}{\sin(\pi 3(\tau_i \bmod D_{\mathrm{F}})/D_{\mathrm{u}})}$$

$$\times\sum_n g(n)g^*(n+\tau_i \bmod D_{\mathrm{F}})e^{-j2\pi\alpha n}, \tag{2.22}$$

and the set of CFs as

$$\mathcal{K}=\{\alpha:\alpha=\nu D_{\mathrm{F}}^{-1},\ \nu \text{ integer}\}. \tag{2.23}$$

By following the same procedure, one can easily show that the CAF of the mobile WiMAX signal at delays $\overline{\tau}_i=\mu D_{\mathrm{F}}+\lfloor iD_{\mathrm{u}}/3\rfloor$, μ integer and $i=1,\ 2,$ is given by

$$R_r(\alpha,\overline{\tau}_i)=D_{\mathrm{F}}^{-1}a_{\mathrm{P}}^2\sigma_u^2 e^{-j2\pi(-\frac{K_{\mathrm{P}}}{2}+S_{\mathrm{P},d})(\overline{\tau}_i \bmod D_{\mathrm{F}})/D_{\mathrm{u}}}e^{-j\pi 3(\overline{\tau}_i \bmod D_{\mathrm{F}})(K_{\mathrm{P},d}-1)/D_{\mathrm{u}}}\frac{\sin(\pi 3(\overline{\tau}_i \bmod D_{\mathrm{F}})K_{\mathrm{P},d}/D_{\mathrm{u}})}{\sin(\pi 3(\overline{\tau}_i \bmod D_{\mathrm{F}})/D_{\mathrm{u}})}$$

$$\times\sum_n g(n)g^*(n+\overline{\tau}_i \bmod D_{\mathrm{F}})e^{-j2\pi\alpha n}, \tag{2.24}$$

and the set of CFs as

$$\mathcal{K}=\{\alpha:\alpha=\nu D_{\mathrm{F}}^{-1},\ \nu \text{ integer}\}. \tag{2.25}$$

Case (3): Derivations of the analytical expressions for CAF at delays equal to $\lceil iD_{\mathrm{u}}/M_{\mathrm{DL}}\rceil$ and $\lfloor iD_{\mathrm{u}}/M_{\mathrm{DL}}\rfloor$, $i=1, 2,\ldots, M_{\mathrm{DL}}$-1, respectively, and $\lceil iD_{\mathrm{u}}/M_{\mathrm{UL}}\rceil$ and $\lfloor iD_{\mathrm{u}}/M_{\mathrm{UL}}\rfloor$, $i=1, 2,\ldots, M_{\mathrm{UL}}$-1, respectively, and the corresponding set of CFs

We investigate $R_r(n,\tau)$ for delays equal to $\lceil iD_{\mathrm{u}}/M_{\mathrm{DL}}\rceil$ and $\lfloor iD_{\mathrm{u}}/M_{\mathrm{DL}}\rfloor$, $i=1, 2,\ldots, M_{\mathrm{DL}}$-1, respectively, and $\lceil iD_{\mathrm{u}}/M_{\mathrm{UL}}\rceil$ and $\lfloor iD_{\mathrm{u}}/M_{\mathrm{UL}}\rfloor$, $i=1, 2,\ldots, M_{\mathrm{UL}}$-1, respectively, at which we expect $R_r(n,\tau)$ to have non-zero values due to the transmission of

boosted pilot symbols every M_{DL}th and M_{UL}th subcarriers in the DL and UL OFDM symbols, respectively. We start the analysis by considering a single OFDM symbol with such a frequency structure, regardless of its position. A DL OFDM symbol is considered without loss of generality; similar results can be also found for an UL OFDM symbol. Then, we generalize our findings for multiple symbols and multiple frames, and derive the expressions for the CAF at these delays, as well as for the set of CFs.

Consider a single DL OFDM symbol, which includes both data and pilot subcarriers. The pilot symbols are transmitted every M_{DL}th subcarrier, and are boosted over the data symbols. The time domain representation of such a DL OFDM symbol is

$$s_{\mathrm{DL}}(n) = a_{\mathrm{DL}} \sum_{k=-K_{\mathrm{DL}}/2, k\neq 0}^{K_{\mathrm{DL}}/2} c_k e^{j2\pi kn/D_{\mathrm{u}}},\ n = 0, 1, \ldots, D_{\mathrm{u}}\text{-}1, \tag{2.26}$$

where c_k is the (data/pilot) symbol transmitted on the kth subcarrier. Note that the dependency on l is dropped, as the OFDM symbol position is not considered here. Also, as in case (2), a rectangular window is assumed without loss of generality. The DL OFDM symbol can be further expressed as the sum of two parts: a first part which corresponds to symbols over all subcarriers, whose variance is $\sigma^2_{\mathrm{DL},d}$, and a second part which corresponds to symbols only over the pilot subcarriers, whose variance is $\sigma^2_{\mathrm{DL},pd} = \sigma^2_{\mathrm{DL},p} - \sigma^2_{\mathrm{DL},d}$, i.e.,

$$s_{\mathrm{DL}}(n) = s^{(1)}_{\mathrm{DL}}(n) + s^{(2)}_{\mathrm{DL}}(n), \tag{2.27.a}$$

where

$$s^{(1)}_{\mathrm{DL}}(n) = a_{\mathrm{DL}} \sum_{k=-K_{\mathrm{DL}}/2, k\neq 0}^{K_{\mathrm{DL}}/2} c^{(1)}_k e^{j2\pi kn/D_{\mathrm{u}}},\ n = 0, 1, \ldots, D_{\mathrm{u}}\text{-}1, \tag{2.27.b}$$

$$s_{\mathrm{DL}}^{(2)}(n) = a_{\mathrm{DL}} \sum_{k=0}^{K_{\mathrm{DL},p}-1} c_k^{(2)} e^{j2\pi(M_{\mathrm{DL}}k - \frac{K_{\mathrm{DL}}}{2}+S_p)n/D_{\mathrm{u}}}, \; n = 0, 1, \ldots, D_{\mathrm{u}}\text{-}1^{5}, \tag{2.27.c}$$

where $c_k^{(1)}$ and $c_k^{(2)}$ are the symbols with variance $\sigma_{\mathrm{DL},d}^2$ and $\sigma_{\mathrm{DL},pd}^2$, respectively, $K_{\mathrm{DL},p}$ is the number of subcarriers used for pilot transmission in the considered DL OFDM symbol, and $-\frac{K_{\mathrm{DL}}}{2}+S_p$ is the position of the first subcarrier where a pilot symbol is transmitted. $s_{\mathrm{DL}}^{(2)}(n)$ can be further written as

$$s_{\mathrm{DL}}^{(2)}(n) = a_{\mathrm{DL}} \sum_{k=0}^{K_{\mathrm{DL},p}-1} c_k^{(2)} e^{j2\pi(-\frac{K_{\mathrm{DL}}}{2}+S_p)n/D_{\mathrm{u}}} e^{j2\pi(M_{\mathrm{DL}}k)n/D_{\mathrm{u}}}, \; n = 0, 1, \ldots, D_{\mathrm{u}}\text{-}1. \tag{2.28}$$

Similar to case (2), by defining

$$V_k = \begin{cases} c_k^{(2)} e^{j2\pi(-\frac{K_{\mathrm{DL}}}{2}+S_p)n/D_{\mathrm{u}}}, & \text{if } k = 0, 1, \ldots, K_{\mathrm{DL},p}-1 \\ 0, & \text{otherwise.} \end{cases} \quad , k = 0, 1, \ldots, D_{\mathrm{u}}-1, \tag{2.29}$$

and substituting it into (2.26), $s_{\mathrm{DL}}^{(2)}(n)$ can be written as

$$s_{\mathrm{DL}}^{(2)}(n) = a_{\mathrm{DL}} \sum_{k=0}^{D_{\mathrm{u}}-1} V_k e^{j2\pi(M_{\mathrm{DL}}n)k/D_{\mathrm{u}}}, \; n = 0, 1, \ldots, D_{\mathrm{u}}\text{-}1. \tag{2.30}$$

The right hand side of the (2.30) can be seen as $v(M_{\mathrm{DL}}n)$, with $v(n)$ as the IDFT of $\{V_k\}$. By considering all subcarriers (data, pilot, and null subcarriers) in the OFDM symbol, one can notice that $K_{\mathrm{DL},p} < \lceil D_{\mathrm{u}} / M_{\mathrm{DL}} \rceil$ and that there is zero padding in (2.30)

[5] Note that, for simplicity, we assume that one set of pilot symbols are transmitted in an OFDM symbol. In case that another set is transmitted with different distribution, simply, another term e.g., $s_{\mathrm{DL}}^{(3)}(n)$, can be added to represent any additional set. The same analysis for $s_{\mathrm{DL}}^{(2)}(n)$, applies for $s_{\mathrm{DL}}^{(3)}(n)$, with the final result for the CAF is given by the summation of results for all terms.

with more than $\lceil (M_{DL}-1)D_u / M_{DL} \rceil$ zeros. As n goes from 0 to $D_u - 1$, the argument $M_{DL}n$ cycles through the range M_{DL} times. Consequently, one can express $s_{DL}^{(2)}(n)$ as the concatenation of M_{DL} sequences. By defining $v_i(n)$ as $v(M_{DL}n+\gamma_i)$, with $i = 1,\ldots, M_{DL}-1$ and $\gamma_i = M_{DL} - iD_u \bmod M_{DL}$, one can show that

$$s_{DL}^{(2)}(n) = \begin{cases} v(M_{DL}n) & , n= 0, 1,\ldots, \lceil D_u / M_{DL} \rceil - 1 \\ v_1(n - \lceil D_u / M_{DL} \rceil) & , n= \lceil D_u / M_{DL} \rceil,\ldots, \lceil 2D_u / M_{DL} \rceil - 1 \\ \vdots & \\ v_{M_{DL}-1}(n - \lceil (M_{DL}-1)D_u / M_{DL} \rceil) & , n= \lceil (M_{DL}-1)D_u / M_{DL} \rceil,\ldots, D_u - 1. \end{cases} \quad (2.31)$$

Note that we use $\lceil . \rceil$ as D_u may not be divisible by M_{DL} (D_u is usually a power of 2 as it equals the FFT size used with the OFDM signals). To accommodate such cases, we take $s_{DL}^{(2)}(n) = v_i(n - \lceil iD_u / M_{DL} \rceil)$, $n= \lceil iD_u / M_{DL} \rceil,\ldots, \lceil (i+1)D_u / M_{DL} \rceil - 1$, $i = 1, \ldots, M_{DL}-1$. For illustration, we consider $D_u = 512$ and $M_{DL} = 5$. For $n = 0$, (2.30) and (2.31) become $s_{DL}^{(2)}(0) = v(0) = v(512)$ $(i = 0)$. For $n = 103 = \lceil 512/5 \rceil$ $(i = 1)$, $s_{DL}^{(2)}(103) = v(515) = v(3) = v_1(0)$, with $\gamma_1 = 5 - 512 \bmod 5 = 3$. For $n = 205 = \lceil 2\times 512/5 \rceil$ $(i = 2)$, $s_{DL}^{(2)}(205) = v(1025) = v(1) = v_2(0)$, with $\gamma_2 = 5 - 1024 \bmod 5 = 1$. For $n = 308 = \lceil 3\times 512/5 \rceil$ $(i = 3)$, $s_{DL}^{(2)}(308) = v(1540) = v(4) = v_3(0)$, with $\gamma_3 = 5 - 1536 \bmod 5 = 4$. For $n = 410 = \lceil 4\times 512/5 \rceil$ $(i = 4)$, (2.30) gives $s_{DL}^{(2)}(410) = v(2050) = v(2) = v_4(0)$, with $\gamma_4 = 5 - 2048 \bmod 5 = 2$. Furthermore, $s_{DL}^{(2)}(n)$ can be represented as the concatenation of 5 sequences, $\{z(5n)\} = \{z(0),\ldots, z(510)\}$, $\{z(5n+3)\} = \{z(3),\ldots, z(508)\}$, $\{z(5n+1)\} = \{z(1), \ldots, z(511)\}$, $\{z(5n+4)\} = \{z(4),\ldots, z(509)\}$, and $\{z(5n+2)\} = \{z(2),\ldots, z(507)\}$, respectively. By substituting (2.30) into (2.31), one can easily show that there is a correlation between any two of

the previous sequences. One can actually observe that this correlation is practically due to the oversampling with a factor of 5 in (2.30). For example, at delay $\tau = \lceil 512/5 \rceil = 103$, there is a correlation between the first and second sequences, second and third sequences, third and fourth sequences, and fourth and fifth sequences. Furthermore, there is practically a correlation at each delay $\tau_i = \lceil iD_u / M_{DL} \rceil$, $i = 1, 2, ..., M_{DL} - 1$ (note that this is similar to case(2)). At these delays, one can show that the autocorrelation function of $s_{DL}^{(2)}(n)$ is given by

$$
\begin{aligned}
R_{s_{DL}^{(2)}}(n,\tau_i) &= a_{DL}^2 e^{-j2\pi(-\frac{K_{DL}}{2}+S_p)\tau_i/D_u} \sum_{k=0}^{K_{DL,p}-1} E(c_k^{(2)} c_k^{(2)*}) e^{j2\pi k M_{DL} n/D_u} e^{-j2\pi k M_{DL}(n+\tau_i)/D_u} \\
&= a_{DL}^2 \sigma_{DL,pd}^2 e^{-j2\pi(-\frac{K_{DL}}{2}+S_p)\tau_i/D_u} \sum_{k=0}^{K_{DL,p}-1} e^{-j2\pi k M_{DL}\tau_i/D_u} \\
&= a_{DL}^2 \sigma_{DL,pd}^2 e^{-j2\pi(-\frac{K_{DL}}{2}+S_p)\tau_i/D_u} \frac{1-e^{-j2\pi M_{DL}\tau_i K_{DL,p}/D_u}}{1-e^{-j2\pi M_{DL}\tau_i/D_u}} \\
&= a_{DL}^2 \sigma_{DL,pd}^2 e^{-j2\pi(-\frac{K_{DL}}{2}+S_p)\tau_i/D_u} e^{-j\pi M_{DL}\tau_i(K_{DL,p}-1)/D_u} \frac{\sin(\pi M_{DL}\tau_i K_{DL,p}/D_u)}{\sin(\pi M_{DL}\tau_i/D_u)}. \quad (2.32)
\end{aligned}
$$

In addition to delays $\tau_i = \lceil iD_u / M_{DL} \rceil$, $i = 1, 2, ..., M_{DL} - 1$, one can show that the autocorrelation function of $s_P(n)$ is relatively large at delays $\overline{\tau}_i = \lfloor iD_u / M_{DL} \rfloor$, $i = 1, 2, ..., M_{DL} - 1$. Again, we consider $D_u = 512$ and $M_{DL} = 5$ for illustration. For $n = 0$, $s_{DL}^{(2)}(0) = v(0) = v(512)$ and we have the sequence $\{z(5n)\} = \{z(0), z(5), \ldots, z(505)\}$. For $n = 102 = \lfloor 512/5 \rfloor$, $s_{DL}^{(2)}(102) = v(510) = v(-2)$ and we have the sequence $\{z(5n-2)\} = \{z(-2), z(3), \ldots, z(503)\}$. For $n = 204 = \lfloor 2\times 512/5 \rfloor$, $s_{DL}^{(2)}(204) = v(1020) = v(-4)$ and we have the sequence $\{z(5n-4)\} = \{z(-4), z(1), \ldots, z(506)\}$. For $n = 307 = \lfloor 3\times 512/5 \rfloor$, $s_{DL}^{(2)}(307) = v(1535) = v(-1)$ and we have the sequence $\{z(5n-1)\} = \{z(-1), z(4),$

$\ldots, z(504)\}$. For $n = 409 = \lfloor 4\times 512/5 \rfloor$, $s_{\mathrm{DL}}^{(2)}(409) = v(2045) = v(-3)$ and we have the sequence $\{z(5n-3)\} = \{z(-3), z(2), \ldots, z(507)\}$. As in the previous case, there will be a correlation between any two of the previous sequences. Furthermore, there is practically correlation at any delay $\overline{\tau}_i = \lfloor iD_{\mathrm{u}} / M_{\mathrm{DL}} \rfloor$, $i = 1, 2, \ldots, M_{\mathrm{DL}} - 1$ (note that this is similar to case (2)). At these delays, it can be shown that the autocorrelation function of $s_{\mathrm{DL}}^{(2)}(n)$ is given by

$$R_{s_{\mathrm{DL}}^{(2)}}(n, \overline{\tau}_i) = a_{\mathrm{DL}}^2 \sigma_{\mathrm{DL},pd}^2 e^{-j2\pi(-\frac{K_{\mathrm{DL}}+S_p}{2})\overline{\tau}_i / D_{\mathrm{u}}} e^{-j\pi M_{\mathrm{DL}}\overline{\tau}_i (K_{\mathrm{DL},p}-1)/D_{\mathrm{u}}} \frac{\sin(\pi M_{\mathrm{DL}}\overline{\tau}_i K_{\mathrm{DL},p} / D_{\mathrm{u}})}{\sin(\pi M_{\mathrm{DL}}\overline{\tau}_i / D_{\mathrm{u}})}. \quad (2.33)$$

We would like to reiterate that the expressions in (2.32) and (2.33) are for a single DL OFDM symbol. Similar expressions (i.e., $R_{s_{\mathrm{UL}}^{(2)}}(n, \tau_i)$ and $R_{s_{\mathrm{UL}}^{(2)}}(n, \overline{\tau}_i)$, respectively) can be also derived for an UL OFDM symbol, as these may also contain pilot symbols.

In the following, we generalize these results to multiple DL symbols in multiple frames. When the pilot distribution (i.e., the pilot symbols are transmitted every M_{DL}th subcarrier in OFDM symbol) is used in DL OFDM symbols that belong to the frame (the set of these DL OFDM symbols is denoted by $\mathcal{M}_{\mathrm{DL},p}$), $R_r(n, \tau)$ will have non-zero values at delays equal to $\lceil iD_{\mathrm{u}} / M_{\mathrm{DL}} \rceil$ and $\lfloor iD_{\mathrm{u}} / M_{\mathrm{DL}} \rfloor$, $i = 1, 2, \ldots, M_{\mathrm{DL}} - 1$, due to $R_{s_{\mathrm{DL}}^{(2)}}(n, \tau_i)$ and $R_{s_{\mathrm{DL}}^{(2)}}(n, \overline{\tau}_i)$, respectively. Note that M_{DL} can take different values for different groups of symbols within a DL subframe. The dependency of M_{DL} and $\mathcal{M}_{\mathrm{DL},p}$ on the pilot distribution

for diverse groups is not shown by the notation for the reason of simplicity. For any M_{DL}, at delays $\tau_{\mathrm{DL},i} = \lceil iD_{\mathrm{u}} / M_{\mathrm{DL}} \rceil$[6], $i = 1, 2, \ldots, M_{\mathrm{DL}} - 1$, $R_r(n, \tau_{\mathrm{DL},i})$ is given by

$$R_r(n,\tau_{\mathrm{DL},i}) = a_{\mathrm{DL}}^2 \sigma_{\mathrm{DL},pd}^2 e^{-j2\pi(-\frac{K_{\mathrm{DL}}}{2}+S_p)\tau_{\mathrm{DL},i}/D_{\mathrm{u}}} e^{-j\pi M_{\mathrm{DL}}\tau_{\mathrm{DL},i}(K_{\mathrm{DL},p}-1)/D_{\mathrm{u}}} \frac{\sin(\pi M_{\mathrm{DL}}\tau_{\mathrm{DL},i}K_{\mathrm{DL},p}/D_{\mathrm{u}})}{\sin(\pi M_{\mathrm{DL}}\tau_{\mathrm{DL},i}/D_{\mathrm{u}})}$$

$$\times \sum_{\substack{l=-\infty \\ l \bmod N_{\mathrm{F}} = \lambda \in \mathcal{M}_{\mathrm{DL},p}}}^{\infty} g(n - lD - \lfloor lN_{\mathrm{F}}^{-1} \rfloor D_{\mathrm{G}}) g^*(n - lD - \lfloor lN_{\mathrm{F}}^{-1} \rfloor D_{\mathrm{G}} + \tau_{\mathrm{DL},i})$$

$$= a_{\mathrm{DL}}^2 \sigma_{\mathrm{DL},pd}^2 e^{-j2\pi(-\frac{K_{\mathrm{DL}}}{2}+S_p)\tau_{\mathrm{DL},i}/D_{\mathrm{u}}} e^{-j\pi M_{\mathrm{DL}}\tau_{\mathrm{DL},i}(K_{\mathrm{DL},p}-1)/D_{\mathrm{u}}} \frac{\sin(\pi M_{\mathrm{DL}}\tau_{\mathrm{DL},i}K_{\mathrm{DL},p}/D_{\mathrm{u}})}{\sin(\pi M_{\mathrm{DL}}\tau_{\mathrm{DL},i}/D_{\mathrm{u}})}$$

$$\times g(n) g^*(n + \tau_{\mathrm{DL},i}) \otimes \sum_{\substack{l=-\infty \\ l \bmod N_{\mathrm{F}} = \lambda \in \mathcal{M}_{\mathrm{DL},p}}}^{\infty} \delta(n - lD - \lfloor lN_{\mathrm{F}}^{-1} \rfloor D_{\mathrm{G}}), \qquad (2.34)$$

where $K_{\mathrm{DL},p}$ is the number of pilot subcarriers in any DL OFDM symbol that belongs to $\mathcal{M}_{\mathrm{DL},p}$[7]. By expressing l as $l' + \lambda$, with $l' = \lfloor lN_{\mathrm{F}}^{-1} \rfloor N_{\mathrm{F}}$, and using that $D_{\mathrm{F}} = N_{\mathrm{F}} D + D_{\mathrm{G}}$, (2.34) can be written as

$$R_r(n,\tau_{\mathrm{DL},i}) = a_{\mathrm{DL}}^2 \sigma_{\mathrm{DL},pd}^2 e^{-j2\pi(-\frac{K_{\mathrm{DL}}}{2}+S_p)\tau_{\mathrm{DL},i}/D_{\mathrm{u}}} e^{-j\pi M_{\mathrm{DL}}\tau_{\mathrm{DL},i}(K_{\mathrm{DL},p}-1)/D_{\mathrm{u}}} \frac{\sin(\pi M_{\mathrm{DL}}\tau_{\mathrm{DL},i}K_{\mathrm{DL},p}/D_{\mathrm{u}})}{\sin(\pi M_{\mathrm{DL}}\tau_{\mathrm{DL},i}/D_{\mathrm{u}})}$$

$$\times g(n) g^*(n + \tau_{\mathrm{DL},i}) \otimes \sum_{\lambda \in \mathcal{M}_{\mathrm{DL},p}} \sum_{\nu=-\infty}^{\infty} \delta(n - \nu D_{\mathrm{F}} - \lambda D). \qquad (2.35)$$

By taking the Fourier transform of $R_{s_{\mathrm{DL}}^{(2)}}(n, \tau_{\mathrm{DL},i})$, using the convolution theorem and the identity $\Im\{\sum_{\nu} \delta(n - \nu D_{\mathrm{F}})\} = D_{\mathrm{F}}^{-1} \sum_{\nu} \delta(\alpha - \nu D_{\mathrm{F}}^{-1})$, the CAF of mobile WiMAX signal at delays $\tau_{\mathrm{DL},i} = \lceil iD_{\mathrm{u}} / M_{\mathrm{DL}} \rceil$, $i = 1, 2, \ldots, M_{\mathrm{DL}} - 1$, can be shown to be given by

---

[6] At this point we introduce the index DL in the delay notation in order to make the difference between DL and UL in the sequel.

[7] Note that this definition is in agreement with that in p.4, where a single OFDM symbol belonging to $\mathcal{M}_{\mathrm{DL},p}$ is considered.

$$R_r(\alpha,\tau_{\mathrm{DL},i}) = D_{\mathrm{F}}^{-1} a_{\mathrm{DL}}^2 \sigma_{\mathrm{DL},pd}^2 e^{-j2\pi(-\frac{K_{\mathrm{DL}}}{2}+S_p)\tau_{\mathrm{DL},i}/D_{\mathrm{u}}} e^{-j\pi M_{\mathrm{DL}}\tau_{\mathrm{DL},i}(K_{\mathrm{DL},p}-1)/D_{\mathrm{u}}}$$
$$\times \frac{\sin(\pi M_{\mathrm{DL}}\tau_{\mathrm{DL},i}K_{\mathrm{DL},p}/D_{\mathrm{u}})}{\sin(\pi M_{\mathrm{DL}}\tau_{\mathrm{DL},i}/D_{\mathrm{u}})} \sum_{\lambda\in\mathcal{M}_{\mathrm{DL},p}} e^{-j2\pi\alpha\lambda D} \sum_n g(n)g^*(n+\tau_{\mathrm{DL},i})e^{-j2\pi\alpha n}, \quad (2.36)$$

and

$$\mathcal{K} = \{\alpha : \alpha = \nu D_{\mathrm{F}}^{-1},\ \nu \text{ integer}\}. \quad (2.37)$$

Following the same steps, one can easily show that the CAF of the mobile WiMAX signal at delays equal to $\overline{\tau}_{\mathrm{DL},i} = \lfloor iD_{\mathrm{u}}/M_{\mathrm{DL}} \rfloor$, $i = 1,\ 2,\ ...,\ M_{\mathrm{DL}}-1$ and the set of CFs are given respectively as

$$R_r(\alpha,\overline{\tau}_{\mathrm{DL},i}) = D_{\mathrm{F}}^{-1} a_{\mathrm{DL}}^2 \sigma_{\mathrm{DL},pd}^2 e^{-j2\pi(-\frac{K_{\mathrm{DL}}}{2}+S_p)\overline{\tau}_{\mathrm{DL},i}/D_{\mathrm{u}}} e^{-j\pi M_{\mathrm{DL}}\overline{\tau}_{\mathrm{DL},i}(K_{\mathrm{DL},p}-1)/D_{\mathrm{u}}}$$
$$\times \frac{\sin(\pi M_{\mathrm{DL}}\overline{\tau}_{\mathrm{DL},i}K_{\mathrm{DL},p}/D_{\mathrm{u}})}{\sin(\pi M_{\mathrm{DL}}\overline{\tau}_{\mathrm{DL},i}/D_{\mathrm{u}})} \sum_{\lambda\in\mathcal{M}_{\mathrm{DL},p}} e^{-j2\pi\alpha\lambda D} \sum_n g(n)g^*(n+\overline{\tau}_{\mathrm{DL},i})e^{-j2\pi\alpha n}, \quad (2.38)$$

and

$$\mathcal{K} = \{\alpha : \alpha = \nu D_{\mathrm{F}}^{-1},\ \nu \text{ integer}\}. \quad (2.39)$$

Similarly, when the pilot distribution (pilot symbols are transmitted every M_{UL}th subcarrier in an UL OFDM symbol) is used in UL OFDM symbols in the frame that belong to the set $\mathcal{M}_{\mathrm{UL},p}$, $R_r(n,\tau)$ will have non-zero values at delays equal to $\tau_{\mathrm{UL},i} = \lceil iD_{\mathrm{u}}/M_{\mathrm{UL}} \rceil$ and $\overline{\tau}_{\mathrm{UL},i} = \lfloor iD_{\mathrm{u}}/M_{\mathrm{UL}} \rfloor$, $i = 1, 2, \ldots, M_{\mathrm{UL}}-1$, due to $R_{s_{\mathrm{UL}}^{(2)}}(n,\tau_{\mathrm{UL},i})$ and $R_{s_{\mathrm{UL}}^{(2)}}(n,\overline{\tau}_{\mathrm{UL},i})$, respectively. Following the same steps in the previous discussion for the DL case, one can show that for every M_{UL}, the CAF of mobile WiMAX signal at delays $\tau_{\mathrm{UL},i} = \lceil iD_{\mathrm{u}}/M_{\mathrm{UL}} \rceil$, $i = 1,\ 2,\ ...,\ M_{\mathrm{UL}}-1$, can be shown to be given by

$$R_r(\alpha,\tau_{\mathrm{UL},i}) = D_{\mathrm{F}}^{-1} a_{\mathrm{UL}}^2 \sigma_{\mathrm{UL},pd}^2 e^{-j2\pi(-\frac{K_{\mathrm{UL}}}{2}+S_p)\tau_{\mathrm{UL},i}/D_{\mathrm{u}}} e^{-j\pi M_{\mathrm{UL}}\tau_{\mathrm{UL},i}(K_{\mathrm{UL},p}-1)/D_{\mathrm{u}}} \frac{\sin(\pi M_{\mathrm{UL}}\tau_{\mathrm{UL},i}K_{\mathrm{UL},p}/D_{\mathrm{u}})}{\sin(\pi M_{\mathrm{UL}}\tau_{\mathrm{UL},i}/D_{\mathrm{u}})}$$

$$\times e^{-j2\pi\alpha D_{\mathrm{TG}}} \sum_{\lambda\in\mathcal{M}_{\mathrm{UL},p}} e^{-j2\pi\alpha\lambda D} \sum_n g(n)g^*(n+\tau_{\mathrm{UL},i})e^{-j2\pi\alpha n}, \qquad (2.40)$$

and the set of CFs as

$$\mathcal{K} = \{\alpha : \alpha = \nu D_{\mathrm{F}}^{-1},\ \nu \text{ integer}\}. \qquad (2.41)$$

Similarly, one can easily show that the CAF of the mobile WiMAX signal at delays $\overline{\tau}_{\mathrm{UL},i} = \lfloor iD_{\mathrm{u}}/M_{\mathrm{UL}} \rfloor$, $i = 1, 2, \ldots, M_{\mathrm{UL}}-1$ and the set of CFs are respectively given as

$$R_r(\alpha,\overline{\tau}_{\mathrm{UL},i}) = D_{\mathrm{F}}^{-1} a_{\mathrm{UL}}^2 \sigma_{\mathrm{UL},pd}^2 e^{-j2\pi(-\frac{K_{\mathrm{UL}}}{2}+S_p)\overline{\tau}_{\mathrm{UL},i}/D_{\mathrm{u}}} e^{-j\pi M_{\mathrm{UL}}\overline{\tau}_{\mathrm{UL},i}(K_{\mathrm{UL},p}-1)/D_{\mathrm{u}}} \frac{\sin(\pi M_{\mathrm{UL}}\overline{\tau}_{\mathrm{UL},i}K_{\mathrm{UL},p}/D_{\mathrm{u}})}{\sin(\pi M_{\mathrm{UL}}\overline{\tau}_{\mathrm{UL},i}/D_{\mathrm{u}})}$$

$$\times e^{-j2\pi\alpha D_{\mathrm{TG}}} \sum_{\lambda\in M_{\mathrm{UL},p}} e^{-j2\pi\alpha\lambda D} \sum_n g(n)g^*(n+\overline{\tau}_{\mathrm{UL},i})e^{-j2\pi\alpha n}, \qquad (2.42)$$

and

$$\mathcal{K} = \{\alpha : \alpha = \nu D_{\mathrm{F}}^{-1},\ \nu \text{ integer}\}. \qquad (2.43)$$

Case (4): Derivation of the analytical expressions for CAF at delays equal to integer multiples of the frame duration, D_{F}, and the corresponding set of CFs

We further investigate (2.6) for delays equal to integer multiples of D_{F}. At these delays, one can easily show that the only non-zero term corresponds to $E(u_{k_1}u_{k_2}^*)$ when $k_1 = k_2 (= k)$, which is due to the time repetition of the preamble every frame. Thus, (2.6) becomes

$$R_r(n,\tau)=a_{\mathrm{p}}^2\sigma_u^2\sum_{\substack{l_1=-\infty\\ l_1 \bmod N_{\mathrm{F}}=0}}^{\infty}\sum_{\substack{l_2=-\infty\\ l_2 \bmod N_{\mathrm{F}}=0}}^{\infty}\sum_{k=0}^{K_{\mathrm{P},d}-1} g(n-l_1D-l_1N_{\mathrm{F}}^{-1}D_{\mathrm{G}})$$
$$\times g^*(n-l_2D-l_2N_{\mathrm{F}}^{-1}D_{\mathrm{G}}+\tau)e^{j2\pi(3k-\frac{K_{\mathrm{P}}}{2}+S_{\mathrm{P},d})(n-l_1D-l_1N_{\mathrm{F}}^{-1}D_{\mathrm{G}})/D_u}$$
$$\times e^{-j2\pi(3k-\frac{K_{\mathrm{P}}}{2}+S_{\mathrm{P},d})(n-l_2D-l_2N_{\mathrm{F}}^{-1}D_{\mathrm{G}}+\tau)/D_u}. \qquad (2.44)$$

Note that at these delays $g(n-l_1D-l_1N_{\mathrm{F}}^{-1}D_{\mathrm{G}})g^*(n-l_2D-l_2N_{\mathrm{F}}^{-1}D_{\mathrm{G}}+\tau)=0$ unless $l_2-l_1=\tau N_F D_{\mathrm{F}}^{-1}$ (otherwise the pulses do not overlap, yielding zero product). Here we present two cases for illustration: (1) $\tau=D_{\mathrm{F}}$, $l_1=0$, and $l_2=2N_{\mathrm{F}}$: this yields $g(n)g^*(n-2N_{\mathrm{F}}D-2D_{\mathrm{G}}+D_{\mathrm{F}})=g(n)g^*(n-D_{\mathrm{F}})=0$. (2) $\tau=D_{\mathrm{F}}$, $l_1=0$, and $l_2=N_{\mathrm{F}}$: this yields $g(n)g^*(n-N_{\mathrm{F}}D-D_{\mathrm{G}}+D_{\mathrm{F}})=g(n)g^*(n)\neq 0$. Based on the above observation, by using that $D_{\mathrm{F}}=N_{\mathrm{F}}D+D_{\mathrm{G}}$, and after some mathematical manipulations, (2.44) can be re-expressed as

$$R_r(n,\tau)=a_{\mathrm{p}}^2\sigma_u^2K_{\mathrm{P},d}\,g(n)g^*(n)\otimes\sum_{\nu=-\infty}^{\infty}\delta(n-\nu D_{\mathrm{F}}). \qquad (2.45)$$

Furthermore, by following the same steps as in cases (1)-(3) one obtains

$$\Im\{R_r(n,\tau)\}=D_{\mathrm{F}}^{-1}a_{\mathrm{p}}^2\sigma_u^2K_{\mathrm{P},d}\sum_n|g(n)|^2e^{-j2\pi\alpha n}\sum_{\nu=-\infty}^{\infty}\delta(\alpha-\nu D_{\mathrm{F}}^{-1}), \qquad (2.46)$$

and, thus, the CAF and set of CFs are given respectively as

$$R_r(\alpha,\tau)=D_{\mathrm{F}}^{-1}a_{\mathrm{p}}^2\sigma_u^2K_{\mathrm{P},d}\sum_n|g(n)|^2e^{-j2\pi\alpha n}, \qquad (2.47)$$

and

$$\mathcal{K} = \{\alpha : \alpha = \nu D_F^{-1},\ \nu \text{ integer}\}. \tag{2.48}$$

To sum up, for the closed form expressions for the CAF and corresponding set of CFs of mobile WiMAX OFDM-based signals, one can refer to equations:

- (2.11) and (2.12) for Case (1);

- (2.22) and (2.23), and (2.24) and (2.25) for Case (2);

- (2.36) and (2.37), (2.38) and (2.39), (2.40) and (2.41), and (2.42) and (2.43) for Case (3); and

- (2.47) and (2.48) for Case (4), each of the 4 cases corresponding to certain delays.

2.3.3. OFDM Parameters of the Mobile WiMAX Signals

The OFDM parameters for mobile WiMAX signals are presented in Table 2.1. As one can notice, the FFT size is scalable with the bandwidth: when the available bandwidth increases, the FFT size also increases such that the subcarrier spacing is fixed. This in turn leads to a constant useful OFDM symbol duration.

Table 2.1. OFDM parameters for the mobile WiMAX signal [19].

Channel bandwidth (MHz)	1.25	5	10	20
FFT size	128	512	1024	2048
Subcarrier spacing Δf (kHz)	10.94			
Useful symbol time (μs)	91.4			

2.3.4. CAF and CFs of Mobile WiMAX Signal: Comparison between Analytical and Simulation Results

In the following, the analytical results obtained in Subsection 2.3.2 for the CAF and CFs of mobile WiMAX OFDM-based signals are compared with results obtained from simulations. We consider mobile WiMAX signals with 5 MHz double-sided bandwidth and 512 subcarriers. The CP duration equals 1/8 of the useful OFDM symbol duration. The data subcarriers are modulated using 16-QAM with unit variance constellation. The scheme employed for the subcarrier mapping in both DL and UL subframes is the partial usage of subchannels [18]. Boosted pilots are transmitted only in the downlink OFDM symbols every 14th subcarriers. In the even DL OFDM symbols, two sets of pilot symbols are transmitted. With both sets, the pilot symbols are transmitted every 14th subcarriers. Each set a has different value of S_p. The values of S_p are 5 and 9 respectively. In the odd DL OFDM symbols, two sets of pilot symbols are transmitted. With both sets, the pilot symbols are transmitted every 14 subcarriers. Each set has a different value of S_p. The values of S_p are 1 and 13 respectively. A raised root cosine pulse shape window with 0.025 roll-off factor is employed at the transmit-side. The number of symbols in the DL and UL subframes equals 35 and 12, respectively. The RTG duration is $D_{\mathrm{RG}} = 60\mu s \times f_s$ whereas the TTG duration equals $D_{\mathrm{F}} - N_{\mathrm{F}}D - D_{\mathrm{RG}}$ [16]. The signal is oversampled with a factor of 28/25 [16]. Table 2.2 summarizes the second order cyclostationarity of the mobile WiMAX signal with the chosen parameters.

Table 2.2. Second-order cyclostationarity of the mobile WiMAX signal with the parameters given in Section 2.3.4.

Delay	CFs	Dependency of the CFs with non-zero and considerable CAF magnitude
$\tau = 0$ and $\tau = D_u = 512$ ($T_u = 91.4$ μs) (Case(1))	νD_F^{-1}, ν integer, $D_F = 28{,}000$	CAF magnitude at CFs close to integer multiples of D^{-1} predominates, (depends on D[8]).
$\tau_i = \lceil iD_u / 3 \rceil$, $i = 1, 2$, i.e., $\tau_1 = 171$ (30.54 μs) and $\tau_2 = 342$. (Case(2))	νD_F^{-1}, ν integer	Depends on D_F.
$\overline{\tau}_i = \lfloor iD_u / 3 \rfloor$, $i = 1, 2$, i.e., $\overline{\tau}_1 = 170$ and $\overline{\tau}_2 = 341$. (Case(2))	νD_F^{-1}, ν integer	Depends on D_F.
$\tau_{DL,i} = \lceil iD_u / M_{DL} \rceil$, $i = 1, 2, \ldots, M_{DL}-1$, $M_{DL} = 14$ (Case(3))[9]	νD_F^{-1}, ν integer	CAF magnitude at CFs close to integer multiples of $(2D)^{-1}$ predominates, (depends on the distribution of the pilot symbols)
$\overline{\tau}_{DL,i} = \lfloor iD_u / M_{DL} \rfloor$, $i = 1, 2, \ldots, M_{DL}-1$, $M_{DL} = 14$ (Case(3))[9]	νD_F^{-1}, ν integer	CAF magnitude at CFs close to integer multiples of $(2D)^{-1}$ predominates, (depends on the distribution of the pilot symbols)
$\tau = \mu D_F$, μ integer, $D_F = 28{,}000$ ($T_F = 5$ ms) (Case(4))	νD_F^{-1}, ν integer	Depends on D_F.

The estimated results are obtained without noise and channel dispersion, with a relatively large observation interval (500 ms). The theoretical and estimated CAF magnitude for the Mobile WiMAX OFDM-based signal at zero CF versus delay is shown in Fig. 2.5 a) and b), respectively. As expected, one can see from Fig. 2.5 that the CAF magnitude has a peak at $\tau = D_u = 512$ (due to the existence of CP, Case (1)), peaks at $\tau = \lceil 512/3 \rceil = 171$, $\tau = \lfloor 512/3 \rfloor = 170$, $\tau = \lceil 1024/3 \rceil = 342$, and $\tau = \lfloor 1024/3 \rfloor = 341$ (due to the structure of

[8] Note that the OFDM symbol duration depends on the CP duration ($D = D_u + D_{cp}$).

[9] Note that in Case (3), not only the CFs depend on the distribution of the pilot subcarriers, but also the delays.

the preamble symbol in the frequency domain, Case (2)), peaks at $\tau = \lceil 512i/14 \rceil$ and $\tau = \lfloor 512i/14 \rfloor$, $i =$ 1, 2,..., 13, (due to the transmission of boosted pilot symbols every 14th subcarrier in the DL OFDM symbols, Case (3)). Furthermore, we have checked that there is a peak in the CAF of mobile WiMAX signal at $\tau = D_F = 28000$, which is not shown in Fig. 2.4 because of the large required range.

Figs. 2.6 to 2.9 show the theoretical and estimated CAF magnitude of the mobile WiMAX signal versus CF at delays equal to $\tau = D_u = 512$ (Case (1)), $\tau = \lceil 512/3 \rceil = 171$ (as an example for Case (2)), $\tau = \lceil 3 \times 512/14 \rceil = 110$ (as an example for Case (3)), and $\tau = 28000$ (Case (4)), respectively. Note that the estimated CAFs in Figs. 2.6 to 2.9 are given for CFs (νD_F^{-1}, ν integer). Furthermore, we estimated the CAF for non-CFs and a reasonably large observation interval (0.5 ms), and $R(\alpha, \tau) \approx 0$ is always the case for non-CFs.

As one can see from Figs. 2.6 a) and b), the CAF magnitude of the mobile WiMAX OFDM signal at delay equal to the useful OFDM symbol duration has CFs at νD_F^{-1}, ν integer. Due to the CP, there seems to be a periodicity in the autocorrelation function of the mobile WiMAX signal with period D; nevertheless, the existence of the transitions gaps in the WiMAX frame impairs this periodicity. As such, the CAF has CFs at νD_F^{-1}, ν integer. However, the CAF magnitude at CFs close to integer multiples of D^{-1} predominates. This can be explained based on the short duration of the transition gaps when compared with the frame duration.

As it can be seen from Figs. 2.7 a) and b), and 2.9 a) and b), the CAF magnitude of the mobile WiMAX OFDM signal has CFs at νD_F^{-1}, ν integer, at $\tau = 171$ and $\tau = 28000$, respectively.

This is due to the periodicity of the autocorrelation function at these delays with period D_F, as the correlation due to the preamble in both cases repeats every frame.

As it can be revealed from Figs. 2.8 a) and b), the CAF magnitude of the mobile WiMAX OFDM signal at $\tau = 110$ has CFs at νD_F^{-1}, ν integer, as expected from the theoretical findings. Due to the distribution of the pilot symbols which repeats every 2 OFDM symbols, there seems to be a periodicity in the autocorrelation function of the mobile WiMAX signals with period $2D$; nevertheless; the existence of this periodicity only in the DL OFDM symbols impairs it. As such, the CAF has CFs at νD_F^{-1}, ν integer. However, the CAF magnitude at CFs close to integer multiples of $1/2D$ predominates. This can be explained based on the relatively large number of DL OFDM symbols in the frame.

2.4. Summary

In this chapter, a description of the structure of the mobile WiMAX OFDM-based signals and a signal model of these signals are provided. Furthermore, the second-order cyclostationarity of the mobile WiMAX signals is investigated and closed-from expressions for the CAF and CFs are derived. Finally, we compare analytical findings with simulation results, which are in agreement.

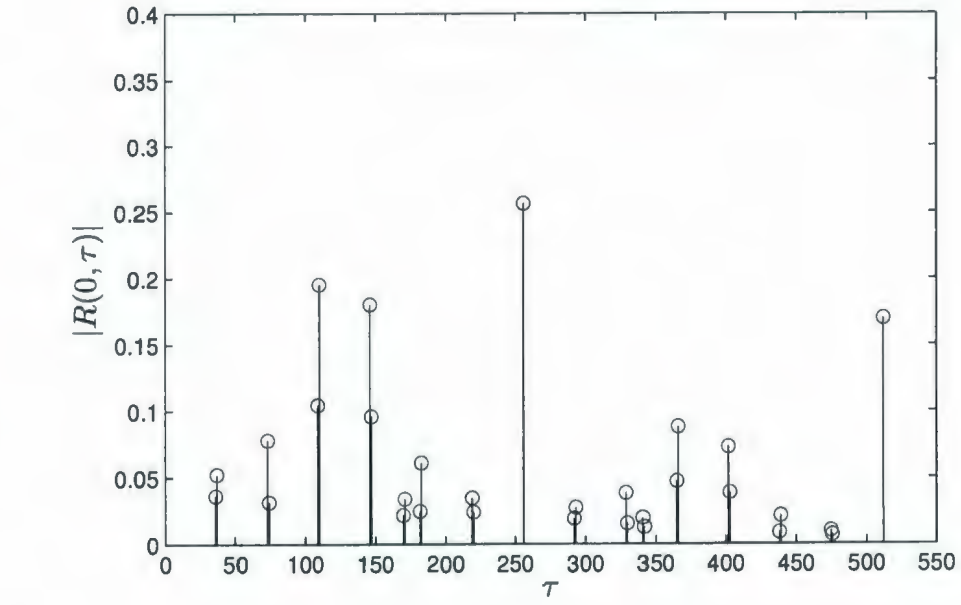

a)

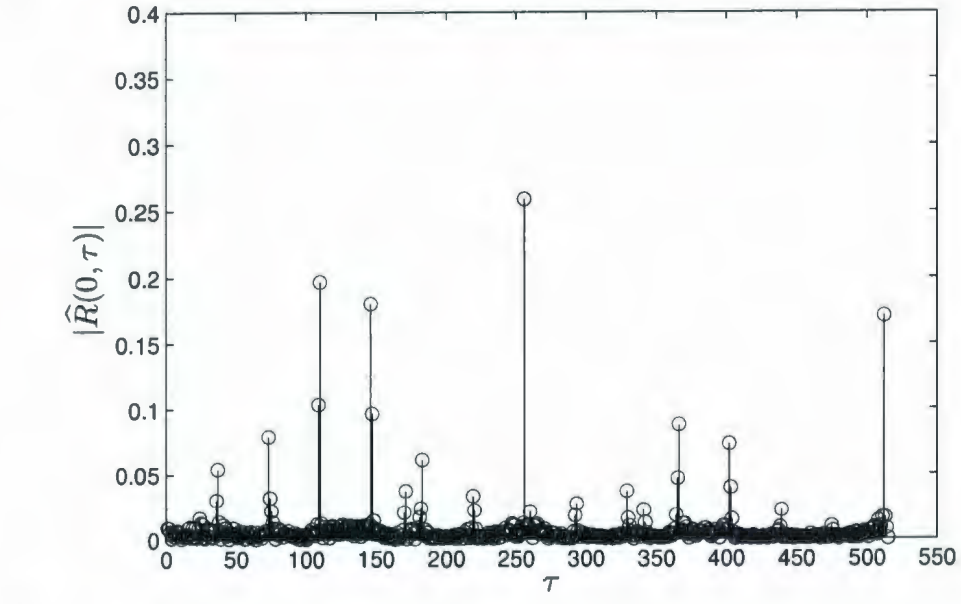

b)

Fig. 2.5. The CAF magnitude for the mobile WiMAX signal at $\alpha = 0$ versus delay a) theoretical b) estimated.

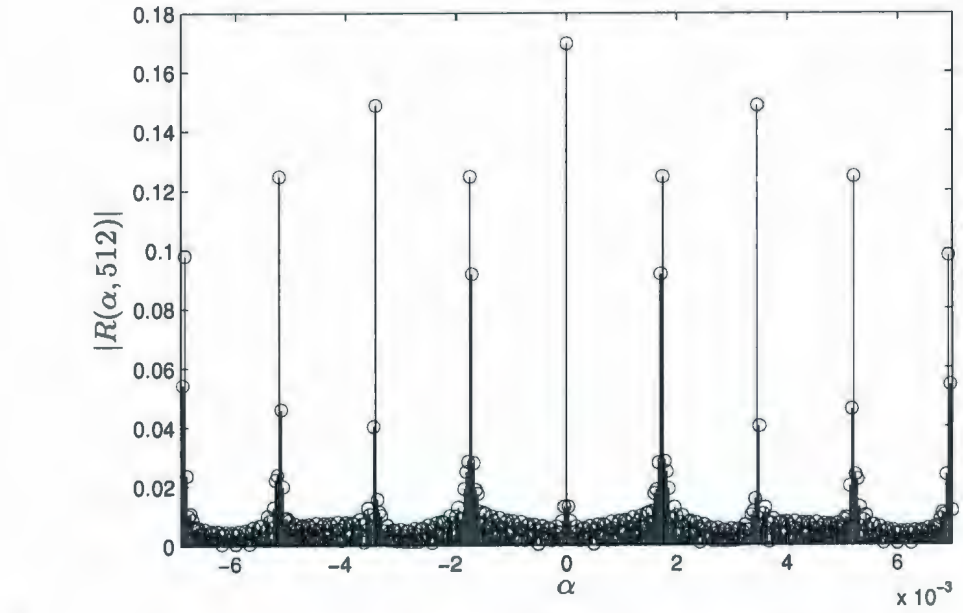

a)

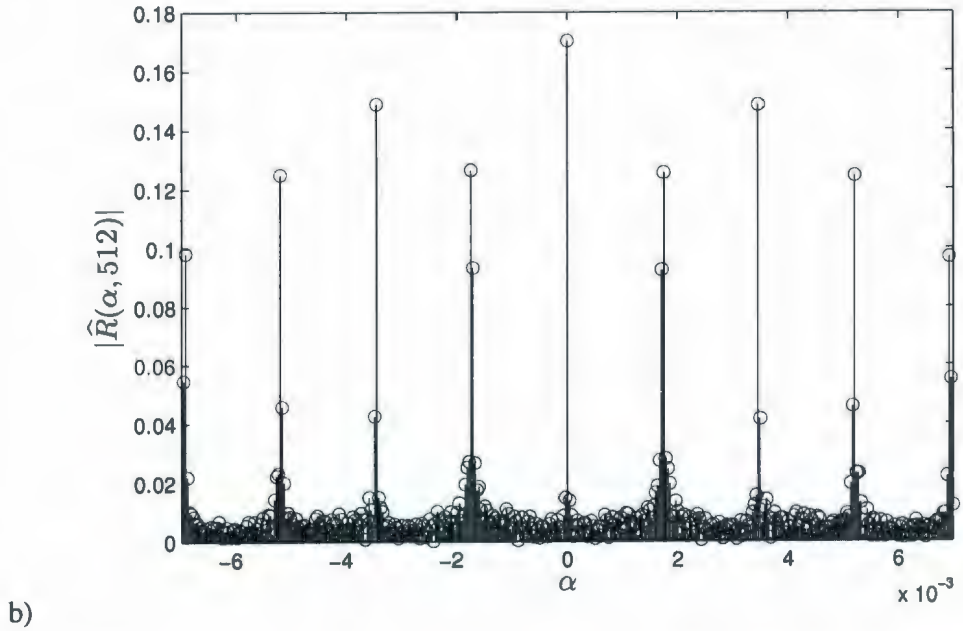

b)

Fig. 2.6. The CAF magnitude for the mobile WiMAX signal at $\tau = D_u = 512$ versus CF a) theoretical b) estimated.

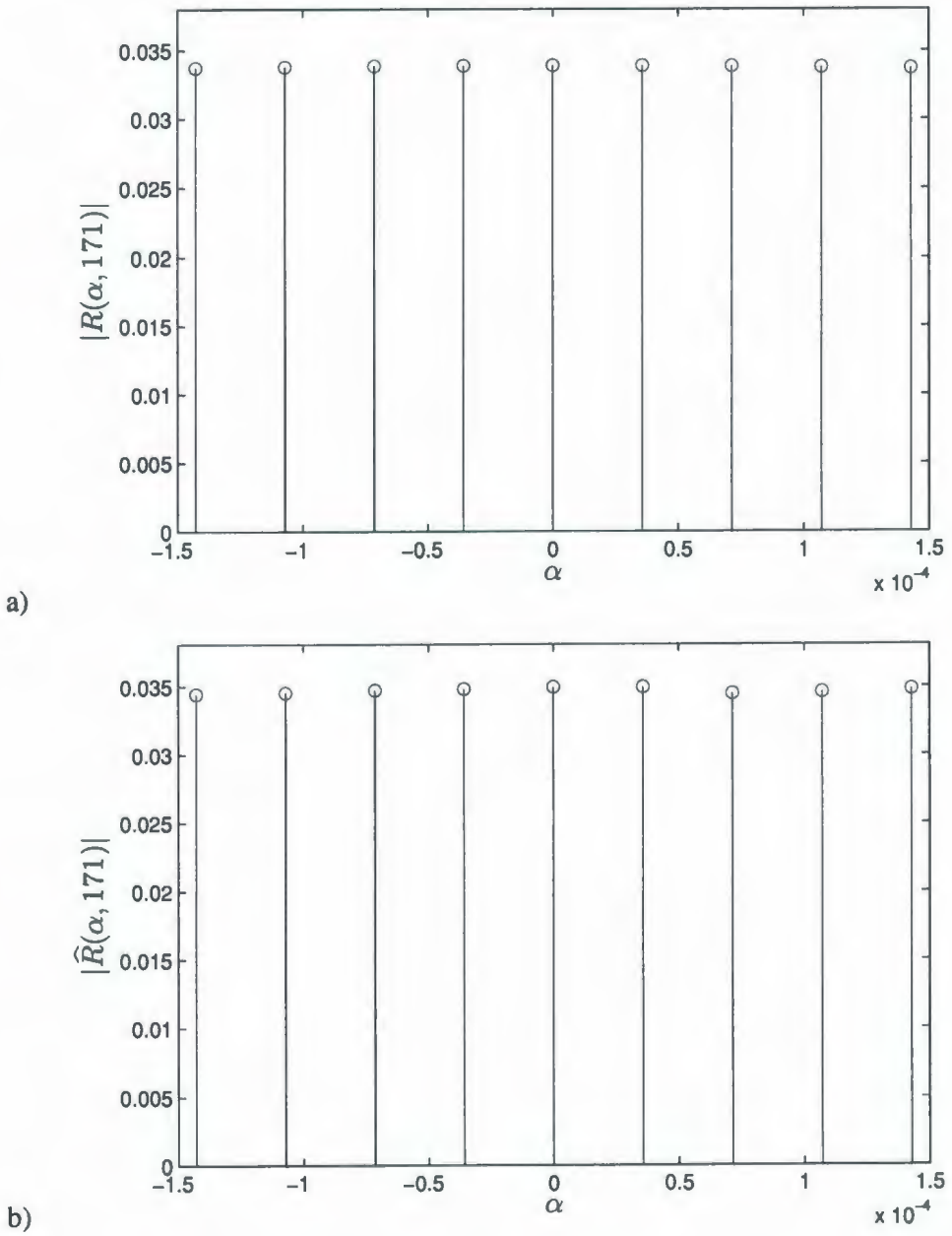

Fig. 2.7. The CAF magnitude for the mobile WiMAX signal at $\tau = \lceil 512/3 \rceil = 171$ versus CF a) theoretical b) estimated.

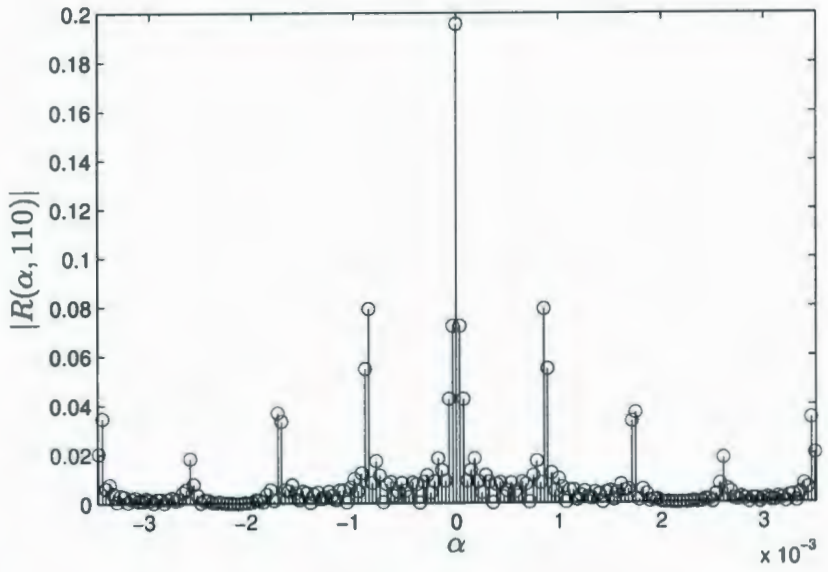

a)

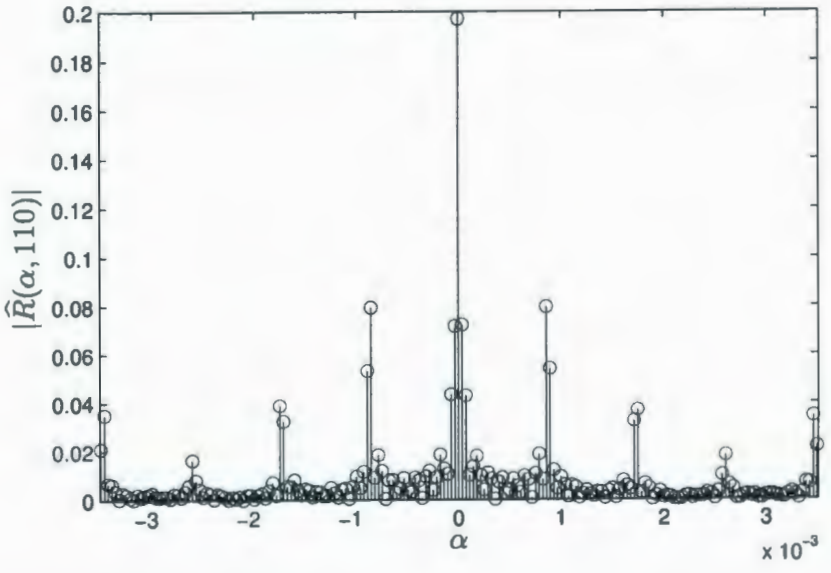

b)

Fig. 2.8. The CAF magnitude for the mobile WiMAX signal at $\tau = \lceil 3 \times 512/14 \rceil = 110$ versus CF a) theoretical b) estimated.

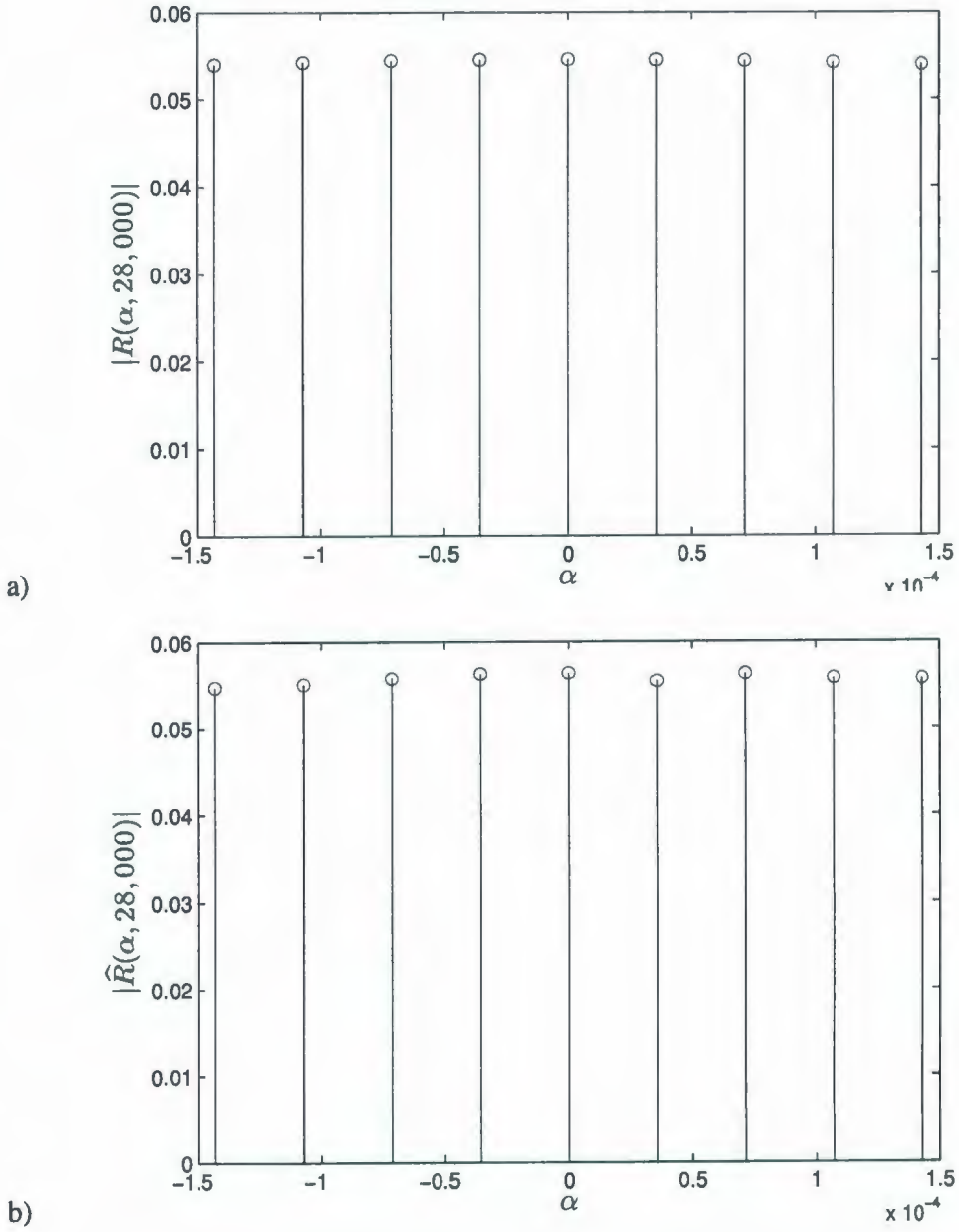

Fig. 2.9. The CAF magnitude for the mobile WiMAX signal at $\tau = D_F = 28000$ versus CF a) theoretical b) estimated.

Chapter 3

Second-Order Cyclostationarity of the OFDM-based LTE Signals

3.1. Introduction

LTE is the one of the most popular standards that uses the OFDM at the physical layer of its DL traffic. Scalable OFDM is employed, which allows bandwidth scalability [22], [23]. This chapter starts with a description of the OFDM-based LTE signals and their structure. Then, signal models for such signals are provided. Furthermore, the second-order cyclostationarity of these signals is studied and closed form expressions for their CAF and corresponding set of CFs are derived. Finally, the CAF results obtained from both analytical findings and computer simulations are presented.

3.2. OFDM-based LTE Signal Model

3.2.1. Signal Description

Fig. 3.1 shows the FDD DL frame structure used in the LTE systems [22]. The frame time duration is 10 ms, and each frame is divided into 20 slots, with the slot duration equal to 0.5 ms.

Each slot contains N_{symb}^{DL} OFDM symbols, where N_{symb}^{DL} depends on the CP length and useful symbol duration (equal to the reciprocal of the subcarrier frequency spacing) parameters of the OFDM signal. The LTE standard allows multimedia broadcast multicast services be performed either in a single cell mode or in a multi-cell mode. For the latter, transmissions from different cells are synchronized to form a Multicast Broadcast Single Frequency Network (MBSFN) [22]. Here we consider the case where a single operational mode is employed in each cell, i.e., either MBSFN or non-MBSFN [22]. The MBSFN mode uses either $\Delta f = 7.5$ KHz or 15 kHz subcarrier spacing and long CP, with $N_{symb}^{DL} = 3$ and $N_{symb}^{DL} = 6$, respectively. On the other hand, the non-MBSFN mode employs $\Delta f = 15$ kHz subcarrier spacing and either short or long CP. With the long CP $N_{symb}^{DL} = 6$, while with the short CP $N_{symb}^{DL} = 7$. The ratio between the CP length and the useful OFDM symbol duration T_{cp} / T_u equals 1/4 for long CP, while for short CP this is 10/128 for the first OFDM symbol in the slot and 9/128 for the remaining OFDM symbols in the slot. Table 3.1 summarizes the different LTE operation modes along with their parameters.

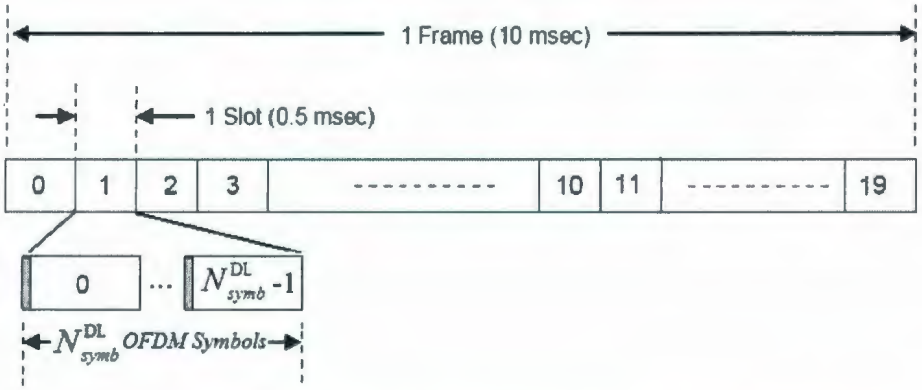

Fig. 3.1. The FDD downlink frame structure in the LTE OFDM-based systems.

Table 3.1. Operation modes of the LTE signals and associated parameters[10].

Operation mode	Associated CP length	Associated subcarrier spacing (Δf)
Non-MBSFN	Long CP	15 kHz
	Short CP	
MBSFN	Long CP	15 kHz
		7.5 kHz

The slot structure and associated resource grid used in the FDD downlink frame are illustrated in Fig. 3.2.

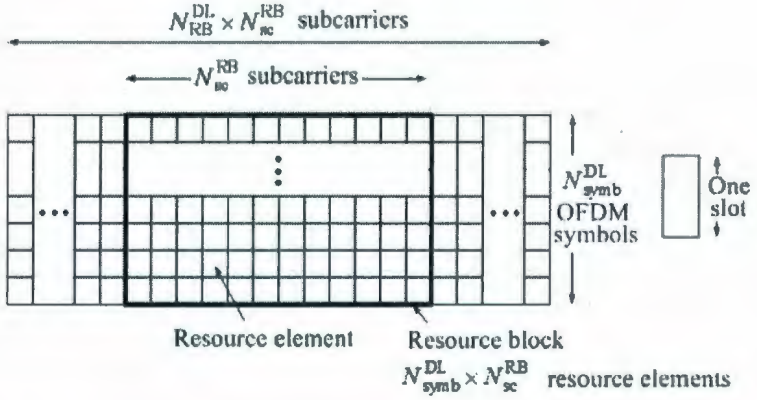

Fig. 3.2. The slot structure and resource grid in the FDD downlink frame (modified from [22]).

The slot can be represented as a two dimensional resource grid consisting of N_{symb}^{DL} OFDM symbols in time domain and $K = N_{RB}^{DL} N_{sc}^{RB}$ subcarriers in frequency domain, with N_{RB}^{DL} as the number of resource blocks and N_{sc}^{RB} as the number of subcarriers in a resource block. Note that K represents the number of subcarriers in an OFDM symbol. A resource block is defined as N_{symb}^{DL} consecutive OFDM symbols in time domain and N_{sc}^{RB} consecutive

[10] Henceforth, the LTE signal will be referred to, by its distinctive features, i.e., we will have 4 different possible combinations of the different modes/parameters, which are non-MBSFN with long CP, non-MBSFN with short CP, MBSFN with $\Delta f = 15$ kHz, and MBSFN and $\Delta f = 7.5$ kHz.

subcarriers in frequency domain. N_{sc}^{RB} equals 12 and 24 for the LTE signals with $\Delta f = 15$ kHz and 7.5 kHz subcarrier spacing, respectively. N_{RB}^{DL} then depends on the signal bandwidth; for possible values of this parameter the reader is referred to [23]. The smallest entity of the resource grid is called resource element; a resource block consists of $N_{symb}^{DL} \times N_{sc}^{RB}$ resource elements.

Reference signals (RSs) are embedded in the resource blocks of the transmission frame for channel estimation and cell search/ acquisition purposes [22]. An RS is assigned to each cell of the network and acts as a cell identifier. Therefore, the RS repeats each downlink frame. Here we study two types of RSs: the cell-specific RS associated with the non-MBSFN mode and the MBSFN RS associated with the MBSFN mode. Note that the terminology used here is according to [22]. The RSs are interspersed over the resource elements, usually transmitted on some of the subcarriers of one or two non-consecutive symbols in each slot. Figs. 3.3 to 3.6 show the distribution of the RSs over one resource block and two consecutive slots. Fig. 3.3 shows the distribution of the cell-specific RS for long CP over one resource block and two consecutive slots ($N_{symb}^{DL} = 6$ OFDM symbols per slot and $N_{sc}^{RB} = 12$ subcarriers per resource block): the cell-specific RS is transmitted on the first and seventh subcarriers of the first OFDM symbol and on the fourth and tenth subcarriers of the fourth OFDM symbol in each slot. Fig. 3.4 shows the distribution of the cell-specific RS for short CP over one resource block and two consecutive slots ($N_{symb}^{DL} = 7$ OFDM symbols per slot and $N_{sc}^{RB} = 12$ subcarriers per resource block): the cell-specific RS is transmitted on the first and seventh subcarriers of the first OFDM symbol and on the fourth and tenth subcarriers of the fifth OFDM symbol in each slot. Fig. 3.5 shows the

distribution of the MBSFN RS over one resource block and two consecutive slots of LTE signal with $\Delta f = 15$ KHz ($N_{symb}^{DL} = 6$ OFDM symbols per slot and $N_{sc}^{RB} = 12$ subcarriers per resource block): the MBSFN RS is transmitted every second subcarrier starting from the first subcarrier in the third OFDM symbol of the odd-numbered slots and the fifth OFDM symbol of the even-numbered slots. Also the MBSFN RS is transmitted every second subcarrier starting from the second subcarrier in the first OFDM symbol of the even-numbered slots. Finally, Fig. 3.6 shows the distribution of the MBSFN RS over one resource block and two consecutive slots of LTE signal with $\Delta f = 7.5$ KHz ($N_{symb}^{DL} = 3$ OFDM symbols per slot and $N_{sc}^{RB} = 24$ subcarriers per resource block): the MBSFN RS is transmitted every second subcarrier starting from the first subcarrier in the second OFDM symbol of the odd-numbered slots and the third OFDM symbol of the even-numbered slots. Also the MBSFN RS is transmitted every fourth subcarrier starting from the third subcarrier in the first OFDM symbol of the even-numbered slots.

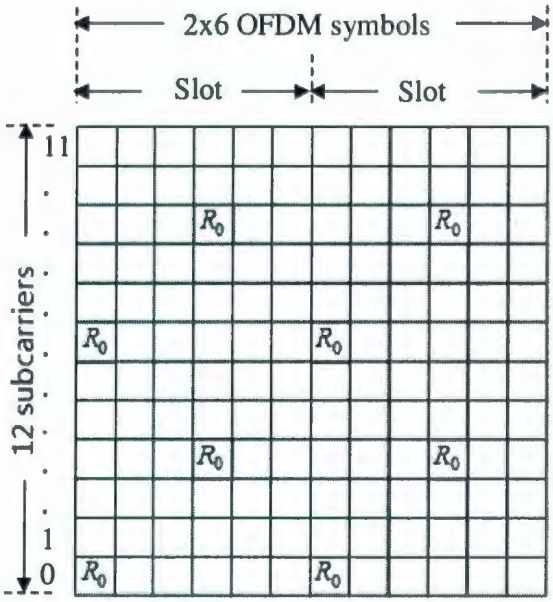

Fig. 3.3. Resource element mapping of cell-specific RS in LTE signal with non-MBSFN mode and long CP (taken from [22]).

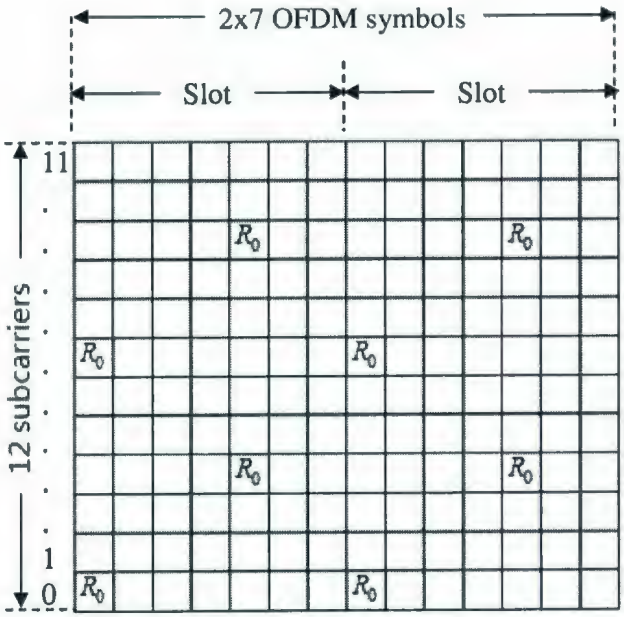

Fig. 3.4. Resource element mapping of cell-specific RS in LTE signal with non-MBSFN mode and short CP (taken from [22]).

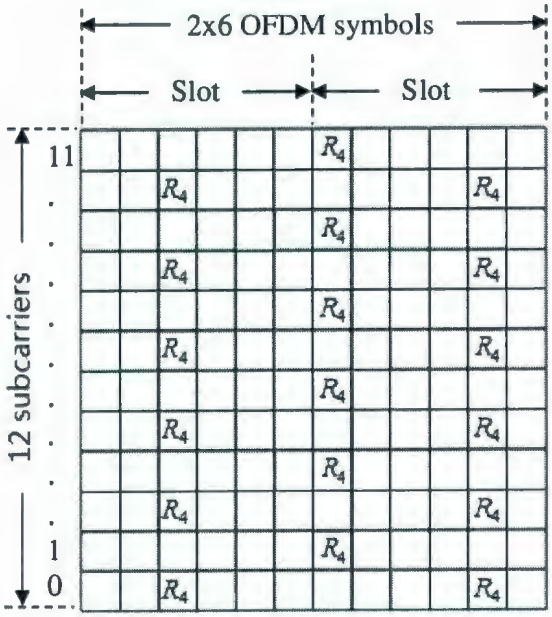

Fig. 3.5. Resource element mapping of MBSFN RS in LTE signal with MBSFN mode and $\Delta f = 15$ KHz (taken from [22]).

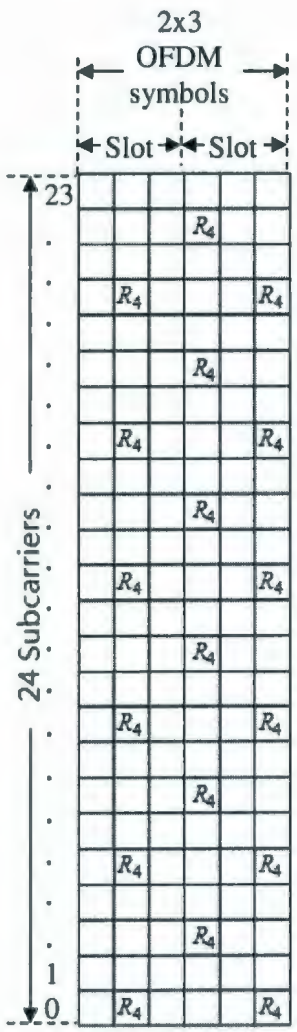

Fig. 3.6. Resource element mapping of MBSFN RS in LTE signal with MBSFN mode and $\Delta f = 7.5$ KHz (taken from [22]).

3.2.2. Signal Model for the LTE Signals with Long CP

According to the above description, a general model for the LTE OFDM signals with long CP and any RS distribution is provided here. This model includes LTE signals with non-MBSFN mode and long CP and LTE signals with MBSFN mode (these signals have a similar structure, with different parameters values and RS distributions). The corresponding discrete-time signal at the receive-side, affected by additive Gaussian noise, can be expressed as,

$$
\begin{aligned}
r(n) = a[& \sum_{\substack{l=-\infty \\ l \bmod N_z = \beta \in \mathcal{Z}_1}}^{\infty} \sum_{\substack{k=-K/2, k\neq 0 \\ k \in A_1}}^{K/2} b_{k,l} g(n-lD) e^{j2\pi k(n-lD)/D_u} \\
& + \sum_{\substack{l=-\infty \\ l \bmod N_z = \beta \in \mathcal{Z}_1}}^{\infty} \sum_{\substack{k=-K/2, k\neq 0 \\ k \in A_1}}^{K/2} c_{k,l} g(n-lD) e^{j2\pi k(n-lD)/D_u}] \\
& + a[\sum_{\substack{l=-\infty \\ l \bmod N_z = \beta \in \mathcal{Z}_2}}^{\infty} \sum_{\substack{k=-K/2, k\neq 0 \\ k \in A_2}}^{K/2} b_{k,l} g(n-lD) e^{j2\pi k(n-lD)/D_u} \\
& + \sum_{\substack{l=-\infty \\ l \bmod N_z = \beta \in \mathcal{Z}_2}}^{\infty} \sum_{\substack{k=-K/2, k\neq 0 \\ k \in A_2}}^{K/2} c_{k,l} g(n-lD) e^{j2\pi k(n-lD)/D_u}] \\
& + a \sum_{\substack{l=-\infty \\ l \bmod N_z = \beta \notin \mathcal{Z}_1, \mathcal{Z}_2}}^{\infty} \sum_{k=-K/2, k\neq 0}^{K/2} b_{k,l} g(n-lD) e^{j2\pi k(n-lD)/D_u} + w(n),
\end{aligned}
\tag{3.1}
$$

where a is the amplitude factor equal to $1/\sqrt{K}$, N_z is the repetition period for the RS distribution (in number of OFDM symbols), which equals either N_{symb}^{DL} or $2N_{symb}^{DL}$, $\mathcal{Z}_1$ and $\mathcal{Z}_2$ are the sets of the OFDM symbols in which the RS is transmitted, A_1 and A_2 are the sets of subcarriers on which the RS is transmitted in the OFDM symbols belonging to $\mathcal{Z}_1$ and $\mathcal{Z}_2$, respectively, D is the OFDM symbol period equal to the useful symbol duration,

D_u, plus the CP length, D_{cp}, $g(n)$ is the impulse response of the transmit and the receive filters in cascade, $b_{k,l}$ and $c_{k,l}$ are the data and RS symbols transmitted on the kth subcarrier and within the lth OFDM symbol, respectively, and $w(n)$ is the additive zero-mean Gaussian noise. Note that the data symbols $b_{k,l}$ are taken either from a QAM or PSK signal constellation, while the RS symbols $c_{k,l}$ are taken from the BPSK signal constellation. Both data and RS symbols are zero-mean i.i.d. random variables.

To ease the understanding of the expressions for the signal model in (3.1), here we provide an explanation for that. In all the terms on the right hand-side of (3.1), the inner summation is over the number of subcarriers, while the outer summation is over the OFDM symbol index. The first four terms model the OFDM symbols which include RS, while the fifth term expresses the remaining OFDM symbols. In the OFDM symbols with RS, there can be only two different assignments of the RS symbols on subcarriers. As such, the second and fourth terms in (3.1) represent the subcarriers where the RS is induced for the two possible assignments, whereas the first and third terms represent the data subcarriers within the same OFDM symbols. Here, we give the values of the parameters N_z, $\mathcal{Z}_1$, $\mathcal{Z}_2$, for each of the cases in Figs 3.3, 3.5, and 3.6. The values of N_z are 6, 12, and 6, respectively. The values of $\mathcal{Z}_1$ are {0}, {2, 10}, and {1, 5}, respectively. The values of $\mathcal{Z}_2$ are {3}, {6}, and {3}, respectively.

3.2.3. Signal Model for the non-MBSFN LTE Signals with Short CP

According to the above description for the LTE signal, a model for the LTE OFDM signal with short CP and RS distribution as in Fig. 3.4 is provided here. The corresponding discrete-time signal at the receive-side, affected by additive Gaussian noise, can be expressed as,

$$
\begin{aligned}
r(n) = a & \sum_{\substack{l=-\infty \\ l \bmod N_z=\beta=0}}^{\infty} \sum_{\substack{k=-K/2,k\neq 0 \\ k\in A_1}}^{K/2} b_{k,l} g_1(n - lN_z^{-1}D_z) e^{j2\pi k(n-lN_z^{-1}D_z)/D_u} \\
& + a \sum_{\substack{l=-\infty \\ l \bmod N_z=\beta=0}}^{\infty} \sum_{\substack{k=-K/2,k\neq 0 \\ k\in A_1}}^{K/2} c_{k,l} g_1(n - lN_z^{-1}D_z) e^{j2\pi k(n-lN_z^{-1}D_z)/D_u} \\
& + a \sum_{\substack{l=-\infty \\ l \bmod N_z=\beta=4}}^{\infty} \sum_{\substack{k=-K/2,k\neq 0 \\ k\in A_2}}^{K/2} b_{k,l} g(n - \lfloor lN_z^{-1} \rfloor D_z - 3D - D_1) e^{j2\pi k(n-\lfloor lN_z^{-1} \rfloor D_z-3D-D_1)/D_u} \\
& + a \sum_{\substack{l=-\infty \\ l \bmod N_z=\beta=4}}^{\infty} \sum_{\substack{k=-K/2,k\neq 0 \\ k\in A_2}}^{K/2} c_{k,l} g(n - \lfloor lN_z^{-1} \rfloor D_z - 3D - D_1) e^{j2\pi k(n-\lfloor lN_z^{-1} \rfloor D_z-3D-D_1)/D_u} \\
& + a \sum_{\substack{l=-\infty \\ l \bmod N_z=\beta\neq 0,4}}^{\infty} \sum_{k=-K/2,k\neq 0}^{K/2} b_{k,l} g(n - \lfloor lN_z^{-1} \rfloor D_z - (\beta-1)D - D_1) \\
& \times e^{j2\pi k(n-\lfloor lN_z^{-1} \rfloor D_z-(\beta-1)D-D_1)/D_u} + w(n),
\end{aligned}
\tag{3.2}
$$

where $N_z = 7$ in this case, which corresponds to the number of OFDM symbols in one slot, $g_1(n)$ is the transmit pulse shape window (associated with the first symbol in the slot) and the impulse response of the receive filter in cascade, $g(n)$ is the transmit pulse shape window (associated with remaining symbols in the slot) and the impulse response of the receive filter in cascade, D_1, D, and D_z here are the duration of the first OFDM symbol in the slot, the duration of the remaining OFDM symbols in the slot, and the

duration of the slot, respectively. To ease the understanding of the expressions for the signal model in (3.2), here we provide an explanation for that. In all the terms on the right hand-side of (3.2), the inner summation is over the number of subcarriers, while the outer summation is over the OFDM symbol index. The first two terms model the first OFDM symbol in the slot, which includes data and RS symbols, respectively. The first term represents the subcarriers where data symbols are transmitted, while the second term represents those where RS symbols are transmitted. Furthermore, for the position of the first symbol in the slot, we need to take into account the duration of the preceding slots, which yields the shift of $g_1(n)$ and $e^{j2\pi k/D_u}$ by $lN_z^{-1}D_z$, with $\left\lfloor lN_z^{-1} \right\rfloor = lN_z^{-1}$ providing the slot index. Similarly, the third and fourth terms model the fifth OFDM symbol in the slot, which includes data and RS symbols. Furthermore, for the position of the fifth symbol in the slot, we need to take into account the duration of the preceding slots, as well as the duration of the preceding OFDM symbols in the same slot, which are the first OFDM symbol in the slot, D_1 (which is longer than the other symbols) along with other 3 OFDM symbols, $3D$. This yields the shift of $g(n)$ and $e^{j2\pi k/D_u}$ by $\left\lfloor lN_z^{-1} \right\rfloor D_z + 3D + D_1$. The fifth term expresses the remaining OFDM symbols where only data symbols are transmitted. Here, for the position of the OFDM symbol in the slot, we need to take into account the duration of the preceding slots, as well as the duration of the preceding OFDM symbols in the same slot, which are the first OFDM symbol in the slot, D_1, along with other $(\beta - 1)$ OFDM symbols, $(\beta - 1)D$. This yields the shift of $g(n)$ and $e^{j2\pi k/D_u}$ by $\left\lfloor lN_z^{-1} \right\rfloor D_z + (\beta - 1)D + D_1$.

3.3. Second-Order Cyclostationarity of the OFDM-based LTE Signals

3.3.1. Second-Order Cyclostationarity of LTE signals with Long CP

By using the signal model in (3.1), the autocorrelation function of $r(n)$ can be expressed as the sum of the autocorrelation functions corresponding to any two signal components, signal and noise components, and noise component,

$$
\begin{aligned}
R_r(n,\tau) = a^2 & \sum_{\substack{l_1=-\infty \\ l_1 \bmod N_z=\beta\in\mathcal{Z}_1}}^{\infty} \sum_{\substack{l_2=-\infty \\ l_2 \bmod N_z=\beta\in\mathcal{Z}_1}}^{\infty} \sum_{\substack{k_1=-K/2,k_1\neq 0 \\ k_1\in A_1}}^{K/2} \sum_{\substack{k_2=-K/2,k_2\neq 0 \\ k_2\in A_1}}^{K/2} E(b_{l_1,k_1} b^*_{l_2,k_2}) \\
& \times g(n-l_1D)e^{j2\pi k_1(n-l_1D)/D_u} g^*(n-l_2D+\tau)e^{-j2\pi k_2(n-l_2D+\tau)/D_u} \\
& + a^2 \sum_{\substack{l_1=-\infty \\ l_1 \bmod N_z=\beta\in\mathcal{Z}_1}}^{\infty} \sum_{\substack{l_2=-\infty \\ l_2 \bmod N_z=\beta\in\mathcal{Z}_1}}^{\infty} \sum_{\substack{k_1=-K/2,k_1\neq 0 \\ k_1\in A_1}}^{K/2} \sum_{\substack{k_2=-K/2,k_2\neq 0 \\ k_2\in A_1}}^{K/2} E(c_{l_1,k_1} c^*_{l_2,k_2}) \\
& \times g(n-l_1D)e^{j2\pi k_1(n-l_1D)/D_u} g^*(n-l_2D+\tau)e^{-j2\pi k_2(n-l_2D+\tau)/D_u} \\
& + \ldots + E(w(n)w^*(n+\tau)),
\end{aligned}
\tag{3.3}
$$

where $E(.)$ is the expectation operator. To ease the understanding of (3.3), here we provide an explanation. The first term on the right hand side represents the autocorrelation of the first term on the right hand side of (3.1). The second shown term represents the autocorrelation of the second term on the right hand side of (3.1), and the last shown term represents the autocorrelation of $w(n)$. the remaining components on the right hand side of (3.3) involve the autocorrelation of the remaining terms on the right hand side of (3.1) as well as the correlation of these terms with each others.

We expect that non-zero significant values of $R_r(n,\tau)$ are attained only in the following cases:

1) Delays equal to zero (due to the correlation of the signal with itself) and D_u (due to the existence of the CP). This is referred to as Case (1) in the sequel.

2) Delays equal to integer multiples of D_F (due to the repetition of the RS every frame). This is subsequently referred to as Case (2).

We study $R_r(\alpha,\tau)$ at these delays and its representation as a Fourier series, and determine the expressions for $R_r(\alpha,\tau)$ and set of CFs $\{\alpha\}$.

Case (1): Derivation of the analytical expressions for CAF at delays equal to zero and useful OFDM symbol duration and the corresponding set of CFs

Assuming that the symbols on each subcarrier are i.i.d. and mutually independent for different subcarriers, one can easily see that only $E(b_{k_1,l_1}b^*_{k_2,l_2})$ and $E(c_{k_1,l_1}c^*_{k_2,l_2})$ are non-zero at delays equal to zero and the useful OFDM symbol duration, and this occurs when $k_1 = k_2 = k$ and $l_1 = l_2 = l$, for which (3.3) becomes

$$R_r(n,\tau) = a^2[\sigma_b^2 K_d + \sigma_c^2 K_r] \sum_{\substack{l=-\infty \\ l \bmod N_z = \beta \in \mathcal{Z}_1}}^{\infty} g(n-lD)g^*(n-lD+\tau)$$
$$+ a^2[\sigma_b^2 K_d + \sigma_c^2 K_r] \sum_{\substack{l=-\infty \\ l \bmod N_z = \beta \in \mathcal{Z}_2}}^{\infty} g(n-lD)g^*(n-lD+\tau)$$
$$+ a^2\sigma_b^2 K \sum_{\substack{l=-\infty \\ l \bmod N_z = \beta \in \mathcal{Z}_1,\mathcal{Z}_2}}^{\infty} g(n-lD)g^*(n-lD+\tau), \qquad (3.4)$$

where K_d and K_r are the number of data and RS subcarriers respectively, where $K_d + K_r = K$, $\sigma_b^2 = E(b_{l,k} b_{l,k}^*)$, and $\sigma_c^2 = E(c_{l,k} c_{l,k}^*)$. Note that the symbols $c_{k,l}$ and $b_{k,l}$ are taken from a unit variance constellation, which means that $\sigma_c^2 = \sigma_b^2 = \sigma^2 (= 1)$ and (3.4) becomes

$$R_r(n,\tau) = a^2 \sigma^2 K \sum_{l=-\infty}^{\infty} g(n - lD) g^*(n - lD + \tau) = \sigma^2 g(n) g^*(n+\tau) \otimes \sum_{l=-\infty}^{\infty} \delta(n - lD) \qquad (3.5)$$

By taking the Fourier transform of (3.5), using the convolution theorem and the identity $\Im\{\sum_l \delta(n - lD)\} = T^{-1} \sum_l \delta(\alpha - lD^{-1})$, one can write

$$\Im\{R_r(n,\tau)\} = D^{-1} \sigma^2 \sum_n g(n) g^*(n+\tau) e^{-j2\pi\alpha n} \sum_{l=-\infty}^{\infty} \delta(\alpha - lD^{-1}). \qquad (3.6)$$

As one can see from (3.6), $\Im\{R_r(n,\tau)\}$ is non zero only at $\alpha = lD^{-1}$, where l is an integer. By using the inverse Fourier transform of (3.6), one can easily see that the autocorrelation function has a Fourier series representation. This means that the CF domain is discrete. Furthermore, the CAF at CF α and delay τ, and the set of CFs, $\mathcal{K}$, are given respectively as

$$R_r(\alpha,\tau) = D^{-1} \sigma^2 \sum_n g(n) g^*(n+\tau) e^{-j2\pi\alpha n} \qquad (3.7)$$

and

$$\mathcal{K} = \{\alpha : \alpha = lD^{-1},\ l \text{ integer}\}. \qquad (3.8)$$

Case (2): Derivation of the analytical expressions for CAF at delays equal to integer multiples of the frame duration and the corresponding set of CFs

We further investigate (3.3) for delays equal to integer multiples of the frame time duration. At these delays, one can show that the only non-zero terms are due to the repetition of the RS, and correspond to $E(c_{l_1,k_1}c^*_{l_2,k_2}) \neq 0$ when $k_1 = k_2 (= k)$ and $l_2 - l_1 = \mu N_F$, with μ as an integer and N_F as the number of the OFDM symbols in the transmission frame. Thus, (3.3) becomes

$$R_r(n,\tau) = a^2\sigma_c^2 \sum_{\substack{l_1=-\infty \\ l_1 \bmod N_z=\beta\in\mathcal{Z}_1}}^{\infty} \sum_{\substack{l_2=-\infty \\ l_2 \bmod N_z=\beta\in\mathcal{Z}_1 \\ l_2=l_1+\mu N_F}}^{\infty} g(n-l_1D)g^*(n-l_2D+\tau) \sum_{\substack{k=-K/2,k\neq 0 \\ k\in A_1}}^{K/2} e^{-j2\pi k(\tau+l_1D-l_2D)/D_u}$$

$$+a^2\sigma_c^2 \sum_{\substack{l_1=-\infty \\ l_1 \bmod N_z=\beta\in\mathcal{Z}_2}}^{\infty} \sum_{\substack{l_2=-\infty \\ l_2 \bmod N_z=\beta\in\mathcal{Z}_2 \\ l_2=l_1+\mu N_F}}^{\infty} g(n-l_1D)g^*(n-l_2D+\tau) \sum_{\substack{k=-K/2,k\neq 0 \\ k\in A_2}}^{K/2} e^{-j2\pi k(\tau+l_1D-l_2D)/D_u}. \quad (3.9)$$

Note that in this case, $g(n-l_1D)g^*(n-l_2D+\tau)=0$ unless $l_2 - l_1 = N_F\tau D_F^{-1}$ (otherwise the pulses do not overlap, yielding a zero product). Here we present two cases for illustration: (1) $\tau = D_F$, $l_1 = 0$, and $l_2 = 2N_F$: this yields $g(n)g^*(n-D_F)=0$; (2) $\tau = D_F$, $l_1 = 0$, and $l_2 = N_F$: this yields $g(n)g^*(n-N_FD+D_F) = g(n)g^*(n) \neq 0$. Based on this observation and after some mathematical manipulations, (3.9) can be rewritten as

$$R_r(n,\tau) = a^2\sigma_c^2[K_1 \sum_{\substack{l=-\infty \\ l \bmod N_z=\beta\in\mathcal{Z}_1}}^{\infty} |g(n-lD)|^2 + K_2 \sum_{\substack{l=-\infty \\ l \bmod N_z=\beta\in\mathcal{Z}_2}}^{\infty} |g(n-lD)|^2], \quad (3.10)$$

where K_1 and K_2 are the number of subcarriers in A_1 and A_2 respectively. Given that $K_1 = K_2 = K_r$ (see Figs 3.3, 3.5, and 3.6), (3.10) becomes

$$R_r(n,\tau) = a^2\sigma_c^2 K_r |g(n)|^2 \otimes [\sum_{\substack{l=-\infty \\ l \bmod N_z = \beta \in \mathcal{Z}_1}}^{\infty} \delta(n-lD) + \sum_{\substack{l=-\infty \\ l \bmod N_z = \beta \in \mathcal{Z}_2}}^{\infty} \delta(n-lD)]. \quad (3.11)$$

By expressing l as $l' + \beta$, with $l' = \lfloor lN_z^{-1} \rfloor N_z$, (3.11) can be rewritten as,

$$R_r(n,\tau) = a^2\sigma_c^2 K_r |g(n)|^2 \otimes [\sum_{\beta \in \mathcal{Z}_1} \sum_{\substack{l'=-\infty \\ l' \bmod N_z = 0}}^{\infty} \delta(n-l'D-\beta D) + \sum_{\beta \in \mathcal{Z}_2} \sum_{\substack{l'=-\infty \\ l' \bmod N_z = 0}}^{\infty} \delta(n-l'D-\beta D)],$$

$$= a^2\sigma_c^2 K_r |g(n)|^2 \otimes [\sum_{\beta \in \mathcal{Z}_1} \sum_{\nu=-\infty}^{\infty} \delta(n-\nu D_z-\beta D) + \sum_{\beta \in \mathcal{Z}_2} \sum_{\nu=-\infty}^{\infty} \delta(n-\nu D_z-\beta D)]. \quad (3.12)$$

where $D_z = N_z D$. By taking the Fourier transform of (3.12), and using the convolution theorem and the identity $\Im\{\sum_\nu \delta(n-\nu D_z)\} = D_z^{-1} \sum_\nu \delta(\alpha - \nu D_z^{-1})$, one can write

$$\Im\{R_r(n,\tau)\} = D_z^{-1} a^2\sigma_c^2 K_r [\sum_{\beta \in \mathcal{Z}_1} e^{-j2\pi\alpha\beta D} + \sum_{\beta \in \mathcal{Z}_2} e^{-j2\pi\alpha\beta D}] \sum_n |g(n)|^2 e^{-j2\pi\alpha n} \sum_{\nu=-\infty}^{\infty} \delta(\alpha - \nu D_z^{-1}), \quad (3.13)$$

and the CAF at CF α and delay τ, and the set of CFs, $\mathcal{K}$, can be shown to be given respectively as

$$R_r(\alpha,\tau) = D_z^{-1} a^2\sigma_c^2 K_r [\sum_{\beta \in \mathcal{Z}_1} e^{-j2\pi\alpha\beta D} + \sum_{\beta \in \mathcal{Z}_2} e^{-j2\pi\alpha\beta D}] \sum_n |g(n)|^2 e^{-j2\pi\alpha n}, \quad (3.14)$$

and

$$\mathcal{K} = \{\alpha : \alpha = \nu D_z^{-1},\ \nu \text{ integer}\}. \quad (3.15)$$

To sum up, for the closed form expressions for the CAF and corresponding set of CFs of LTE signals with long CP, one can refer to equations:

- (3.7) and (3.8) for delays equal to zero and D_u (Case (1)), and
- (3.14) and (3.15) for delays equal to integer multiples of D_F (Case (2)).

3.3.2. Second-Order Cyclostationarity of the non-MBSFN LTE Signals with Short CP

By using the signal model in (3.2), the autocorrelation function of $r(n)$ can be expressed as the sum of the autocorrelation functions corresponding to any two signal components, signal and noise components, and noise component as

$$
\begin{aligned}
R_r(n,\tau) = a^2 & \sum_{\substack{l_1=-\infty \\ l_1 \bmod N_z=\beta=0}}^{\infty} \sum_{\substack{l_2=-\infty \\ l_2 \bmod N_z=\beta=0}}^{\infty} \sum_{\substack{k_1=-K/2, k_1\neq 0 \\ k_1\in A_1}}^{K/2} \sum_{\substack{k_2=-K/2, k_2\neq 0 \\ k_2\in A_1}}^{K/2} E(b_{l_1,k_1} b^*_{l_2,k_2}) \\
& \times g_1(n-l_1N_z^{-1}D_z) e^{j2\pi k_1 (n-l_1N_z^{-1}D_z)/D_u} g_1^*(n-l_2N_z^{-1}D_z+\tau) e^{-j2\pi k_2 (n-l_2N_z^{-1}D_z+\tau)/D_u} \\
& + a^2 \sum_{\substack{l_1=-\infty \\ l_1 \bmod N_z=\beta=0}}^{\infty} \sum_{\substack{l_2=-\infty \\ l_2 \bmod N_z=\beta=0}}^{\infty} \sum_{\substack{k_1=-K/2, k_1\neq 0 \\ k_1\in A_1}}^{K/2} \sum_{\substack{k_2=-K/2, k_2\neq 0 \\ k_2\in A_1}}^{K/2} E(c_{l_1,k_1} c^*_{l_2,k_2}) \\
& \times g_1(n-l_1N_z^{-1}D_z) e^{j2\pi k_1 (n-l_1N_z^{-1}D_z)/D_u} g_1^*(n-l_2N_z^{-1}D_z+\tau) e^{-j2\pi k_2 (n-l_2N_z^{-1}D_z+\tau)/D_u} \\
& + ... + E(w(n)w^*(n+\tau)).
\end{aligned}
\tag{3.16}
$$

To ease the understanding of (3.16), here we provide an explanation. The first term on the right hand side represents the autocorrelation of the first term on the right hand side of (3.2). The second shown term represents the autocorrelation of the second term on the right hand side of (3.2), and the last shown term represents the autocorrelation of $w(n)$. the remaining components on the right hand side of (3.16) involve the autocorrelation of the remaining terms on the right hand side of (3.2) as well as the correlation of these terms with each others.

We expect that non-zero significant values of $R_r(n,\tau)$ are attained only in the following cases:

1) Delays equal to zero (due to the correlation of the signal with itself) and D_u (due to the existence of the CP). This is referred to as Case (1) in the sequel.

2) Delays equal to integer multiples of D_F (due to the repetition of the RS every frame). This is subsequently referred to as Case (2).

We study $R_r(\alpha,\tau)$ at these delays and its representation as a Fourier series, and determine the expressions for $R_r(\alpha,\tau)$ and set of CFs $\{\alpha\}$.

Case (1): Derivation of the analytical expressions for CAF at delays equal to zero and useful OFDM symbol duration, and the corresponding set of CFs

Assuming that the symbols on each subcarrier are i.i.d. and mutually independent for different subcarriers, one can easily see that only $E(b_{k_1,l_1}b^*_{k_2,l_2})$ and $E(c_{k_1,l_1}c^*_{k_2,l_2})$ are non-zero at delays equal to zero and the useful OFDM symbol duration, and this occurs when $k_1=k_2=k$ and $l_1=l_2=l$, for which (3.16) becomes[11]

$$
\begin{aligned}
R_r(n,\tau) &= a^2[\sigma_b^2K_d+\sigma_c^2K_r]\sum_{\substack{l=-\infty\\ l \bmod N_z=\beta=0}}^{\infty} g_1(n-lN_z^{-1}D_z)g_1^*(n-lN_z^{-1}D_z+\tau)\\
&+a^2[\sigma_b^2K_d+\sigma_c^2K_r]\sum_{\substack{l=-\infty\\ l \bmod N_z=\beta=4}}^{\infty} g(n-\lfloor lN_z^{-1}\rfloor D_z-3D-D_1)g^*(n-\lfloor lN_z^{-1}\rfloor D_z-3D-D_1+\tau)\\
&+a^2\sigma_b^2K\sum_{\substack{l=-\infty\\ l \bmod N_z=\beta\neq 0,4}}^{\infty} g(n-\lfloor lN_z^{-1}\rfloor D_z-(\beta-1)D-D_1)g^*(n-\lfloor lN_z^{-1}\rfloor D_z-(\beta-1)D-D_1+\tau)\\
&=a^2\sigma^2Kg_1(n)g_1^*(n+\tau)\otimes\sum_{\substack{l=-\infty\\ l \bmod N_z=\beta=0}}^{\infty}\delta(n-lN_z^{-1}D_z)\\
&+a^2\sigma^2Kg(n)g^*(n+\tau)\otimes\sum_{\substack{l=-\infty\\ l \bmod N_z=\beta=4}}^{\infty}\delta(n-\lfloor lN_z^{-1}\rfloor D_z-3D-D_1)
\end{aligned}
$$

[11] Note that as for the LTE OFDM signals with long CP, in this case the number of subcarriers is equal for both sets A_1 and A_2, and equals K_r ($K_1=K_2=K_r$). Also ($\sigma_b^2=\sigma_c^2=\sigma^2$).

$$+a^2\sigma^2 Kg(n)g^*(n+\tau)\otimes \sum_{\substack{l=-\infty \\ l \bmod N_z=\beta\neq 0,4}}^{\infty} \delta(n-\left\lfloor lN_z^{-1}\right\rfloor D_z-(\beta-1)D-D_1)]$$

$$=\sigma^2\Big[g_1(n)g_1^*(n+\tau)\otimes \sum_{\substack{l=-\infty \\ l \bmod N_z=\beta=0}}^{\infty} \delta(n-lN_z^{-1}D_z)$$

$$+g(n)g^*(n+\tau)\otimes[\sum_{\substack{l=-\infty \\ l \bmod N_z=\beta=4}}^{\infty} \delta(n-\left\lfloor lN_z^{-1}\right\rfloor D_z-3D-D_1)$$

$$+\sum_{\substack{l=-\infty \\ l \bmod N_z=\beta\neq 0,4}}^{\infty} \delta(n-\left\lfloor lN_z^{-1}\right\rfloor D_z-(\beta-1)D-D_1)]\Big]$$

$$=\sigma^2\Big[g_1(n)g_1^*(n+\tau)\otimes \sum_{\substack{l=-\infty \\ l \bmod N_z=\beta=0}}^{\infty} \delta(n-lN_z^{-1}D_z)$$

$$+g(n)g^*(n+\tau)\otimes \sum_{\substack{l=-\infty \\ l \bmod N_z=\beta\neq 0}}^{\infty} \delta(n-\left\lfloor lN_z^{-1}\right\rfloor D_z-(\beta-1)D-D_1)\Big]. \qquad (3.17)$$

By expressing l as $l'+\beta$, with $l'=\left\lfloor lN_z^{-1}\right\rfloor N_z$, (3.17) can be rewritten as

$$R_r(n,\tau)=\sigma^2\Big[g_1(n)g_1^*(n+\tau)\otimes \sum_{\substack{l'=l=-\infty \\ l' \bmod N_z=0}}^{\infty} \delta(n-l'N_z^{-1}D_z)$$

$$+g(n)g^*(n+\tau)\otimes \sum_{\beta=1}^{N_z-1}\sum_{\substack{l'=-\infty \\ l' \bmod N_z=0}}^{\infty} \delta(n-l'N_z^{-1}D_z-(\beta-1)D-D_1)\Big]$$

$$=\sigma^2\Big[g_1(n)g_1^*(n+\tau)\otimes \sum_{\nu=-\infty}^{\infty} \delta(n-\nu D_z)$$

$$+g(n)g^*(n+\tau)\otimes \sum_{\beta=1}^{N_z-1}\sum_{\nu=-\infty}^{\infty} \delta(n-\nu D_z-(\beta-1)D-D_1)\Big]. \qquad (3.18)$$

Furthermore, by taking the Fourier transform of (3.18), using the convolution theorem and the identity $\Im\{\sum_\nu \delta(n-\nu D_z)\}=D_z^{-1}\sum_\nu \delta(\alpha-\nu D_z^{-1})$, one obtains

$$\Im\{R_r(n,\tau)\} = D_z^{-1}\sigma^2\Big[\sum_n g_1(n)g_1^*(n+\tau)e^{-j2\pi n\alpha} + \sum_{\beta=1}^{N_z-1} e^{-j2\pi\alpha((\beta-1)D+D_1)}\sum_n g(n)g^*(n+\tau)e^{-j2\pi n\alpha}\Big]$$

$$\times \sum_{\nu=-\infty}^{\infty}\delta(\alpha-\nu D_z^{-1}), \tag{3.19}$$

and the CAF at CF α and delay τ, and the set of CFs, $\mathcal{K}$, can be shown to be given respectively as

$$R_r(\alpha,\tau) = D_z^{-1}\sigma^2\Big[\sum_n g_1(n)g_1^*(n+\tau)e^{-j2\pi n\alpha} + \sum_{\beta=1}^{N_z-1} e^{-j2\pi\alpha((\beta-1)D+D_1)}\sum_n g(n)g^*(n+\tau)e^{-j2\pi n\alpha}\Big] \tag{3.20}$$

and

$$\mathcal{K} = \{\alpha : \alpha = \nu D_z^{-1},\ \nu \text{ integer}\}. \tag{3.21}$$

Case (2): Derivation of the analytical expressions for CAF at delays equal to integer multiples of the frame duration and the corresponding set of CFs

We further investigate (3.16) for delays equal to integer multiples of the frame time duration. At these delays, one can show that the only non-zero terms are due to the repetition of the RS, and correspond to $E(c_{l_1,k_1}c^*_{l_2,k_2}) \neq 0$ when $k_1 = k_2 (= k)$ and $l_2 - l_1 = \mu N_F$, with μ as an integer and N_F as the number of the OFDM symbols in the transmission frame. Thus, it is straightforward that (3.16) becomes

$$R_r(n,\tau) = a^2\sigma_c^2 \sum_{\substack{l_1=-\infty \\ l_1 \bmod N_z = 0}}^{\infty} \sum_{\substack{l_2=-\infty \\ l_2 \bmod N_z = 0 \\ l_2 = l_1 + \mu N_F}}^{\infty} g_1(n - l_1 N_z^{-1} D_z) g_1^*(n - l_2 N_z^{-1} D_z + \tau) \sum_{\substack{k=-K/2, k\neq 0 \\ k\in A_1}}^{K/2} e^{-j2\pi k(\tau + (l_1 - l_2)N_z^{-1}D_z)/D_u}$$

$$+ a^2\sigma_c^2 \sum_{\substack{l_1=-\infty \\ l_1 \bmod N_z = 4}}^{\infty} \sum_{\substack{l_2=-\infty \\ l_2 \bmod N_z = 4 \\ l_2 = l_1 + \mu N_F}}^{\infty} g(n - \lfloor l_1 N_z^{-1} \rfloor D_z - 3D - D_1) g^*(n - \lfloor l_2 N_z^{-1} \rfloor D_z - 3D - D_1 + \tau)$$

$$\times \sum_{\substack{k=-K/2, k\neq 0 \\ k\in A_2}}^{K/2} e^{-j2\pi k(\tau + (\lfloor l_1 N_z^{-1} \rfloor - \lfloor l_2 N_z^{-1} \rfloor)D_z)/D_u}. \tag{3.22}$$

Note that in this case $g_1(n-l_1N_z^{-1}D_z)g_1^*(n-l_2N_z^{-1}D_z+\tau) = g(n-\lfloor l_1N_z^{-1}\rfloor D_z-3D-D_1)$ $\times g^*(n-\lfloor l_2N_z^{-1}\rfloor D_z-3D-D_1+\tau)=0$ unless $l_2-l_1=N_F\tau D_F^{-1}$. Here we present two cases with $g_1(n-l_1N_z^{-1}D_z)g_1^*(n-l_2N_z^{-1}D_z+\tau)$ for illustration: (1) $\tau=D_F$, $l_1=0$, and $l_2=2N_F$: this yields $g_1(n)g_1^*(n-D_F)=0$; (2) $\tau=D_F$, $l_1=0$, and $l_2=N_F$: this yields $g_1(n)g_1^*(n-D_F+D_F) = g(n)g^*(n)\neq 0$. Based on this observation and after some mathematical manipulations, (3.22) can be rewritten as

$$R_r(n,\tau)=a^2\sigma_c^2[K_1\sum_{\substack{l=-\infty\\ l \bmod N_z=0}}^{\infty}\left|g_1(n-lN_z^{-1}D_z)\right|^2+K_2\sum_{\substack{l=-\infty\\ l \bmod N_z=4}}^{\infty}\left|g(n-\lfloor lN_z^{-1}\rfloor D_z-3D-D_1)\right|^2], \quad (3.23)$$

where K_1 and K_2 are the number of subcarriers that belong to A_1 and A_2 respectively. Given that $K_1=K_2=K_r$, (3.23) becomes

$$\begin{aligned}R_r(n,\tau)&=a^2\sigma_c^2K_r[\left|g_1(n)\right|^2\otimes\sum_{\substack{l=-\infty\\ l \bmod N_z=0}}^{\infty}\delta(n-lN_z^{-1}D_z)+\left|g(n)\right|^2\otimes\sum_{\substack{l=-\infty\\ l \bmod N_z=4}}^{\infty}\delta(n-\lfloor lN_z^{-1}\rfloor D_z-3D-D_1)]\\ &=a^2\sigma_c^2K_r[\left|g_1(n)\right|^2\otimes\sum_{\substack{l=-\infty\\ l \bmod N_z=0}}^{\infty}\delta(n-lN_z^{-1}D_z)+\left|g(n)\right|^2\otimes\sum_{\substack{l=-\infty\\ l \bmod N_z=0}}^{\infty}\delta(n-lN_z^{-1}D_z-3D-D_1)]\\ &=a^2\sigma_c^2K_r[\left|g_1(n)\right|^2\otimes\sum_{\nu=-\infty}^{\infty}\delta(n-\nu D_z)+\left|g(n)\right|^2\otimes\sum_{\nu=-\infty}^{\infty}\delta(n-\nu D_z-3D-D_1)]. \quad (3.24)\end{aligned}$$

By taking the Fourier transform of (3.24), using the convolution theorem and the identity $\Im\{\sum_\nu\delta(n-\nu D_z)\}=D_z^{-1}\sum_\nu\delta(\alpha-\nu D_z^{-1})$, one can write that

$$\begin{aligned}\Im\{R_r(n,\tau)\}&=D_z^{-1}a^2\sigma_c^2K_r[\sum_n\left|g_1(n)\right|^2e^{-j2\pi\alpha n}+e^{-j2\pi\alpha(3D+D_1)}\sum_n\left|g(n)\right|^2e^{-j2\pi\alpha n}]\\ &\quad\times\sum_{\nu=-\infty}^{\infty}\delta(\alpha-\nu D_z^{-1}), \quad (3.25)\end{aligned}$$

and the CAF at CF α and delay τ, and the set of CFs, $\mathcal{K}$, can be shown to be given respectively as

$$R_r(\alpha,\tau) = D_z^{-1} a^2 \sigma_c^2 K_r [\sum_n |g_1(n)|^2 e^{-j2\pi\alpha n} + e^{-j2\pi\alpha(3D+D_1)} \sum_n |g(n)|^2 e^{-j2\pi\alpha n}], \quad (3.26)$$

and

$$\mathcal{K} = \{\alpha : \alpha = \nu D_z^{-1},\ \nu \text{ integer}\}. \quad (3.27)$$

To sum up, for the closed form expressions for the CAF and corresponding set of CFs of the non-MBSFN LTE signals with short CP, one can refer to equations:

- (3.20) and (3.21) for delays equal to zero and D_u (Case (1)), and
- (3.26) and (3.27) for delays equal to integer multiples of D_F (Case (2)).

3.3.3. OFDM Parameters of the OFDM-based LTE Signals

The OFDM parameters for LTE signals are presented in Table 3.2. As one can notice, the FFT size is scalable with the bandwidth: when the available bandwidth increases, the FFT size also increases such that the subcarrier spacing is fixed. This in turn leads to a constant useful OFDM symbol duration. As previously mentioned, two different values are used for the subcarrier spacing with the LTE signal (Δf = 7.5 KHz and 15 kHz), and this results in two different values for the useful OFDM symbol duration (133.33 μs and 66.67 μs, respectively).

Table 3.2. OFDM parameters for the LTE signals[12] (taken from [22]).

Channel bandwidth (MHz)	1.25	2.5	5	10	15	20
FFT size	128, 256	256, 512	512, 1024	1024, 2048	1536, 3072	2048, 4096
Subcarrier spacing Δf (kHz)	15, 7.5					
Useful symbol time (μs)	66.67, 133.33					

3.3.4. Results for CAF of the OFDM-based LTE Signals

In the following, the results obtained for the CAF of LTE signals are presented. LTE signals with 5 MHz double-sided bandwidth are considered. The data subcarriers are modulated using 16-QAM, while the RS subcarriers are modulated using BPSK. Unit variance constellations are considered. A raised root cosine pulse shape window with 0.025 roll-off factor is employed at the transmit-side. Table 3.3 summarizes the second order cyclostationarity of the LTE signal with the chosen parameters.

Table 3.3. Second-order cyclostationarity of the LTE signal with the parameters given in Section 3.3.4.

Mode	Delay	CFs	Dependency of the CFs with non-zero and considerable CAF magnitude
Non-MBSFN, Long CP	$\tau = 0$ and $\tau = D_u = 512$ ($T_u = 66.6$ μs) (Case (1))	lD^{-1}, l integer	Depends on D[13].
	$\tau = \mu D_F$, μ integer, $D_F = 76{,}800$ ($T_F = 10$ ms) (Case (2))	νD_z^{-1}, ν integer	Depends on the distribution of the RS subcarriers.
Non-MBSFN,	$\tau = 0$ and $\tau = D_u = 512$	νD_z^{-1},	CAF magnitude at CFs close to integer multiples

[12] The first line in the FFT size row corresponds to the signals with $\Delta f = 15$ kHz, whereas the second line corresponds to the the signals with $\Delta f = 7.5$ kHz.

[13] Note that the OFDM symbol duration depends on the CP duration ($D = D_u + D_{cp}$).

short CP	($T_u = 66.6$ μs) (Case (1))	ν integer	of D^{-1} predominates (Depends on D).
	$\tau = \mu D_F$, μ integer, $D_F = 76{,}800$ ($T_F = 10$ ms) (Case (2))	νD_z^{-1}, ν integer	Depends on the distribution of the RS subcarriers.
MBSFN, $\Delta f = 15$ KHz	$\tau = 0$ and $\tau = D_u = 512$ ($T_u = 66.6$ μs) (Case (1))	lD^{-1}, l integer	Depends on D.
	$\tau = \mu D_F$, μ integer, $D_F = 76{,}800$ ($T_F = 10$ ms) (Case (2))	νD_z^{-1}, ν integer	Depends on the distribution of the RS subcarriers.
MBSFN, $\Delta f = 7.5$ KHz	$\tau = 0$ and $\tau = D_u = 1{,}024$ ($T_u = 133.3$ μs) (Case (1))	lD^{-1}, l integer	Depends on D.
	$\tau = \mu D_F$, μ integer, $D_F = 76{,}800$ ($T_F = 10$ ms) (Case (2))	νD_z^{-1}, ν integer	Depends on the distribution of the RS subcarriers.

The estimated results are obtained without noise and channel dispersion, with relatively large observation interval (500 ms). Note that the estimated CAFs are only given for CFs. Furthermore, we estimated the CAF for non-CFs and reasonably large observation interval (500 ms), and $R(\alpha, \tau) \approx 0$ is always the case for non-CFs.

The theoretical and estimated CAF magnitudes for the LTE signal with non-MBSFN mode and long CP, LTE signal with non-MBSFN mode and short CP, LTE signal with MBSFN mode and $\Delta f = 15$ kHz, and LTE signal with MBSFN mode and $\Delta f = 7.5$ kHz

at $\tau = D_u$ are presented versus CF in Figs. 3.7 to 3.10, respectively. The range corresponding to the first 4 positive and negative CFs is shown. As one can notice from these Figures, the CAF magnitude is lower for the LTE signal with the non-MBSFN mode and short CP. This is due to the fact that with this mode of the LTE signal, the value of D_{cp} / D_u is lower. The autocorrelation function of the LTE signals with long CP at $\tau = D_u$ is periodic with period T due to the CP. As it can be seen in Figs. 3.7, 3.9, and 3.10, the CAF of LTE signals with long CP has CFs at integer multiples of D^{-1}, as expected. On the other hand, for the LTE signal with short CP, this periodicity in the autocorrelation function is impaired due to the longer duration of the first symbol in the slot when compared with that of the remaining symbols, and that is the reason for which the CAF of the LTE signal with short CP has CFs equal to integer multiples of D_z^{-1}. However, the CAF magnitude at CFs close to integer multiples of D^{-1} predominates, as one can see from Figs. 3.8 a) and b), as the duration of the first symbol in the slot is only slightly longer than that of the remaining symbols.

The theoretical and estimated CAF magnitude for the LTE signal with non-MBSFN mode and long CP, LTE signal with non-MBSFN mode and short CP, LTE signal with MBSFN mode and $\Delta f = 15$ kHz, and LTE signal with MBSFN mode and $\Delta f = 7.5$ kHz at $\tau = D_F$ is presented versus CF in Figs. 3.11 to 3.14, respectively. As one can see from these figures, the CAF magnitude is higher for the case of MBSFN mode. This can be easily explained, as the MBSFN RS is induced on more subcarriers when compared with

the cell-specific RS. Also, due to diverse RS distributions for different transmission modes, the non-zero CF values depend on the mode.

3.4. Summary

In this chapter, a description of the structure of the OFDM-based LTE signals is discussed and signal models for these signals are provided. Furthermore, the second-order cyclostationarity of the OFDM-based LTE signals is investigated and closed-from expressions for the CAF and CFs are derived. Finally, we compare analytical findings with simulation results, which are in agreement.

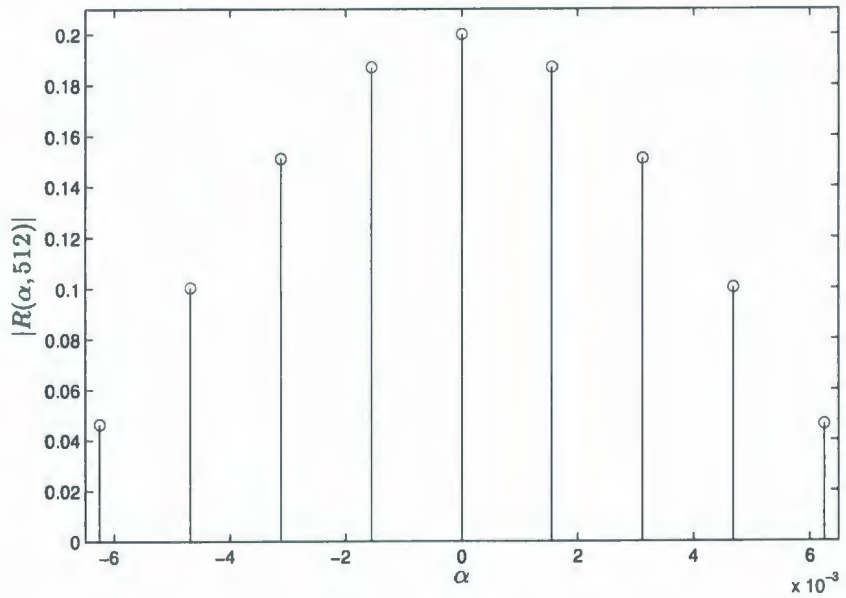

a)

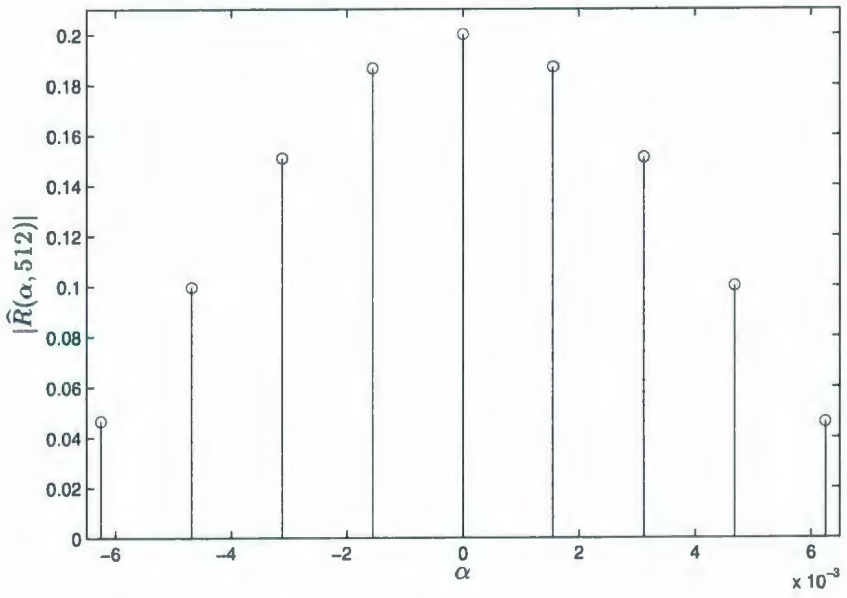

b)

Fig. 3.7. The CAF magnitude for the LTE signal with non-MBSFN mode and long CP at $\tau = D_u = 512$ versus CF a) theoretical b) estimated.

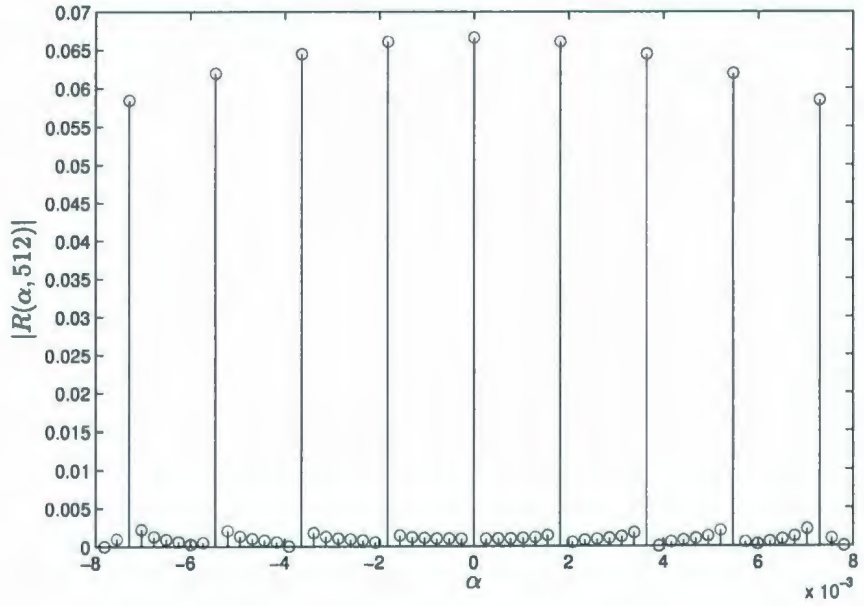

a)

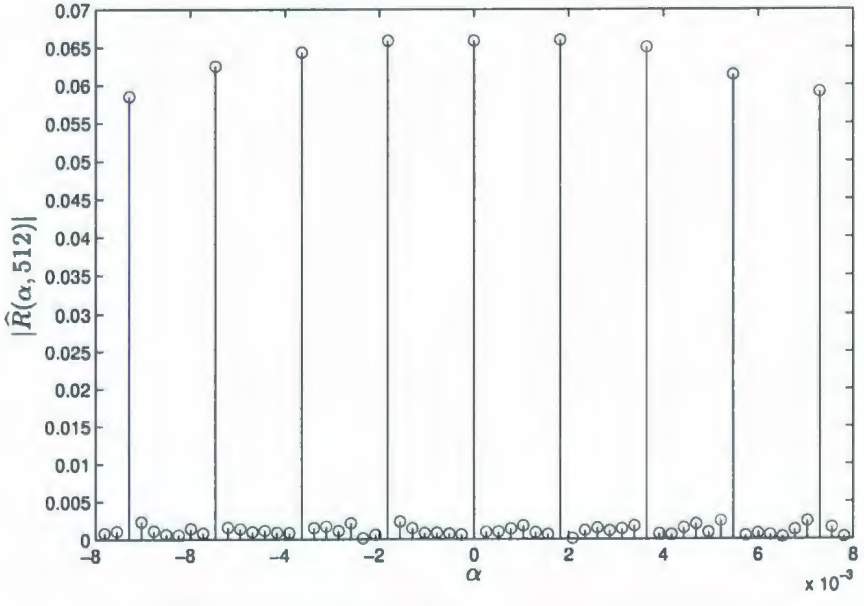

b)

Fig. 3.8. The CAF magnitude for the LTE signal with non-MBSFN mode and short CP at $\tau = D_u = 512$ versus CF a) theoretical b) estimated.

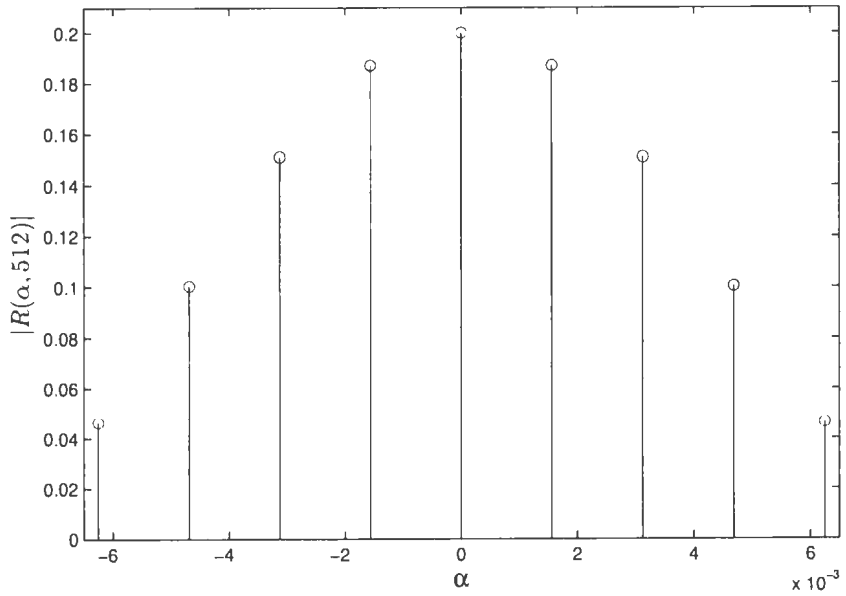

a)

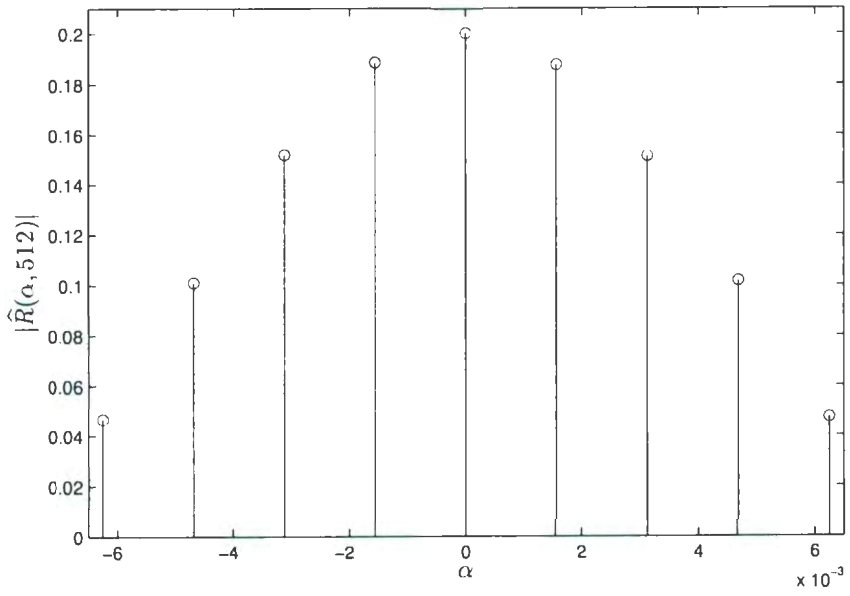

b)

Fig. 3.9. The CAF magnitude for the LTE signal with MBSFN mode and $\Delta f = 15$ kHz at $\tau = D_u = 512$ versus CF a) theoretical b) estimated.

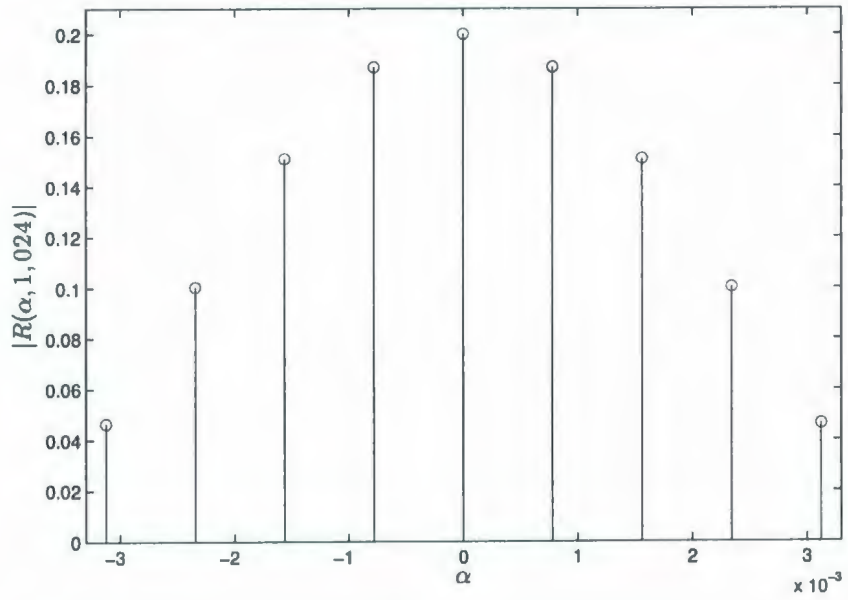

a)

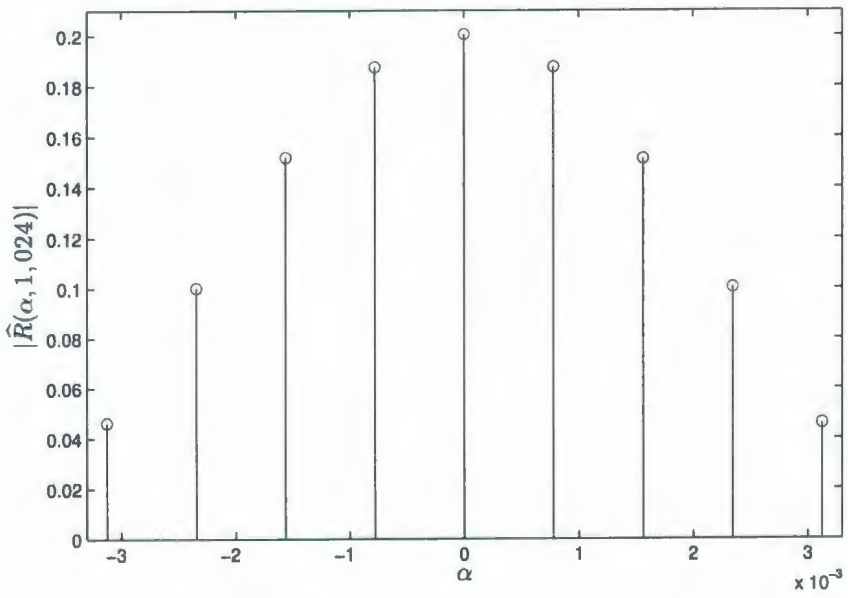

b)

Fig. 3.10. The CAF magnitude for the LTE signal with MBSFN mode and $\Delta f = 7.5$ kHz at $\tau = D_u = 1,024$ versus CF a) theoretical b) estimated.

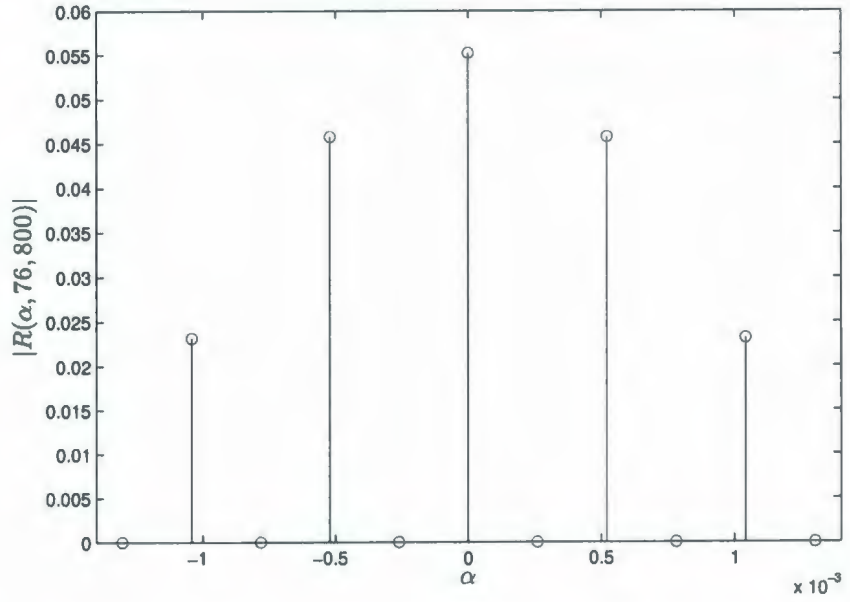

a)

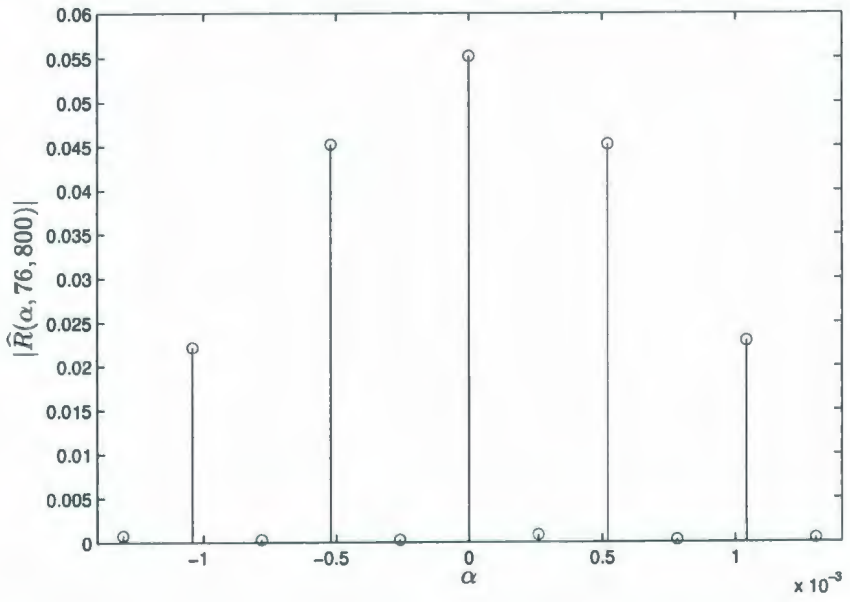

b)

Fig. 3.11. The CAF magnitude for the LTE signal with non-MBSFN mode and long CP at $\tau = D_F = 76,800$ versus CF a) theoretical b) estimated.

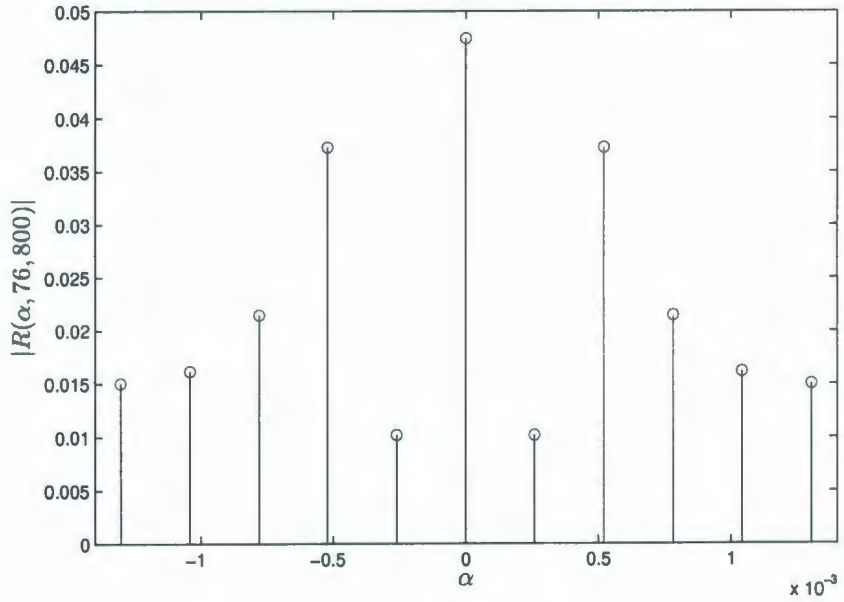

a)

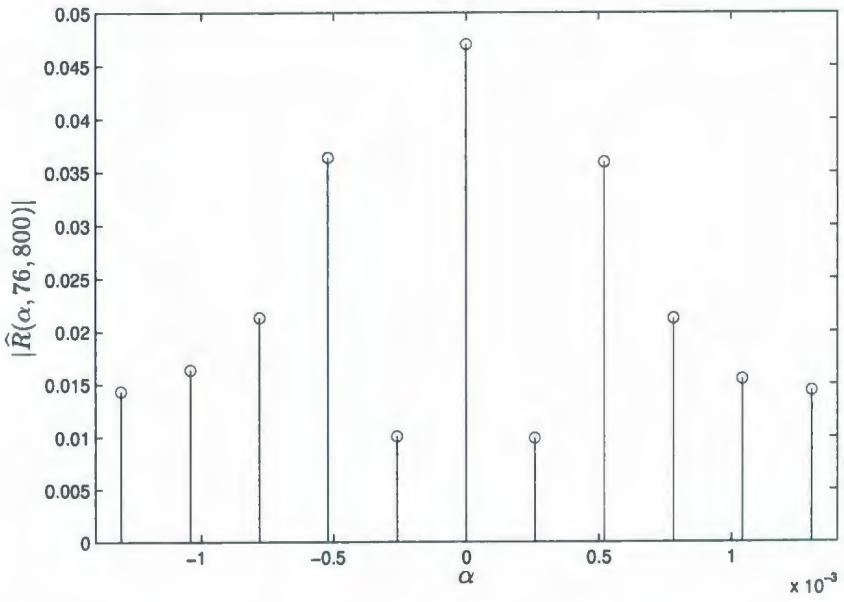

b)

Fig. 3.12. The CAF magnitude for the LTE signal with non-MBSFN mode and short CP at $\tau = D_F = 76,800$ versus CF a) theoretical b) estimated.

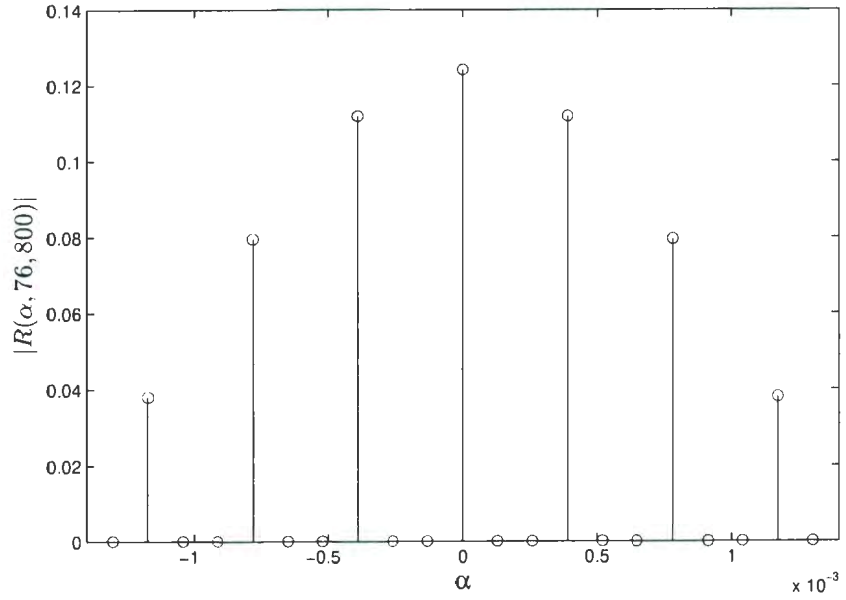

a)

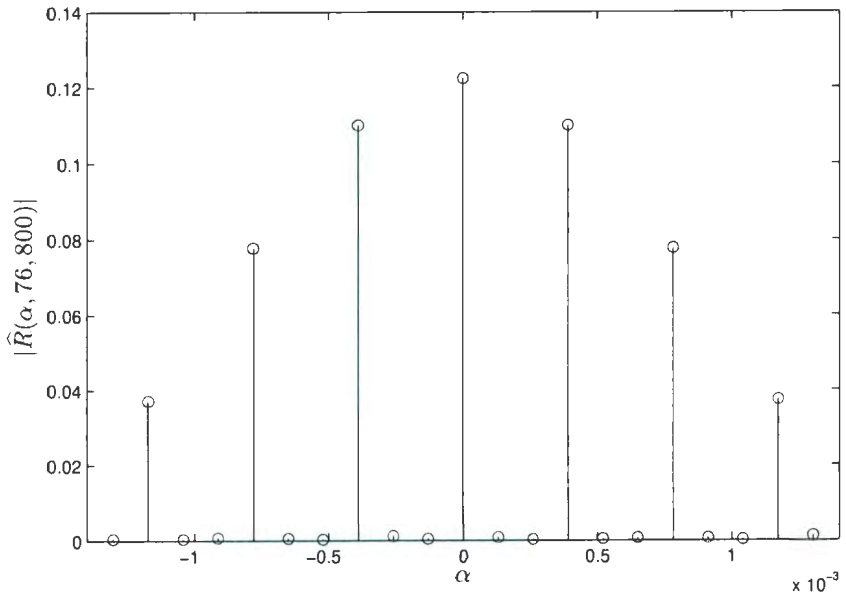

b)

Fig. 3.13. The CAF magnitude for the LTE signal with MBSFN mode and $\Delta f = 15$ kHz at $\tau = D_F = 76,800$ versus CF a) theoretical b) estimated.

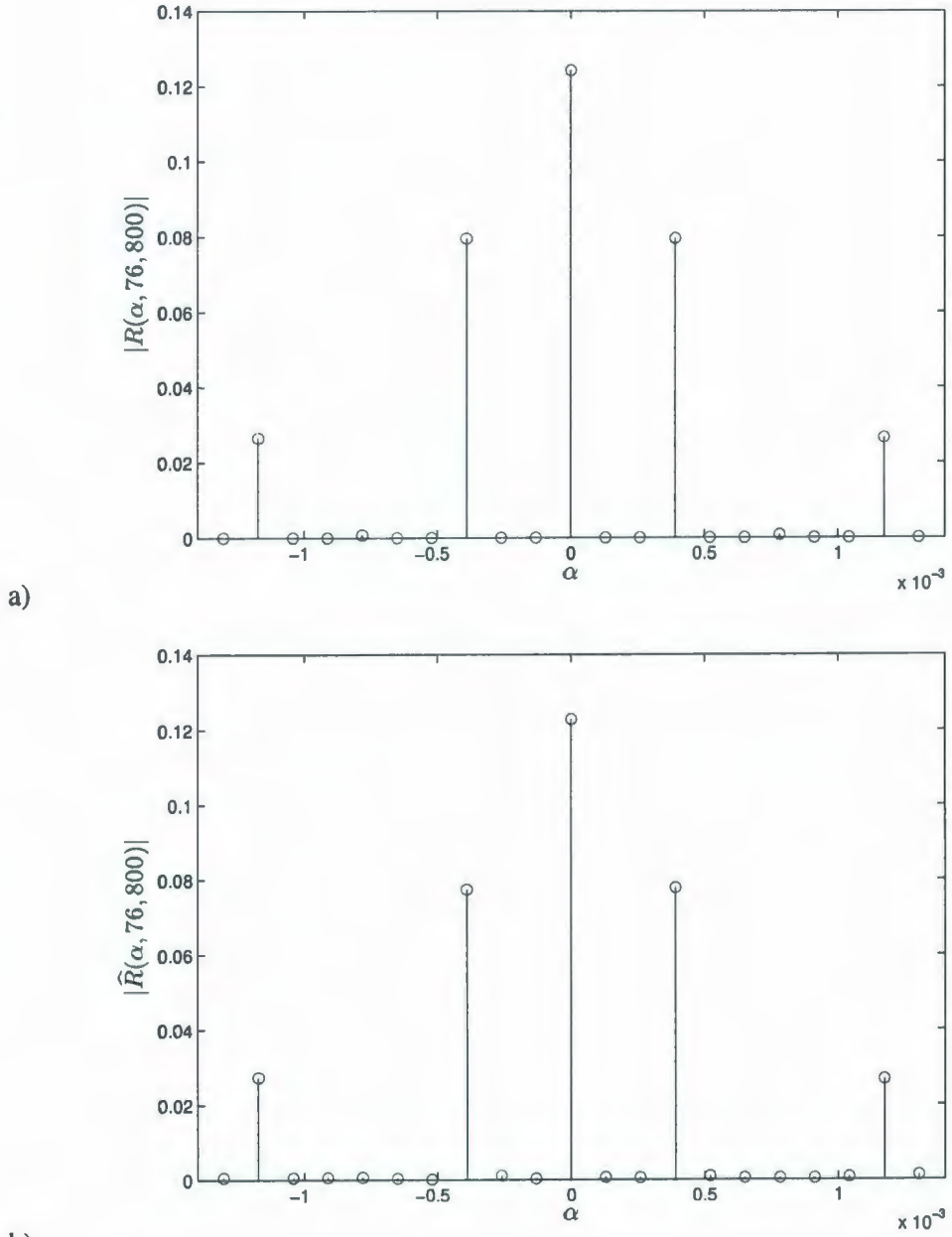

Fig. 3.14. The CAF magnitude for the LTE signal with MBSFN mode and $\Delta f = 7.5$ kHz at $\tau = D_F = 76,800$ versus CF a) theoretical b) estimated.

Chapter 4

Joint Signal Detection and Classification of the OFDM-based Mobile WiMAX and LTE Signals

4.1. Introduction

In this chapter, the results obtained in Chapters 2 and 3 for the CAF of the OFDM-based mobile WiMAX and LTE signals are exploited to develop two cyclostationarity-based algorithms for joint detection and classification of these signals. The proposed algorithms exploit the information that is *a priori* known on the signal parameters, i.e., the useful OFDM symbol duration (equivalently, subcarrier spacing) and frame duration. The proposed algorithms are applied in frequency bands that are common to both signal types.

4.2. Proposed Joint Signal Detection and Classification Algorithm based on the CP-Induced Cycolstationarity

The CP-induced cyclostationarity of the OFDM-based mobile WiMAX and LTE signals is the property that the CAF $R_r(\alpha,\tau)$ is non-zero at CFs α and delay $\tau = D_u$. Here we use this property at zero CF ($\alpha = 0$) in order to jointly detect and classify these signals. Note that only $\alpha = 0$ is used at $\tau = D_u$, as other CFs depend on the length of the

CP, which is unknown (see Sections 2.3.4 and 3.3.4). Note that this is actually the signal autocorrelation at delay ($\tau = D_u$). However, the CAF term will be used for consistency with the rest of the thesis. The proposed joint detection and classification algorithm is a binary decision tree classifier, as presented in Fig. 4.1.

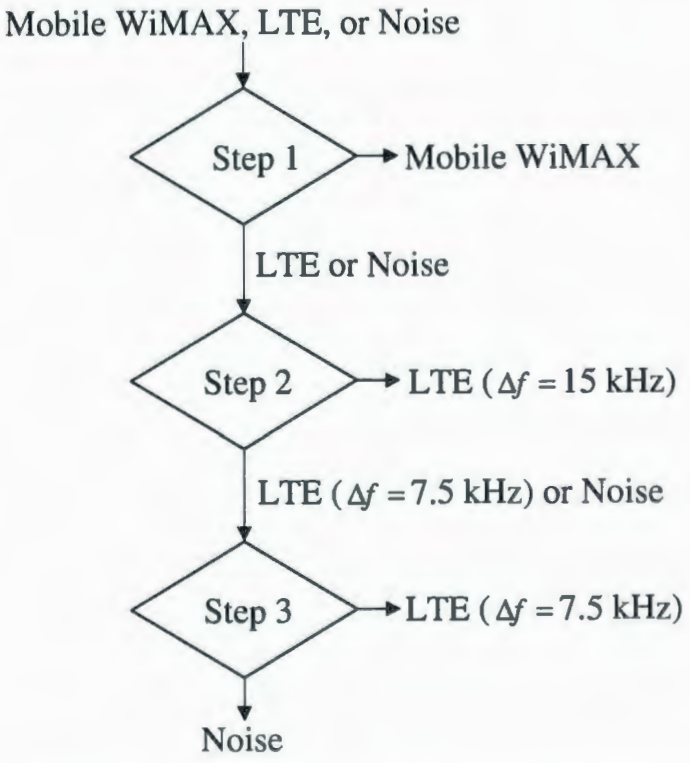

Fig. 4.1. Flowchart of the proposed joint signal detection and classification algorithm.

At Step 1, the existence of a peak at zero CF and $\tau = D_u$ (with $T_u = 91.4$ μs) in the CAF of mobile WiMAX is exploited to distinguish the mobile WiMAX signal from the LTE/noise class. Note that the CAF of LTE signals (any mode/subcarrier spacing) does not have a peak at this delay and CF (see Section 3.3.4) and that the CAF of noise is zero at zero CF and non-zero delay. The cyclostationarity test developed in [24] is used to check

whether or not $\alpha = 0$ is indeed a CF for the selected delay. If $\alpha = 0$ is found to be a CF at this delay, the decision is mobile WiMAX; otherwise, it is LTE/noise class. At Step 2, the existence of a peak at zero CF and $\tau = D_u$ (with $T_u = 66.67$ μs) in the CAF of the LTE signals with 15 kHz subcarrier spacing is used to distinguish the LTE signals ($\Delta f = 15$ kHz) from the LTE signals ($\Delta f = 7.5$ kHz)/noise class. Note that the CAF of LTE signals ($\Delta f = 7.5$ kHz)/noise class do not have a peak at this delay and CF (See Section 3.3.4). The cyclostationarity test in [24] is employed to check whether or not $\alpha = 0$ is a CF at $\tau = D_u$ (with $T_u = 66.67$ μs). The decision that the LTE signal with 15 kHz subcarrier spacing (MBSFN or non MBSFN) is present is made if $\alpha = 0$ is found to be a CF at this delay; otherwise, it is assumed that either the LTE signals with 7.5 kHz subcarrier spacing (MBSFN) or noise is present in the channel. Finally, At Step 3, the existence of a peak at zero CF and $\tau = D_u$ (with $T_u = 133.3$ μs) in the CAF of the LTE signals with 7.5 kHz subcarrier spacing is used to distinguish the LTE signals ($\Delta f = 7.5$ kHz) from noise. Note that the CAF of noise is zero at zero CF and non-zero delay. The cyclostationarity test is used to check whether or not $\alpha = 0$ is a CF at $\tau = D_u$ (with $T_u = 133.33$ μs). The decision that the LTE signal with this subcarrier spacing is present is made if $\alpha = 0$ at this delay is found to be a CF. Otherwise; the decision that only noise is present in the channel is made. Note that joint detection and classification is done in operating bands common to both OFDM standards.

4.3. Proposed Joint Signal Detection and Classification Algorithm based on CP-, Preamble-, and RS-Induced Cyclostationarity

As previously discussed in Section 4.2, both mobile WiMAX and LTE OFDM signals exhibit CP-induced cyclostationarity. However, this information can be unreliable for joint detection and classification, as the cognitive users sharing the spectrum may employ other types of signals with OFDM modulation and close useful symbol duration (equivalently, close subcarrier frequency separation). Hence, the distinctive preamble-induced cyclostationarity of the mobile WiMAX OFDM-based signals (Cases (2) and (4) in Chapter 2) as well as the distinctive RS –induced cyclostationarity of the OFDM-bases LTE signals (Case (2) in Chapter 3) can be used in addition to the CP-induced Cyclostationarity for their joint detection and classification. Here, we propose an algorithm for joint detection and classification of the OFDM-based mobile WiMAX and LTE signals, which makes use of the CP- and preamble-induced cyclostationarity of the mobile WiMAX signal, as well as the CP- and RS-induced cyclostationarity of the LTE signals. In the following, we list the distinctive features of the mobile WiMAX signals used in this algorithm (also summarized in Table 4.1):

- The property that the CAF $R_r(\alpha,\tau)$ is non-zero at CF $\alpha=0$ and delay $\tau=D_u$ (Case (1) in Chapter 2)
- The property that the CAF $R_r(\alpha,\tau)$ is non-zero at CF $\alpha=\nu D_F^{-1},\nu=0,\ 1,\ 2,$ and delay $\tau=\lceil D_u/3\rceil$ (Case (2) in Chapter 2)

- The property that the CAF $R_r(\alpha,\tau)$ is non-zero at CF $\alpha = \nu D_F^{-1}, \nu = 0,\ 1,\ 2,$ and delay $\tau = D_F$ (Case (4) in Chapter 2).

Table 4.1. Distinctive features of the mobile WiMAX signals used in the second algorithm

Delay	CFs
D_u (Case(1))	$\alpha = 0$
$\lceil D_u / 3 \rceil$ (Case(2))	$\alpha = \nu D_F^{-1}, \nu = 0,\ 1,\ 2$
D_F (Case(4))	$\alpha = \nu D_F^{-1}, \nu = 0,\ 1,\ 2$

Note that only $\alpha = 0$ is used at $\tau = D_u$, as other CFs depend on the length of the CP, which is unknown (see Section 2.3.4). Also note that the pilot-induced cyclostationarity is not used here, as different pilot distributions result in different locations for the peaks, and the distribution is not *a priori* known.

In the following, we list the distinctive features of the LTE signals used in the proposed algorithm (also summarized in Table 4.2):

- The property that the CAF $R_r(\alpha,\tau)$ is non-zero at CF $\alpha = 0$ and delay $\tau = D_u$ (Case (1) in chapter 3),
- The property that the CAF $R_r(\alpha,\tau)$ is non-zero at CF $\alpha = 0$ and delay $\tau = D_F$ (Case (2) in chapter 3).

Table 4.2. Distinctive features of the LTE signals used in the second algorithm.

Delay	CFs
D_u (Case(1))	$\alpha = 0$
D_F (Case(2))	$\alpha = 0$

Note that only $\alpha = 0$ is used at $\tau = D_u$, as other CFs depends on the length of the CP, and different CP lengths can be used with the LTE signals (see Section 3.3.4). Also note that only $\alpha = 0$ is used at $\tau = D_F$, as other CFs depend on the distribution of the RS, which is different for different transmission modes. The transmission mode is not known *a priori*.

The proposed joint detection and classification algorithm is a binary decision tree classifier, as shown in Fig. 4.1. At Step 1, we distinguish between WiMAX signals and LTE/noise class. For that we use the distinctive features of the WiMAX signals which were listed before. The test proposed in [24] is applied to check the existence of a peak at $\tau = D_u$ and $\alpha = 0$ (with $T_u = 91.4$ μs). Also the test in [25], which represents an extension of the previous one to multiple CFs, is applied to check the existence of peaks at $\tau = \lceil D_u / 3 \rceil$ and $\alpha = \nu D_F^{-1}$, $\nu = 0, 1, 2$, as well as $\tau = D_F$ and $\alpha = \nu D_F^{-1}$, $\nu = 0, 1, 2$ (with $T_u = 91.4$ μs and $T_F = 5$ ms). Note that the CAF of noise and LTE signals (any mode/subcarrier spacing) do not have peaks at the tested delays and CFs (See Section 3.3.4). If all the tested α's are found to be CFs at the corresponding delays, the decision is mobile WiMAX; otherwise, it is LTE/noise class. At Step 2, we distinguish between LTE signals with 15 kHz subcarrier spacing and LTE signals with 7.5 kHz subcarrier spacing/noise class. For that we use the distinctive features of the LTE signals ($\Delta f = 15$ kHz) that were listed before. The cyclostationarity test in [24] is employed to check whether or not $\alpha = 0$ is a CF for delays equal to D_u and D_F (with $T_u = 66.67$ μs and $T_F = 10$ ms). As these are the T_u and T_F for the LTE signals with 15 kHz subcarrier spacing, the CAF of the LTE signal with this subcarrier spacing has peaks at $\alpha = 0$ for both delays. Note that the CAF of LTE

signals with 7.5 kHz subcarrier spacing do not have a peak at $\alpha = 0$ and delay equal to D_u (with $T_u = 66.67$, See Section 3.3.4) and that the CAF of noise is zero at zero CF and non-zero delay. The decision that the LTE signals with 15 kHz subcarrier spacing (MBSFN or non MBSFN) is present is made if $\alpha = 0$ is found to be a CF at both delays; otherwise, it is assumed that either the LTE signal with 7.5 kHz subcarrier spacing (MBSFN) or noise is present in the channel. Finally, at Step 3, we distinguish between LTE signals with 7.5 kHz subcarrier spacing and noise. The cyclostationarity test in [24] is employed to check whether or not $\alpha = 0$ is a CF for delays equal to D_u and D_F (with $T_u = 133.33$ μs and $T_F = 10$ ms). As these are the T_u and T_F for the LTE signals with 7.5 kHz subcarrier spacing, the CAF of the LTE signals with this subcarrier spacing has peaks at $\alpha = 0$ for both delays. Note that the CAF of noise is zero at zero CF and non-zero delay. The decision that the LTE signal with this subcarrier spacing is present is made if $\alpha = 0$ at both delays is found to be a CF. Otherwise; the decision that only noise is present in the channel is made.

4.4. The Cyclostationarity Tests Used for Decision-Making

The cyclostationarity tests in [24] and [25], which are used for decision-making with the proposed algorithms, are described below. With the test in [24], the presence of a CF is formulated as a binary hypothesis-testing problem, i.e., under hypothesis H_0 the tested frequency α is not a CF at delay τ, and under hypothesis H_1 the tested frequency α is a CF at delay τ. The test consists of the following three steps:

- The CAF of the received signal, $r(n)$, is estimated (from L samples) at tested frequency α and delay τ, and a vector $\hat{\mathbf{R}}_r^{\alpha}$ is formed as

$$\hat{\mathbf{R}}_r^{\alpha} = [\mathrm{Re}\{\hat{R}_r^{\alpha}(\tau)\} \;\; \mathrm{Im}\{\hat{R}_r^{\alpha}(\tau)\}], \tag{4.1}$$

where $\mathrm{Re}\{\cdot\}$ and $\mathrm{Im}\{\cdot\}$ are the real and imaginary parts, respectively.

- A statistic Ψ_r^{α} is computed for the tested frequency α and delay τ as

$$\Psi_r^{\alpha} = L\, \hat{\mathbf{R}}_r^{\alpha}\, \hat{\Sigma}^{-1}\, \hat{\mathbf{R}}_r^{\alpha\,\dagger}, \tag{4.2}$$

where the superscripts -1 and $\dagger$ denote the matrix inverse and transpose, respectively, and $\hat{\Sigma}$ is an estimate of the covariance matrix of $\hat{\mathbf{R}}_r^{\alpha}$

$$\hat{\Sigma} = \begin{bmatrix} \mathrm{Re}\{(Q_0 + Q_1)/2\} & \mathrm{Im}\{(Q_0 - Q_1)/2\} \\ \mathrm{Im}\{(Q_0 + Q_1)/2\} & \mathrm{Re}\{(Q_1 - Q_0)/2\} \end{bmatrix}, \tag{4.3}$$

with the covariances Q_0 and Q_1 are given, for zero-mean process, respectively by [24]

$$Q_0 = \lim_{L\to\infty} L^{-1} \sum_{i=0}^{L-1} \sum_{\xi=-\infty}^{\infty} Cum[f(i;\tau), f(i+\xi;\tau)]\, e^{-j2\pi 2\alpha i} e^{-j2\pi\alpha\xi}, \tag{4.4}$$

and

$$Q_1 = \lim_{L\to\infty} L^{-1} \sum_{i=0}^{L-1} \sum_{\xi=-\infty}^{\infty} \mathrm{Cum}[f(i;\tau), f^*(i+\xi;\tau)] e^{-j2\pi(-\alpha)i}, \tag{4.5}$$

where $\mathrm{Cum}[\cdot]$ is the cumulant operator and $f(i;\tau) = r(i)r^*(i+\tau)$ is the lag product.

The estimators for the covariances Q_0 and Q_1 are given respectively by [24]

$$\hat{Q}_0 = (LL_{sw})^{-1} \sum_{s=-(L_{sw}-1)/2}^{(L_{sw}-1)/2} W^{(L_{sw})}(s) F_{\tau}^{(L)}(\alpha - sL^{-1}) F_{\tau}^{(L)}(\alpha + sL^{-1}), \tag{4.6}$$

and

$$\hat{Q}_1 = (LL_{sw})^{-1} \sum_{s=-(L_{sw}-1)/2}^{(L_{sw}-1)/2} W^{(L_{sw})}(s) F_\tau^{*(L)}(\alpha + sL^{-1}) F_\tau^{(L)}(\alpha + sL^{-1}), \tag{4.7}$$

where $W^{(L_{sw})}$ is a spectral window of length L_{sw} and $F_\tau^{(L)}(\alpha) = \sum_{l=0}^{L-1} r\ (l) r^*(l+\tau)\ e^{-j2\pi\alpha l}$.

- The test statistic Ψ_r^α is compared against a threshold, Γ, for decision making. If $\Psi_r^\alpha \geq \Gamma$, we decide that the tested frequency α is a CF at delay τ. The threshold Γ is set for a given asymptotic probability of false alarm, which is defined as the asymptotic probability to decide that the tested frequency α is a CF at delay τ, when this is actually not. This can be expressed as $\Pr\{\Psi_r^\alpha \geq \Gamma \mid H_0\}$. By using that the statistics Ψ_r^α has an asymptotic chi-square distribution with two degrees of freedom under the hypothesis H_0 [24], the threshold Γ is obtained from the tables of the chi-squared distribution for a given value of this probability.

The cyclostationarity test proposed in [25] represents an extension of the one presented previously to multiple CFs. In this case, the test statistic is

$$\Psi_r = \sum_{\{\alpha\}} \Psi_r^\alpha, \tag{4.8}$$

where $\{\alpha\}$ is the set of tested frequencies and Ψ_r^α is calculated at each tested frequency according to (4.2). The threshold is similarly set, based on the asymptotic distribution of the test statistic Ψ_r under the hypothesis H_0. As shown in [25], this is a chi-square distribution with $2N_\alpha$ degrees of freedom, where N_α represents the number of tested frequencies. Apparently, for $N_\alpha = 1$, this test reduces to the one proposed in [24].

4.5. Summary

Two cyclostationarity-based algorithms for joint detection and classification of the OFDM-based mobile WiMAX and LTE signals are proposed in this chapter. The proposed algorithms exploit information on signal parameters that is known *a priori* i.e., the useful OFDM symbol duration (equivalently, subcarrier spacing) and the frame duration.

Chapter 5

Joint Detection and Classification Performance and Complexity for the Two Proposed Algorithms

In this chapter, the joint detection and classification performance of the proposed algorithms are evaluated through computer simulations, and their computational complexity is investigated. The simulation setup is introduced in Section 5.1, the joint detection and classification performance of the first algorithm is evaluated in Section 5.2, the joint detection and classification performance of the second algorithm is evaluated in Section 5.3, the performance and computational complexity of both algorithms are compared in Section 5.4, and finally, conclusions are drawn in Section 5.5.

5.1. Simulation Setup

The signals are simulated with 5 MHz double-sided bandwidth. For WiMAX, the number of subcarriers used here is 512, while for LTE, this is 512 for the LTE signals with 15 kHz subcarrier spacing, and 1024 kHz for the LTE signal with 7.5 kHz subcarrier spacing. For the mobile WiMAX signal, the value of T_{cp}/T_u is 1/8, as being a common value. For the LTE signal, both long ($T_{cp}/T_u = 1/4$) and short ($T_{cp}/T_u = 10/128$ for the

first symbol in the slot and $T_{cp}/T_u = 9/128$ for the remaining symbols) CPs are used. For both WiMAX and LTE signals, QAM with 16 points and unit variance of the signal constellation is used to modulate the data subcarriers. The pilot subcarriers in mobile WiMAX are modulated according to the IEEE 802.16e standard. A raised root cosine pulse shape window is used at the transmitter with a roll-off factor of 0.025. For the WiMAX signal, the number of symbols in the UL and DL subframes equals 35 and 12, respectively, and the RTG duration (T_{RG}) is 60 μs, whereas the TTG duration equals ($T_F - 47T - 60$ μs) [16]. The sampling frequency at the receiver is set to 8.4 MHz. The AWGN and ITU-R pedestrian and vehicular A fading channels are considered. The maximum delay spreads for the ITU-R pedestrian and vehicular A fading channels are 410 ns and 2.51 μs, respectively. For details on the power-delay profiles of the fading channels one is referred to [26]. The maximum Doppler frequency equals 7.28 Hz and 145.69 Hz for the ITU-R pedestrian and vehicular A fading channels, respectively. At the receive-side, a filter is used to remove the out-of-band noise, SNR is set at the output of this filter. The probability of correct joint detection and classification $P_{dc}(i|i)$, is used as performance measure, with i= WiMAX signal, LTE signals with 15 kHz subcarrier spacing (will be referred to in the figures as LTE_1), and LTE signal with 7.5 kHz subcarrier spacing (will be referred to in the figures as LTE_2). This is estimated based on 1,000 Monte Carlo simulation trials. Unless otherwise mentioned, the observation interval is 30 ms (equivalent to 6 WiMAX frames and 3 LTE frames), the threshold used with the cyclostationarity test is set to 9.2103 at all steps, which corresponds to an asymptotic probability of false alarm of 0.01, and the channel is AWGN.

5.2. Joint Detection and Classification Performance of the First Proposed Algorithm

Fig. 5.1 shows the simulation results for the probability of correct joint signal detection and classification versus SNR for mobile WiMAX, LTE signal with 15 kHz subcarrier spacing and long CP (MBSFN and non-MBSFN have the same results), LTE with non-MBSFN mode and short CP, and LTE with MBSFN mode and 7.5 kHz subcarrier spacing. One can see from these figures that the best results are achieved for the LTE signals with long CP. Lower performance is achieved for the WiMAX signal. The lowest performance is achieved for the LTE signal with non-MBSFN mode and short CP. Note that this is expected and is in agreement with the values for T_{cp} / T_u and the results for the CAF magnitude in Sections 2.3.4 and 3.3.4. From Fig. 5.1, one can see that for the WiMAX signal, the probability of correct detection and classification reaches 1 when the SNR is above -10 dB, while for the LTE signals with long CP, this probability approaches 1 for SNRs above -12 dB. When the short CP is used, the performance of the algorithm degrades. The probability of correct joint detection and classification goes to 1 for SNRs above -7.

Figs. 5.2 a) - d) show the simulation results for the probability of correct joint signal detection and classification for mobile WiMAX, LTE signal with 15 kHz subcarrier spacing and long CP (MBSFN and non-MBSFN have the same results), LTE with non-MBSFN mode and short CP, and LTE with MBSFN mode and 7.5 kHz subcarrier spacing,

respectively, with different observation intervals and thresholds used for decision making[14]. As expected, an improved performance is achieved with increased observation interval for all signals. One can also see from Figs. 5.2 a) – d) that, as expected, a higher probability of correct joint detection and classification is achieved with a lower threshold.

Figs. 5.3 a) – d) show the simulation results for the probability of correct joint signal detection and classification for mobile WiMAX, LTE signal with 15 kHz subcarrier spacing and long CP (MBSFN and non-MBSFN have the same results), LTE with non-MBSFN mode and short CP, and LTE with MBSFN mode and 7.5 kHz subcarrier spacing, respectively, with AWGN, and ITU-R pedestrian and vehicular A channels. Based on these results, one can notice that the probability of correct joint detection and classification in all investigated cases is not influenced by the channel type.

From the above results, one can see that the proposed algorithm does not require an estimation of the channel, signal power, or noise power. However, an estimation of the bandwidth and carrier frequency is required.

[14] Note that the same threshold is used at all the steps of the algorithm. The thresholds used are 9.210 (referred to as Γ_1 in the figures) and 10.597 (referred to as Γ_2 in the figures). The thresholds correspond to $\Pr\{\Psi_r^{\alpha} \geq \Gamma \mid H_0\}$ of 0.01 and 0.005, respectively (See Chapter 4 for details on the cyclostationarity tests).

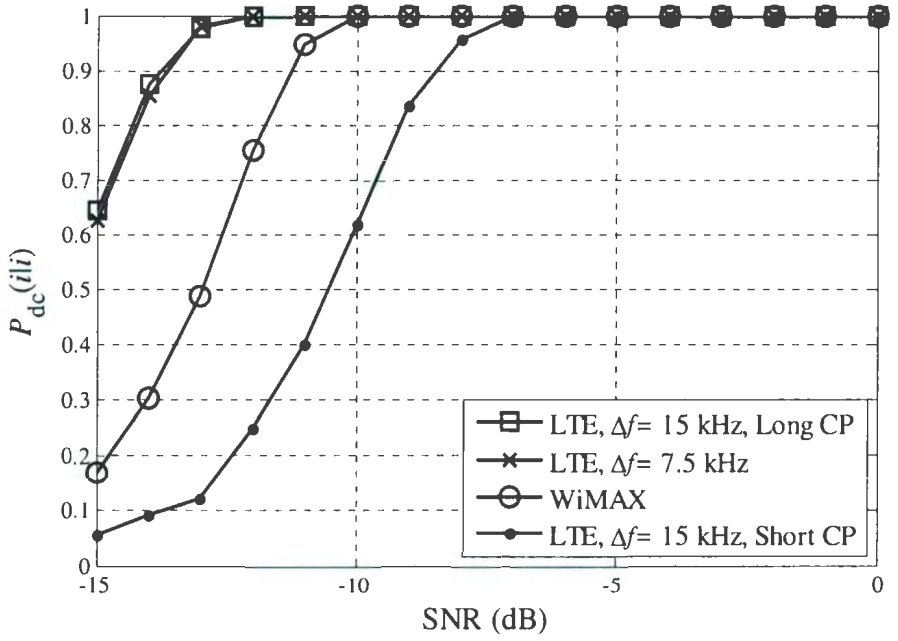

Fig. 5.1. Probability of correct joint detection and classification versus SNR of the signals of interest.

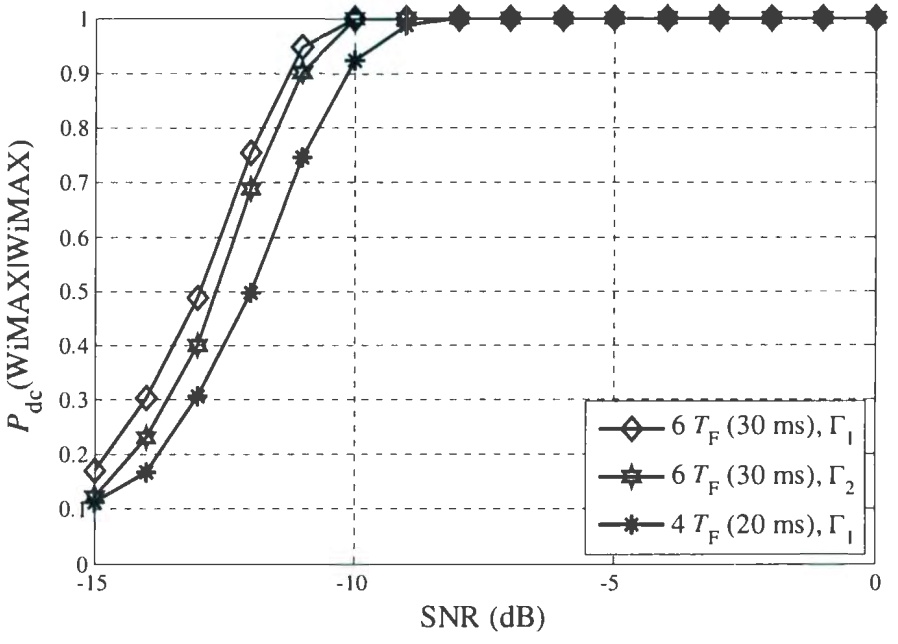

a)

b)

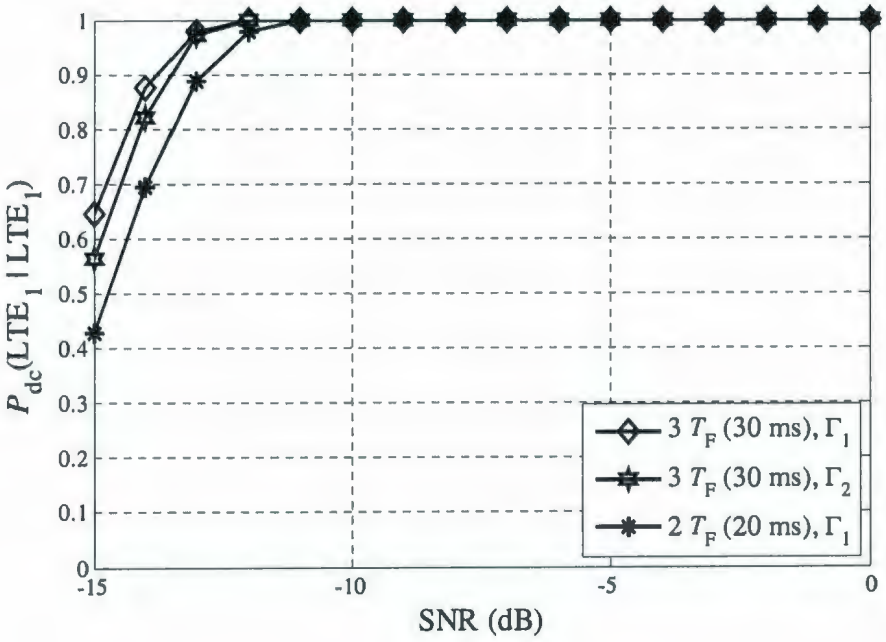
$P_{dc}(LTE_1 | LTE_1)$
SNR (dB)
3 T_F (30 ms), Γ_1
3 T_F (30 ms), Γ_2
2 T_F (20 ms), Γ_1

c)

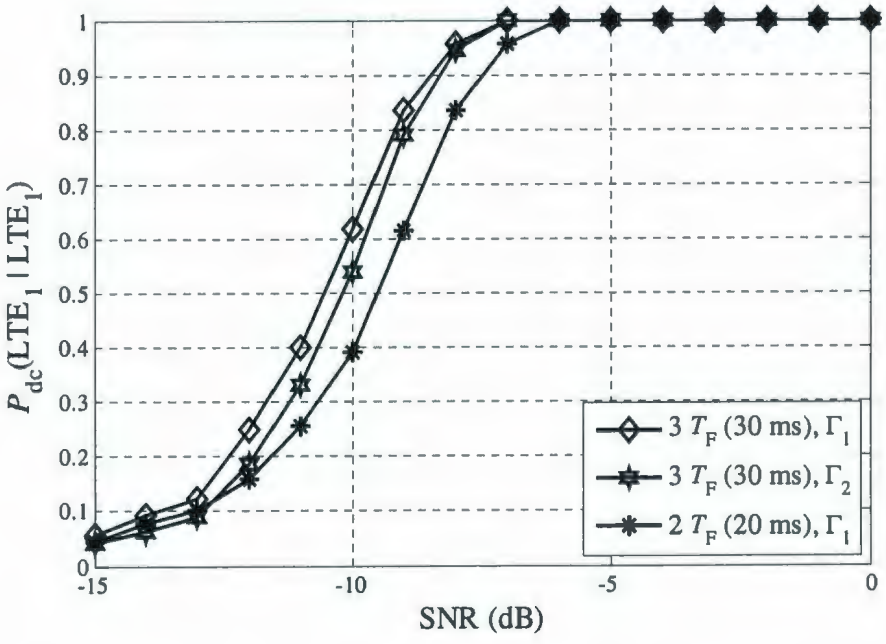
$P_{dc}(LTE_1 | LTE_1)$
SNR (dB)
3 T_F (30 ms), Γ_1
3 T_F (30 ms), Γ_2
2 T_F (20 ms), Γ_1

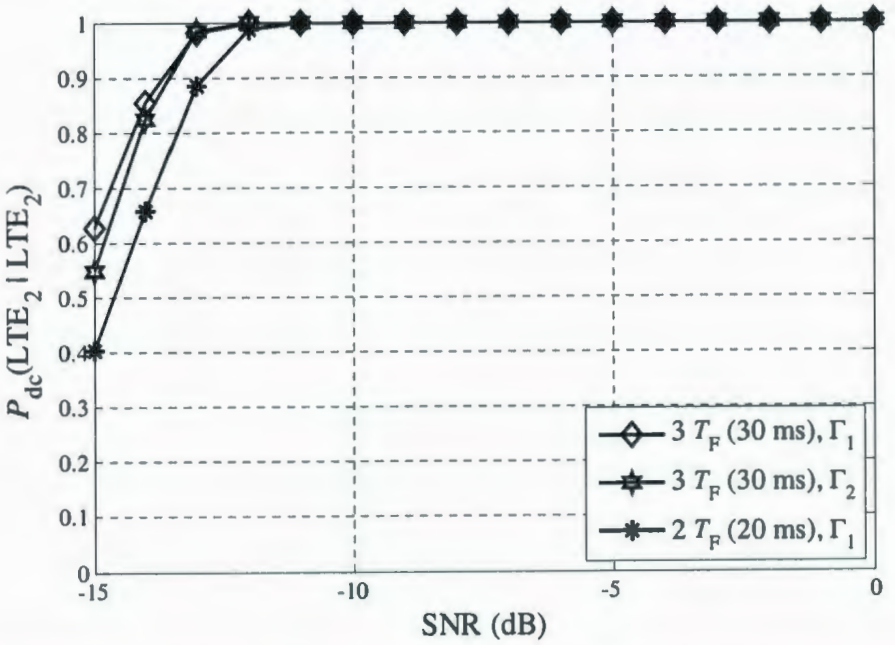

d)

Fig. 5.2. Probability of correct joint detection and classification versus SNR with various observation intervals and thresholds used for decision making a) WiMAX signal b) LTE signal (MBSFN mode with $\Delta f = 15$ kHz, or non MBSFN mode with long CP) c) LTE signal (non-MBSFN mode and short CP) d) LTE signal (MBSFN mode with $\Delta f = 7.5$ kHz).

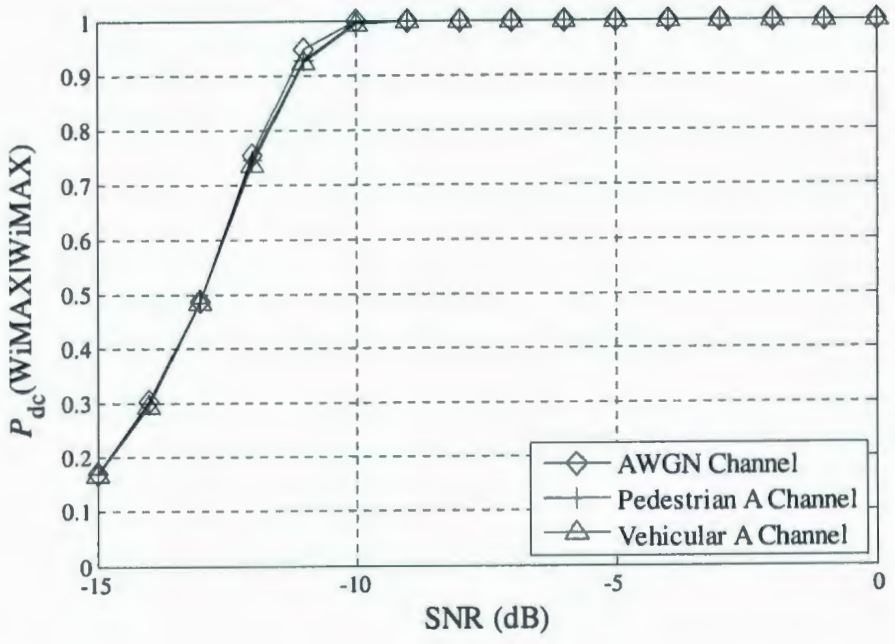

a)

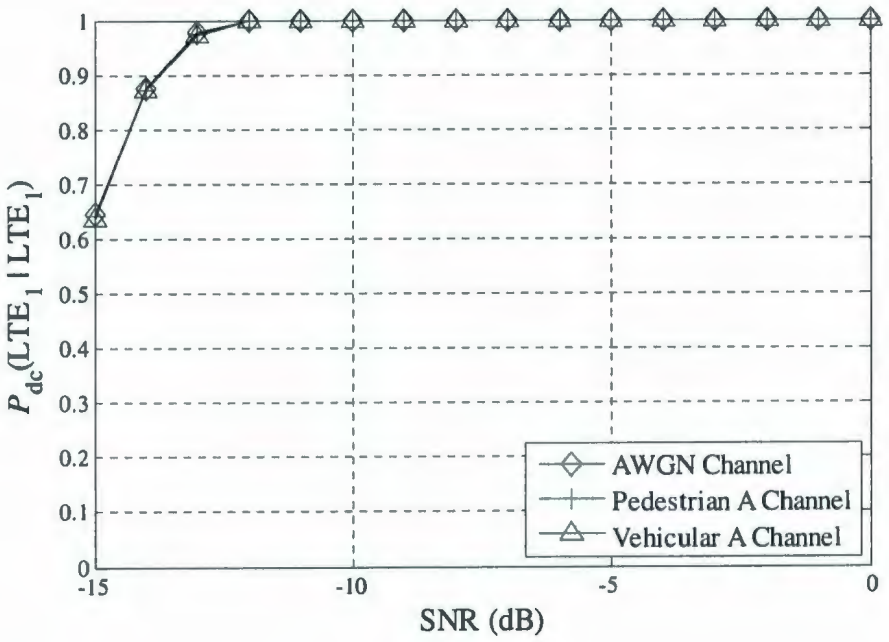
$P_{dc}(LTE_1 | LTE_1)$
SNR (dB)
AWGN Channel
Pedestrian A Channel
Vehicular A Channel

b)

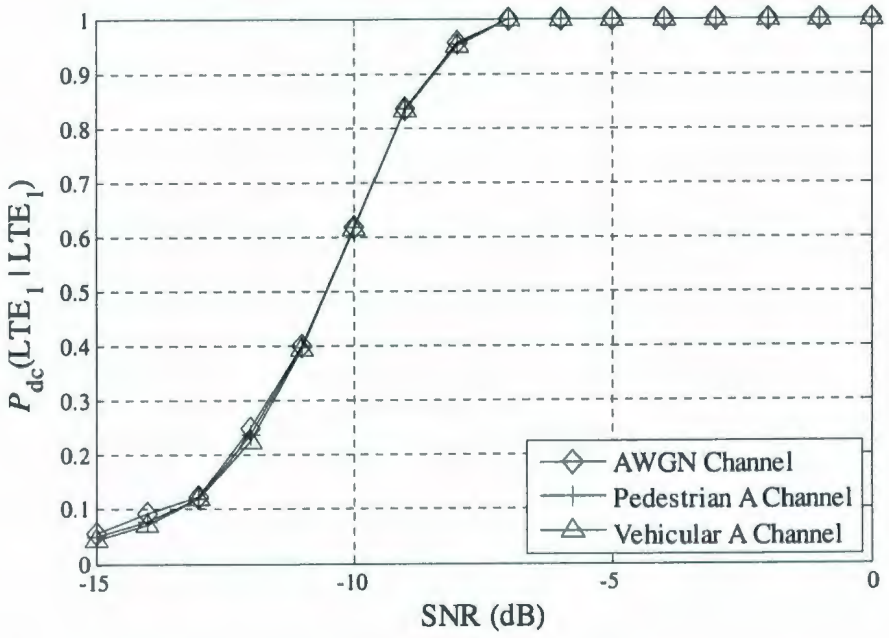
$P_{dc}(LTE_1 | LTE_1)$
SNR (dB)
AWGN Channel
Pedestrian A Channel
Vehicular A Channel

c)

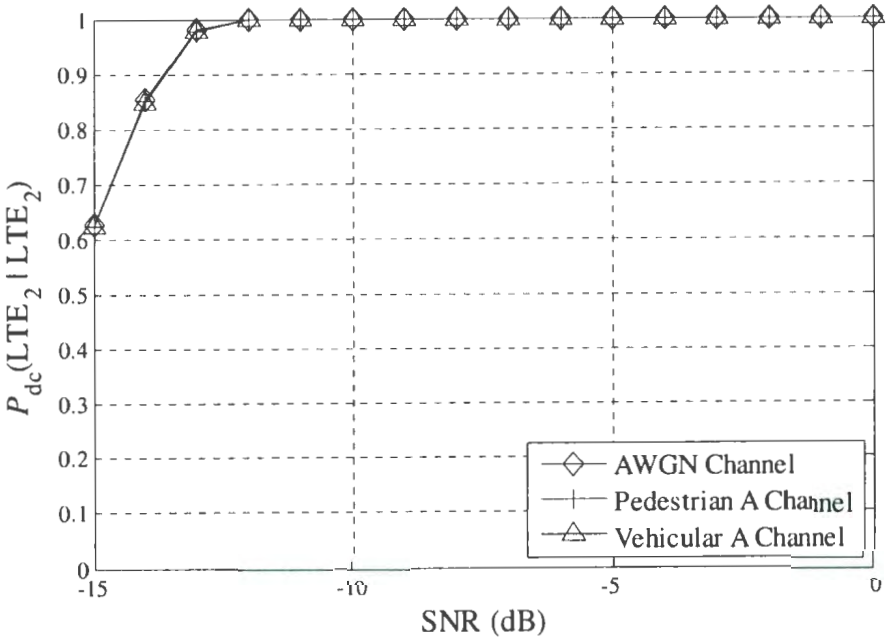

d)

Fig. 5.3. Probability of correct joint detection and classification versus SNR under different channel conditions a) WiMAX signal b) LTE signal (MBSFN mode with $\Delta f = 15$ kHz, or non MBSFN mode with long CP) c) LTE signal (non-MBSFN mode and short CP) d) LTE signal (MBSFN mode with $\Delta f = 7.5$ kHz).

5.3. Joint Detection and Classification Performace of the Second Proposed Algorithm

In this Section, the joint detection and classification performance of the second proposed algorithm is investigated. Note that with the first proposed algorithm (Section 5.2), we consider the simulations for 4 different cases, i.e., mobile WiMAX, LTE signal with 15 kHz subcarrier spacing and long CP (MBSFN and non-MBSFN have the same results), LTE with non-MBSFN mode and short CP, and LTE with MBSFN mode and 7.5 kHz subcarrier spacing. Since the second algorithm gives different results with the LTE signal with non-MBSFN mode and long CP from those with the LTE signal with MBSFN mode and 15 kHz subcarrier spacing, we will consider the simulations here for 5 cases, i.e., mobile WiMAX, LTE with the non-MBSFN mode and long CP, LTE with non-MBSFN mode and short CP, LTE with MB-SFN mode and 15 kHz subcarrier spacing, and LTE with MBSFN mode and 7.5 kHz subcarrier spacing.

Fig. 5.4 shows the probability of correct joint detection and classification of mobile WiMAX signal versus SNR when one, two, and three CFs are respectively employed at both delays of $\lceil D_u / 3 \rceil$ and D_F (with $T_u = 91.4$ μs and $T_F = 5$ ms). At these delays, the CFs of interest are zero, $1/D_F$, and $2/D_F$ (with $T_F = 5$ ms). One can easily see that the detection performance is significantly enhanced at lower SNRs when employing more CFs. This explains the reason for which the second algorithm employs the aforementioned 3 CFs of the WiMAX signals, for their joint detection and classification.

Fig. 5.5 shows the simulation results for the probability of correct joint signal detection and classification versus SNR for mobile WiMAX, LTE with the non-MBSFN mode and long CP, LTE with non-MBSFN mode and short CP, LTE with MB-SFN mode and 15 kHz subcarrier spacing, and LTE with MBSFN mode and 7.5 kHz subcarrier spacing, respectively. One can see that among the LTE signals, the best results are achieved for the LTE signals with the MBSFN mode. Lower performance is achieved for the LTE signal with the non MBSFN mode and long CP. The lowest performance is achieved for the LTE signal with non-MBSFN mode and short CP. Note that this is expected and is in agreement with the results of the CAF magnitude at $\tau = D_F$ (with $T_F = 10$ ms) in Chapter 3. As the magnitude of the CAF at $\tau = D_F$ is less than that at $\tau = D_u$ for all signals, the results for the CAF magnitude at $\tau = D_F$ practically decide the behavior of the algorithm for all LTE signals. Note that, as mentioned previously in Section 4.3, the CP-induced cyclostationarity can be unreliable for joint detection and classification, as the cognitive users sharing the spectrum may employ other types of signals with OFDM modulation and close useful symbol duration, therefore, the preamble- and RS-induced cyclostationarity are employed in this algorithm.

From Fig. 5.5, one can see that for the WiMAX signal, the probability of correct detection and classification reaches 1 when the SNR is above -4 dB, while for the LTE signal with the non-MBSFN mode and long CP, this probability approaches 1 for SNRs above -5 dB. When the LTE signal with the non-MBSFN mode and short CP is used, the probability of correct joint detection and classification goes to 1 for SNRs above -4. For

the LTE signals with the MBSFN mode, the probability of correct detection and classification reaches 1 when the SNR is above -9 dB.

Figs. 5.6 a) – e) show the simulation results for the probability of correct joint signal detection and classification versus SNR for mobile WiMAX, LTE with the non-MBSFN mode and long CP, LTE with non MB-SFN mode and short CP, LTE with MBSFN mode and 15 kHz subcarrier spacing, and LTE with MBSFN mode and 7.5 kHz subcarrier spacing, respectively, with different observation intervals and thresholds used for decision-making. Note that the same thresholds are used at all steps of the algorithm. The thresholds used are 9.210 with 1 CF and 16.812 with 3 CFs (this set of thresholds correspond to $\Pr\{\Psi_r^{\alpha} \geq \Gamma \mid H_0\}$ of 0.01 and is referred to in the figures as Γ_1), and 10.597 with 1 CF and 18.548 with 3 CFs (this set of thresholds correspond to $\Pr\{\Psi_r^{\alpha} \geq \Gamma \mid H_0\}$ of 0.005 and is referred to in the figures as Γ_2). As expected, an improved performance is achieved with increased observation interval for all signals. One can also see from Figs. 5.6 a) – e) that, as expected, higher probability of correct joint detection and classification is achieved with lower thresholds.

Figs. 5.7 a) – e) show the simulation results for the probability of correct joint signal detection and classification versus SNR for mobile WiMAX, LTE with the non-MBSFN mode and long CP, LTE with non MB-SFN mode and short CP, LTE with MB-SFN mode and 15 kHz subcarrier spacing, and LTE with MBSFN mode and 7.5 kHz subcarrier spacing, respectively, with AWGN, and ITU-R pedestrian and vehicular A channels. One can notice that for all cases, the correct joint detection and classification performance degrades at lower SNRs under the ITU-R vehicular channel.

As in the first algorithm, there is no need for the estimation of the channel, signal power, or noise power. However, an estimation of the bandwidth and carrier frequency is required.

5.4. Comparison of the Proposed Algorithms

In this Section, we compare the joint detection and classification performance, as well as the complexity of the proposed algorithms. Based on the previous results in Sections 5.2 and 5.3, one can notice that the first algorithm achieves better performance for all signals. This can be explained based on the fact that the first algorithm depends only on the correlation in the signals of interest due to the CP, while the second algorithm incorporates other types of correlations (preamble- and RS-induced). The CP-induced correlation is the strongest in all cases as can be seen in the results for the CAF magnitude in Chapters 2 and 3. One can also note from the results in Sections 5.2 and 5.3 that the joint detection and classification performance of the first algorithm is not affected by the vehicular A channel, while the performance degrades a little with the second algorithm. This can be explained based on the fact that the correlation due to the CP (on which, the first algorithm is based) is the strongest, where a considerable portion of the OFDM symbol is replicated in time for every single OFDM symbol.

For the computational complexity of the proposed algorithms, we are interested in the computation of the test statistics (see Section 4.4). At each delay, To compute the test statistic at one CF, one needs the estimation of the covariance matrix $\hat{\Sigma}$. This requires the estimation of Q_0 and Q_1. Based on (4.6), one can easily find that the estimation of Q_0 requires $(L+1)L_{sw}+L+4$ complex multiplications and $(L-1)L_{sw}+(L_{sw}-1)/2$ complex

additions, where L is the total number of the processed samples at the received-side and L_{sw} is the length of the spectral window, $W^{(L_{sw})}$. Furthermore, the estimation of Q_1 requires additional $1+2L_{sw}$ complex multiplications and $L_{sw}-1$ complex additions. At each delay, the estimation of the test statistic at a single CF requires $(L+3)L_{sw}+L+22$ complex multiplications and $(L-1)L_{sw}+3(L_{sw}-1)/2+6$ complex additions. Given that L_{sw} is usually set as a percentage multiplied by L, e.g., $L_{sw}=0.01\times L$, the order of complexity for the first algorithm can be given as $O(L^2)$, where $O(.)$ represents the big O notation. Furthermore, with the second algorithm, to estimate the test statistic for each additional CF ($\alpha=\nu D_F^{-1}$, $\nu=1, 2$, at step 1), one additionally needs $I_F(L+1)+2L_{sw}+21$ complex multiplications and $I_F(L-1)+3(L_{sw}-1)/2+6$ complex additions, where I_F is the number of WiMAX frames in the considered observation interval. Therefore, the order of complexity for the second algorithm can also be given as $O(L^2)$. For example, with the parameters considered for the simulation setup in Section 5.1 and with an observation interval of 30 ms (corresponding to 6 WiMAX frames and 3 LTE frames), the numbers of complex computations required with both algorithms are listed in table 5.1, respectively. With a high performance microprocessor, that is able to execute up to 107.550 billion floating point operations per second [27], the highest number of complex computations in table 5.1 can be executed in approximately 142 ms. As can be noticed from table 5.1, the computational complexity of the second algorithm is higher than that of the first algorithm. This is expected, as the second algorithm requires the estimation of test statistics at more delays and CFs.

From the above, one can conclude that the first algorithm gives better joint detection and classification performance and has less computational complexity. However, the CP-induced cyclostationarity can be unreliable for joint detection and classification, as the cognitive users sharing the spectrum may employ other types of signals with OFDM modulation and close useful symbol duration (equivalently, close subcarrier frequency separation), therefore, the preamble- and RS-induced cyclostationarity are employed in the second algorithm.

Table 5.1. Number of complex computations required by the proposed algorithms

		WiMAX	LTE ($\Delta f = 15$ kHz)	LTE ($\Delta f = 7.5$ kHz)
First Algorithm	Number of complex multiplications	1.2703×10^9	2.5407×10^9	3.8110×10^9
	Number of complex Additions	1.2700×10^9	2.5402×10^9	3.8102×10^9
	Total number of complex computations	2.5404×10^9	5.0809×10^9	7.6213×10^9
Second Algorithm	Number of complex multiplications	3.8171×10^9	6.3578×10^9	7.6282×10^9
	Number of complex Additions	3.8163×10^9	6.3565×10^9	7.6266×10^9
	Total number of complex computations	7.6335×10^9	1.2714×10^{10}	1.5255×10^{10}

5.5. Summary

In this chapter, the joint detection and classification performance, as well as the complexity of the proposed algorithms are studied. Results show that both algorithms lead to good joint detection and classification performance with reasonably short sensing time, at low SNRs, and different channel conditions. The first algorithm has better performance in all cases and has less computational complexity. However, the CP-induced cyclostationarity can be unreliable, as there might be other cognitive users around employing OFDM modulation with useful OFDM symbol durations that are the vicinity of detected signal.

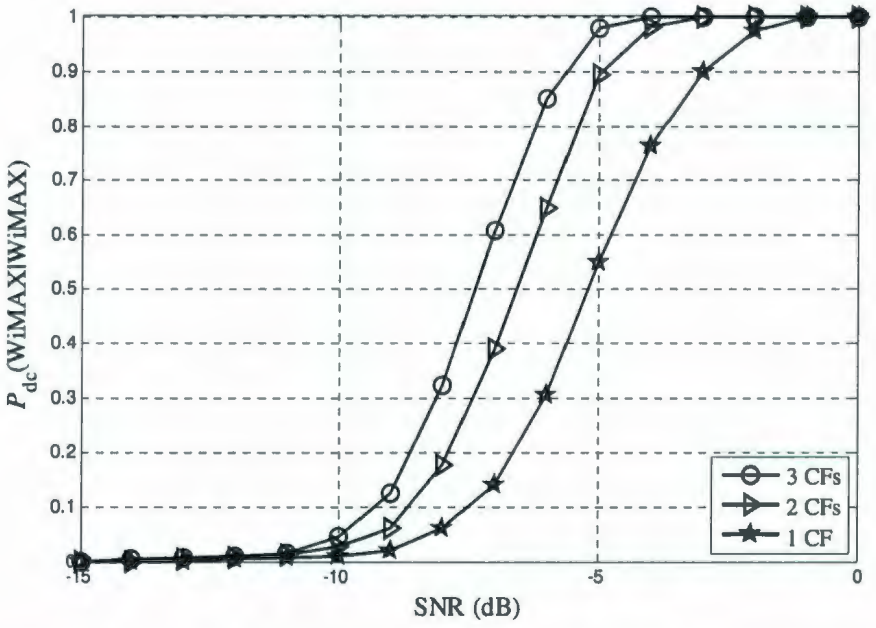

Fig. 5.4. Probability of correct joint detection and classification of the mobile WiMAX signal versus SNR for different number of CFs used in decision making.

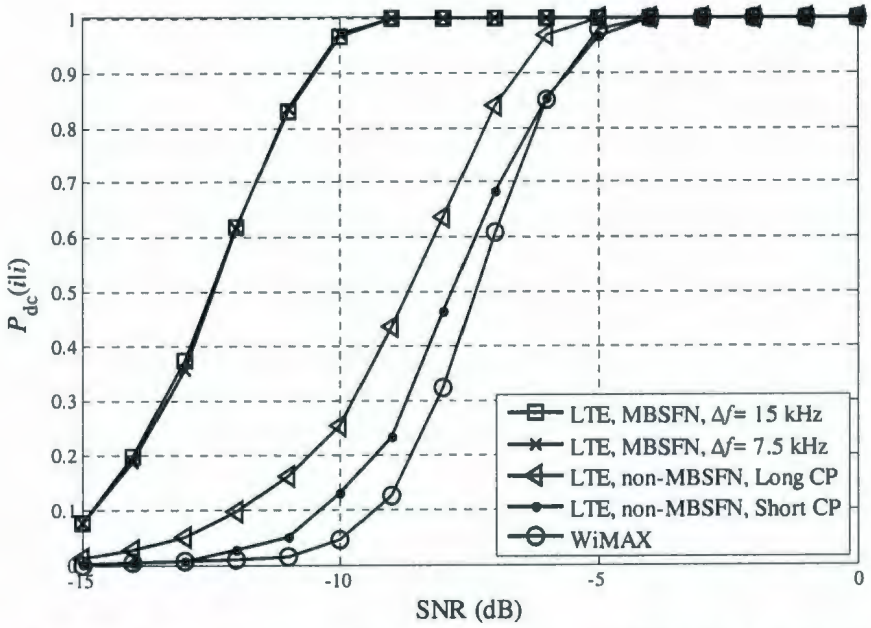

Fig. 5.5. Probability of correct joint detection and classification versus SNR for the signals of interest.

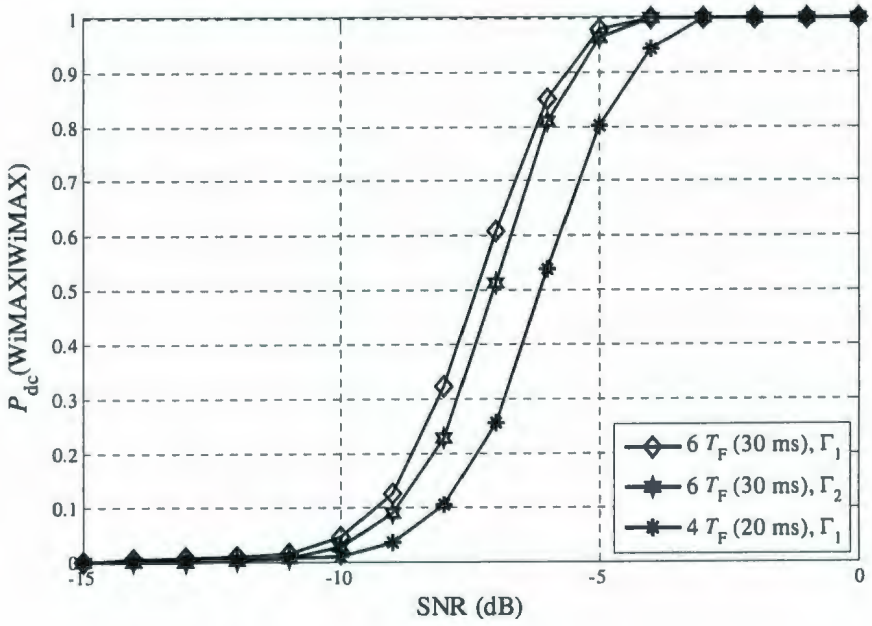

a)

b)

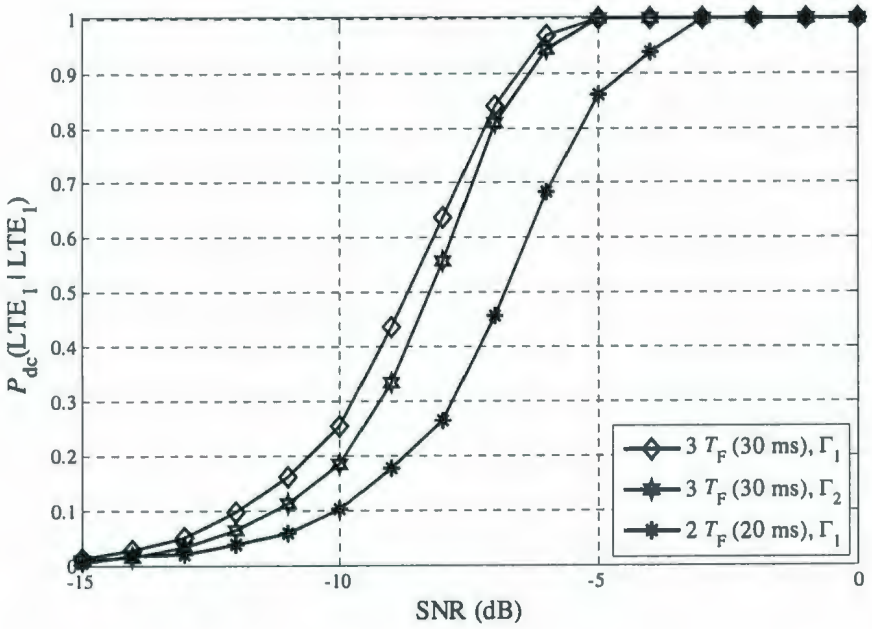
$P_{dc}(LTE_1 | LTE_1)$
SNR (dB)
3 T_F (30 ms), Γ_1
3 T_F (30 ms), Γ_2
2 T_F (20 ms), Γ_1

c)

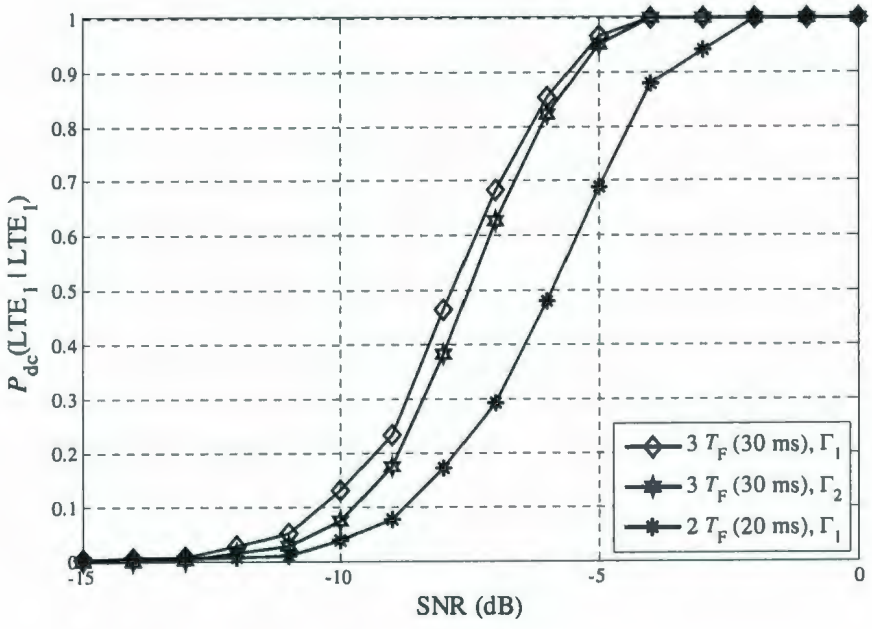
$P_{dc}(LTE_1 | LTE_1)$
SNR (dB)
3 T_F (30 ms), Γ_1
3 T_F (30 ms), Γ_2
2 T_F (20 ms), Γ_1

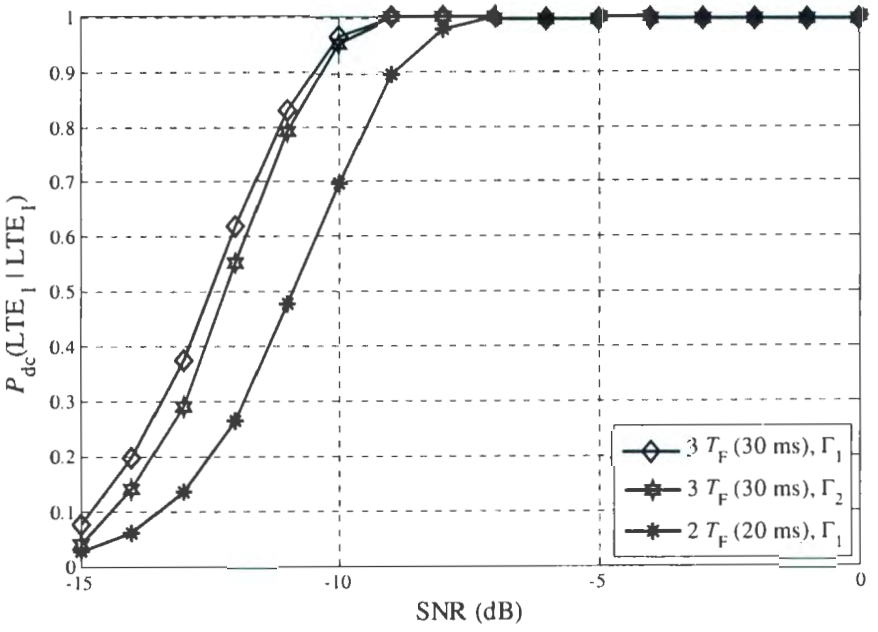

d)

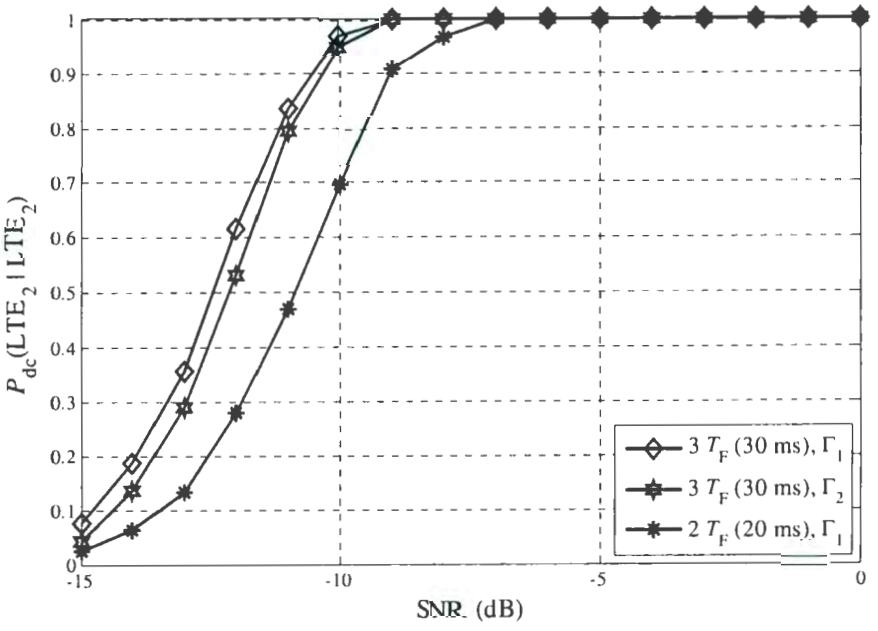

e)

Fig. 5.6. Probability of correct joint detection and classification versus SNR with various observation intervals and thresholds used for decision making a) WiMAX signal b) LTE signal (non-MBSFN mode with long CP) c) LTE signal (non-MBSFN mode with short CP) d) LTE signal (MBSFN mode with $\Delta f = 15$ kHz) e) LTE signal (MBSFN mode with $\Delta f = 7.5$ kHz).

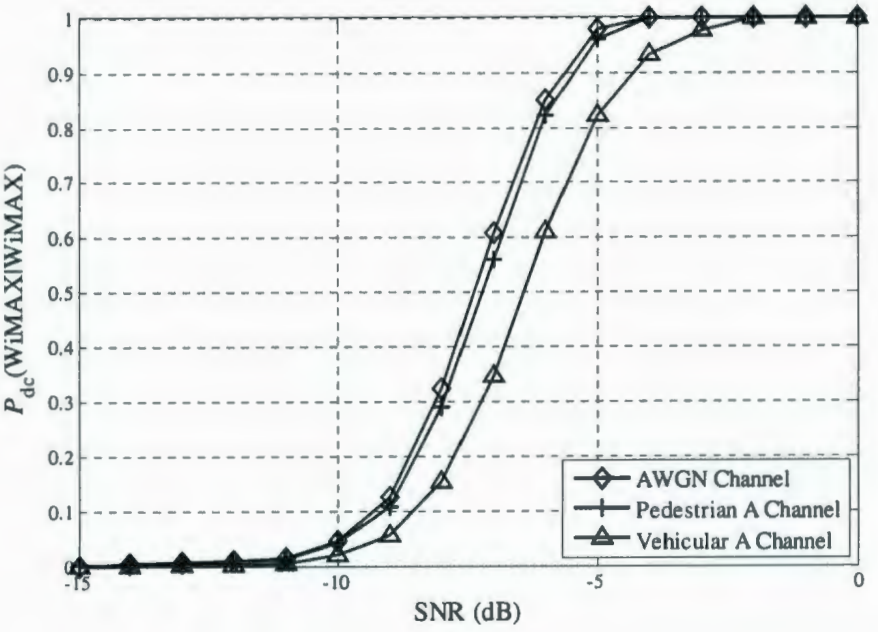
P_{dc}(WiMAX|WiMAX)
SNR (dB)
AWGN Channel
Pedestrian A Channel
Vehicular A Channel

a)

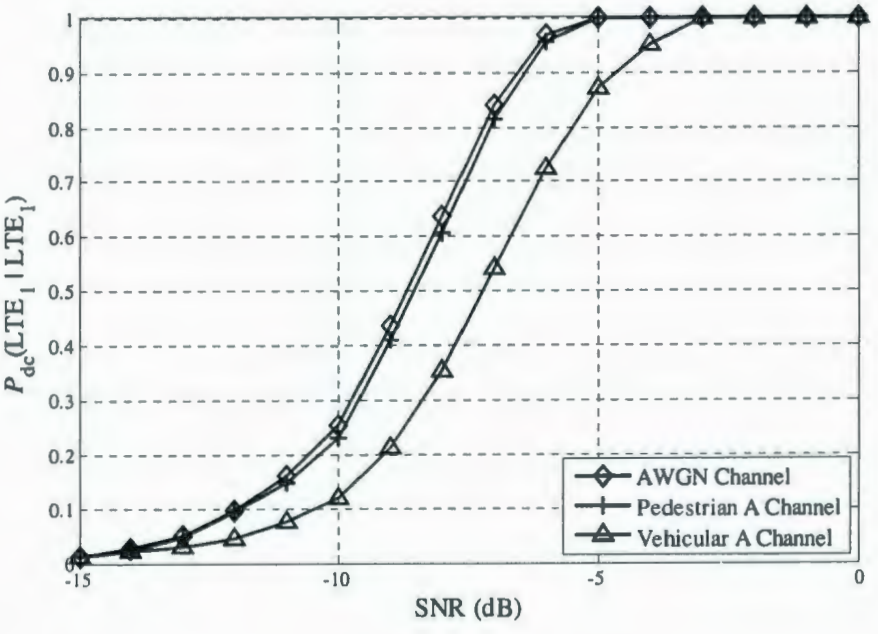
$P_{dc}(LTE_1|LTE_1)$
SNR (dB)
AWGN Channel
Pedestrian A Channel
Vehicular A Channel

b)

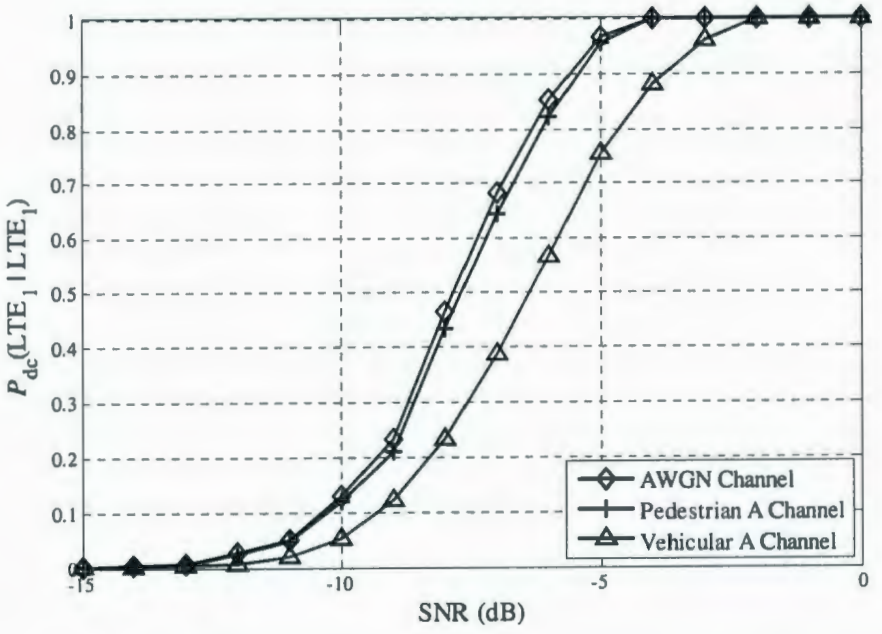
$P_{dc}(LTE_1 | LTE_1)$
SNR (dB)
AWGN Channel
Pedestrian A Channel
Vehicular A Channel

c)

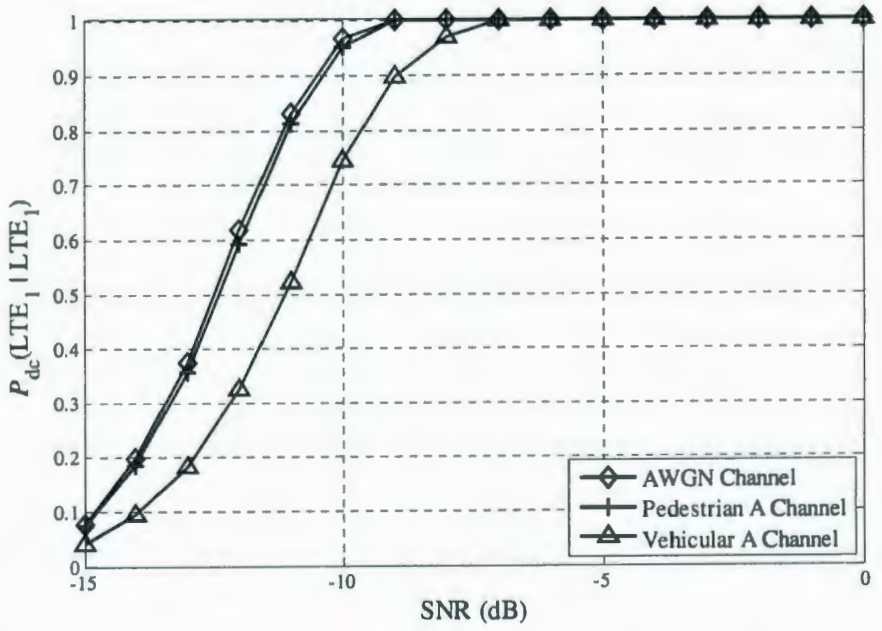
$P_{dc}(LTE_1 | LTE_1)$
SNR (dB)
AWGN Channel
Pedestrian A Channel
Vehicular A Channel

d)

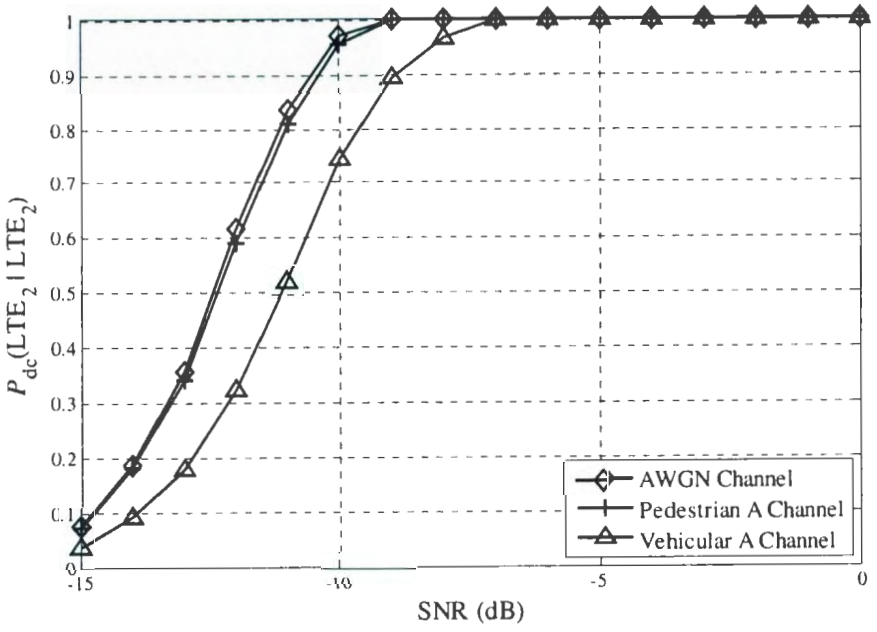

e)

Fig. 5.7. Probability of correct joint detection and classification versus SNR under different channel conditions a) WiMAX signal b) LTE signal (non-MBSFN mode with long CP) c) LTE signal (non MBSFN mode with short CP) d) LTEsignal (MBSFN mode with $\Delta f = 15$ kHz) e) LTE signal (MBSFN mode with $\Delta f = 7.5$ kHz).

Chapter 6

Conclusions and Future Work

In this thesis, the second-order cyclostationarity of OFDM-based signals employed in two popular wireless technologies, namely, the OFDM-based mobile Worldwide Interoperability for Microwave Access (WiMAX) and third Generation Partnership Project Long Term Evolution (3GPP LTE), is studied. Furthermore, the second-order cyclostationarity of these signals are exploited to develop two algorithms for joint detection and classification. The proposed algorithms lead to a good joint detection and classification performance even at low signal-to-noise-ratios (SNRs).

The following are the major contributions of this thesis:

- The OFDM-based mobile WiMAX and LTE signals are studied and models for these signals are developed.

- The second-order cyclostationarity of the OFDM-based mobile WiMAX and LTE signals is investigated, and closed-form expressions of the cyclic autocorrelation function (CAF) and cyclic frequencies (CFs) for these signals are derived.

- As an application to the new findings, an algorithm for joint detection and classification of the OFDM-based mobile WiMAX and LTE signals based on the CP-induced cyclostationarity is proposed.

- Furthermore, a second algorithm which incorporates the CP-, preamble-, and RS-induced second-order cyclostationarity signal features of the mobile WiMAX and LTE signals is proposed for their joint detection and classification.

- The joint detection and classification performance of the proposed algorithms is evaluated through computer simulation, and their computational complexity is investigated.

Both algorithms are used in operating frequency bands that are common to both signals. Simulation results show that both algorithms lead to good joint detection and classification performance under low SNRs, short sensing times, and diverse channel conditions. The proposed algorithms do not require an estimation of the channel, signal power, or noise power. However, an estimation of the bandwidth and carrier frequency is required. Both algorithms have reasonable computational complexity. The first algorithm gives better joint detection and classification performance and has less computational complexity. However, the CP-induced cyclostationarity can be unreliable for joint detection and classification, as the cognitive users sharing the spectrum may employ other types of signals with OFDM modulation and close useful symbol duration, therefore, the preamble- and RS-induced cyclostationarity of the signals of interest are employed in the second algorithm.

Suggested future areas of work are as follows:

- Verifying the proposed algorithms under more realistic conditions, e.g., when the effect of timing offset and carrier frequency offset are considered. The robustness of the proposed algorithms to the accuracy in the bandwidth estimation can also be studied.
- Study of the cyclostationarity of other transmission modes of the mobile WiMAX signals (i.e., the frequency division duplexing (FDD) UL and DL transmission). As LTE employs the single carrier–frequency division multiplexing (SC-FDM) in its UL transmission, the cyclostationarity of these signals can also be studied and employed for their joint detection and classification.
- Study of the cyclostationarity of the new air interface standards of both signals, such as the 802.16m and LTE-advanced.

References:

[1] D. Cabric, "Cognitive Radios: System Design Perspective," Ph.D thesis, University of California, Berkeley, 2007.

[2] I. F. Akyildiz et al., "Next generation/dynamic spectrum access/cognitive radio wireless networks: a survey," *Computer Networks: The International Journal of Computer and Telecommunications Networking*, vol. 50, pp. 2127-2159, Sept. 2006.

[3] T. Yucek and H. Arslan, "A survey of spectrum sensing algorithms for cognitive radio applications," *IEEE Communication Surveys and Tutorials*, vol. 11, pp. 116-130, Mar. 2009.

[4] S. Haykin, "Cognitive radio: brain-empowered wireless communications," *Journal on Selected Areas in Communications*, vol. 23, pp. 201-220, Feb. 2005.

[5] S. M. Mishra et al., "Cognitive technology for Ultra-Wideband/WiMax coexistence" in *Proc. IEEE DySPAN*, 2007, pp. 179-186.

[6] A. Dobre et al., "On the cyclostationarity of OFDM and single carrier linearly digitally modulated signals in time dispersive channels with applications to modulation recognition," in *Proc. IEEE WCNC*, 2008, pp. 1284-1289.

[7] A. Punchihewa, Q. Zhang, O. A. Dobre, C. Spooner, S. Rajan, and R. Inkol, "On the cyclcostationarity of OFDM and single carrier linearly digitally modulated signals in time dispersive channels: Theoretical developments and application," *IEEE Transactions on Wireless Communications*, vol. 9, pp. 2588-2599, June 2010.

[8] N. Han et. al., "Cyclic autocorrelation based blind OFDM detection and identification for cognitive radio," in *Proc. IEEE WiCOM*, 2008, pp. 1-5.

[9] A. Bouzegzi, P. Jallon, and P. Ciblat, "A second order statistics based algorithm for blind recognition of OFDM based systems," in *Proc. IEEE GLOBECOM*, 2008, pp. 1-5.

[10] M. Oner and F. Jondral, "On the extraction of the channel allocation information in spectrum pooling system," *IEEE Journal on Selected Areas in Communications* , vol. 25, pp. 558-565, Apr. 2007.

[11] Z. Lei and F. Chin, "WiMAX signal detection," in *Proc. IEEE MILCOM*, 2008, pp. 1-7.

[12] P. D. Sutton, K. E. Nolan, and L. E. Doyle, "Cyclostationary signatures in practical cognitive radio applications," IEEE *Journal on Selected Areas in Communications*, vol. 26, pp. 13-24, Jan. 2008.

[13] P. D. Sutton et. al., "Cyclostationary signature detection in multipath rayleigh fading enviroment," in *Proc. IEEE CrownCom*, 2008, pp. 408-413.

[14] F.-X. Socheleau, P. Ciblat, and S. Houcke, "OFDM system identification for cognitive radio based on pilot-induced cyclostationarity," *in Proc. IEEE WCNC*, 2009, pp. 1-6.

[15] E. Seagraves, C. Berry, and F. Qian, "Robust mobile WiMAX preamble detection," in *Proc. IEEE MILCOM, 2008*, pp. 1-7.

[16] WiMAX forum, WiMAX Forum Mobile System Profile, 2007.

[17] IEEE Std. 802.16, Part 16: Air Interface for Fixed Broadband Wireless Access Systems, 2004.

[18] IEEE Std. 802.16, Part 16: Air Interface for Fixed and Mobile Broadband Wireless Access Systems, Amendment 2: Physical and medium Access Control Layers for Combined Fixed and Mobile Operations in License Bands and Corrigendum 1, 2005.

[19] J. G. Andrews, A. Ghosh, and R. Muhamed, *Fundamentals of WiMAX: Understanding Broadband Wireless Networking*. Prentice-Hall, 2007.

[20] C. M. Spooner and W. A. Gardner, "The cumulant theory of cyclostationary time-series, part I: foundation and part II: development and applications," *IEEE Trans. Sig. Proc.*, vol. 42, pp. 3387-3429, Dec. 1994.

[21] R. Nee, *OFDM wireless multimidia communications*, Artech house, 2000.

[22] 3GPP TS 36.211: Evolved Universal Terrestrial Radio Access (E-UTRA); Physical channels and modulation, 2009.

[23] 3GPP TS 36.101: Evolved Universal Terrestrial Radio Access (E-UTRA); User Equipment (UE) radio transmission and reception, 2009.

[24] A. V. Dandawate and G. B. Giannakis, "Statistical tests for presence of cyclostationarity," *IEEE Trans. on Signal Processing*, vol. 42, pp. 2355–2369, Sep. 1994.

[25] J. Lunden et al., "Spectrum sensing in cognitive radios based on multiple cyclic frequencies," *in Proc. IEEE CROWNCOM*, 2007, pp. 37-43.

[26] A. F. Molisch, *Wireless Communications*. Wiley, 2005.

[27] [Online]. Available: http://ark.intel.com/ Product.aspx?id=47932&processor= i7-980X&spec-codes=SLBUZ

[28] H. L. van Trees, *Detection, Estimation, and Modulation Theory*. Wiley, 2001.